The Varying Probability of Fission Model for Calculation of Neutron Moments and Applications

A Dissertation Presented for the
Doctor of Philosophy
Degree
The University of Tennessee, Knoxville

Aaron Nowack
August 2023

"I am fain to compare myself with a wanderer on the mountains who, not knowing the path, climbs slowly and painfully upwards and often has to retrace his steps because he can go no further—then, whether by taking thought or from luck, discovers a new track that leads him on a little till at length when he reaches the summit he finds to his shame that there is a royal road by which he might have ascended, had he only the wits to find the right approach to it. In my works, I naturally said nothing about my mistake to the reader, but only described the made track by which he may now reach the same heights without difficulty."

Hermann von Helmholtz

Dedication

This work is dedicated to my wife, Sue Nowack, whose support and presence during this adventure made this work and my graduation possible. I love you forever, Sue. Now it's time for us to embark on your adventure.

Acknowledgements

I attended the University of Tennessee based on the positive recommendations I received about Jason Hayward, who has served my academic advisor. He has lived up to the many positive stories I was told. His unconditional support, understanding, and firm belief in me and this work enabled me to complete this work despite the several challenges. I am incredibly appreciative and thankful of his positive and affirming approach as an advisor, which I hope to emulate in my own professional career.

This work also would not have been completed if it weren't for the many conversations I had with Paul Hausladen of ORNL. When I faced a brick wall in my work, or had an overwhelming sense of frustration, Paul provided the level headed context and advice that I needed to hear. He helped guide this work from a combination of several disparate ideas into a more coherent work. I am very thankful for our weekly conversations. Thank you, Paul.

My fellow students provided much needed moral support and encouragement throughout this work: Micah Folsom for graciously listening to my many frustrations, Matthew Tweardy for engaging in similar work and providing technical insight, and many others for their positive interactions.

Credit is due to the Nuclear Science and Security Consortium and the Department of Energy, who provided financial support for this research and provided me the opportunity to attend several insightful workshops, summer schools, and conferences which advanced and clarified the importance of this field of research and my contribution.

The University of Tennessee and the Department of Nuclear Engineering several times provided help that went beyond what I expected, when it was needed most, and I remain very appreciative of their support.

I would also like to thank my committee members Lawrence Heilbronn, Ronald Pevey, and Jens Gregor for supervising this dissertation and providing feedback.

I thank my father who helped remodel the office this dissertation was written in, and my mother whose many trips together to children's museums and libraries imparted a lasting curiosity.

I am thankful for the conversations about my 'shapes' with my young nieces, Kira and Kitana, who assured me that it's okay if my shapes don't match because sometimes their clothes don't match.

Lastly, I would like to state appreciation to everyone who has taken the time to listen to me.

Abstract

Neutron multiplicity analysis (NMA) is a non-destructive method for estimating fissile mass from the rate of detecting one, two or more emitted fission neutrons within a time gate, known as the neutron moments. NMA relies on the point model which expresses the neutron moments as analytic expressions of a constant and uniform probability for each neutron to induce fission. To use a constant probability of fission the point model approximates the geometry of assemblies of fissile materials as a single point in time and space, neglecting all geometry. This approximation significantly underestimates the fissile mass and enrichment for large assemblies. This work presents the Varying Probability of Fission (VPF) model, which extends the point kinetic model by allowing the probability of fission to vary with position and the number of fissions in each fission chain, termed the neutron collision number. While the VPF model requires a several values of the fission probability, additional constraints can be imposed to reduce the number of solved variables. These constraints can be modelled interpolation functions with parameters determined from Monte Carlo simulation. Additionally, the Associated Particle Imaging (API) technique provides additional information on interrogating neutron direction and transmission images. After applying a back projection step API systems provide imaged data of emitted neutron singles and doubles for induced fission at varying positions in addition to the transmission image. This work presents how the imaged data of neutron transmission, neutron singles and doubles can be incorporated into a VPF analysis and provide images of the spatially dependent induced neutron fission probability and the rate of induced neutron chains. The VPF model could enable a new, real-time quantitative assessment capability for nuclear material assemblies that are imaged by API systems.

Table of Contents

List of Tables

List of Figures

List of Algorithms

List of Abbreviations

NMA	**N**eutron **M**ultiplicity **A**nalysis
DA	**D**estructive **A**ssay
NDA	**N**on **D**estructive **A**ssay
TNI	**T**agged **N**eutron **I**nterrogation
VPF	**V**arying **P**robability of **F**ission
API	**A**ssociated **P**article **I**maging
DT	**D**euterium-**T**ritium
APNIS	**A**dvanced **P**ortable **N**eutron **I**maging **S**ystem
MCNP	**M**onte **C**arlo **N**-**P**article
PGF	**P**robability **G**enerating **F**unction
IAEA	**I**nternational **A**tomic **E**nergy **A**gency

List of Symbols

p_f	probability of fission
$P(\nu)$	fission multiplicity distribution
$G_X(s)$	generating function for discrete random variable X
$\mathbb{E}[X]$	expectation value of X
ν_k	kth factorial moment of a discrete distribution
$\mathcal{M}_i$	ith combinatorial moment
$\mathbf{M_T}$	total multiplication
$\mathbf{M_L}$	net or leakage multiplication
$\mathbf{F}$	number of events initiating fission
$\mathbf{S}$	neutron singles
$\mathbf{D}$	neutron doubles
$\mathbf{T}$	neutron triples
m_{eff}	effective mass (g)
$\boldsymbol{\alpha}$	ratio of neutrons created from (α, n) reactions to neutrons created from spontaneous fission
ϵ	detector efficiency
Σ_x	macroscopic neutron cross section for interaction x

Chapter 1

Introduction

1.1 Overview and Motivation

Neutron multiplicity analysis (NMA) for non-destructive assay of (NDA) nuclear materials has traditionally relied on the point model formalism by Böhnel, which expresses the neutron multiplicity moments as analytic functions of the probability that any neutron within the sample induces fission [1]. The rates of neutron single, double, and triple coincidences measured by an NMA system is proportional to the respective neutron moments and the rate of initiated fission chains. With an estimated fission chain initiation rate, a determination of fissile mass can be made and is the reason NMA is a widely used technique in nonproliferation [2]. The success of applying the point model is tied to how well the measurement meets the point model assumptions: All neutrons are approximated to be at a single point in time and space, with constant values of energy and probability to induce fission. These assumptions break down for subcritical fissile assemblies with large extended geometries, where variations of neutron multiplication "on the position in the active material at which the source of neutrons is introduced" cannot be ignored [3]. The ability to extend the point model and derive a new set of analytic equations applicable for extended or non-point assemblies is an enabling capability in non-proliferation scenarios [4].

This dissertation presents an extension of the point model for extended assemblies of fissile material which allows for real time analysis of imaged data of neutron singles and doubles taken by tagged neutron interrogation (TNI) systems. The traditional point model and equations for neutron moments are derived in Chapter 2. To extend the point model, Chapter 3 creates a Monte Carlo simulation which matches the point model assumptions as close as possible. This allows a direct investigation of how extended geometries violate the point model. Two dominant factors are shown. The first factor is the aforementioned variation of neutron multiplication on the position of the event generating a neutron. The second contributing factor is the changing distribution of induced fission positions as the fission chain distributes throughout the volume. This variation is dependent on the number of collisions preceding each induced fission, termed the collision number. Chapter 4 presents new moment equations which include these two effects by relaxing the assumption that the probability of fission is constant and instead is dependent on the position of the first event in a fission chain and the collision number. This is termed the Varying Probability of Fission (VPF) model. The simplifications of the physics of Chapter 3 are then relaxed, and the accuracy of the VPF model including the effects of neutron energy variation, capture, elastic and inelastic scatter is presented in second portion of Chapter 4.

An application of the VPF model is to interpret 3D images of neutron singles and doubles, where voxel position is the location of induced fission by an external source. Associated Particle Imaging (API) systems generate this data through the use of a position-sensitive alpha particle detector which tags the direction of the recoiling neutron created in a deuterium-tritium (DT) reaction neutron generator. With repeated measurements at different orientation angles, sinograms are created. A forward model of the measurement process is used in an iterative reconstruction method to create 3D images of detected neutron singles and doubles in a voxelized image space [5]. Section 2.5.4 overviews how current interpretation of these images is done through comparison with trial Monte Carlo simulations where geometry and materials are iterated in a specified manner. As the VPF model is dependent on the starting position of the fission chain, applying the VPF for interpreting API imaged data enables real time conversion of imaged data from API measurements into quantifiable images related to enrichment and the probability of a neutron to initiate fission. The application of the VPF model for interpreting API measurements is presented in Chapter 5. This is an enabling capability of API and similar systems for real-time non-proliferation scenarios.

1.2 List of Original Contributions

1. Chapter 3 presents a modified version of the Monte Carlo N-Particle (MCNP) program of neutron transport which matches the point model assumptions except for the point geometry assumption to quantify the accuracy of the point model assumptions.

2. Chapter 3 additionally presents two factors of the point geometry bias. The variation of the probability of fission with position of introduced source neutron, and the changing spatial distribution of neutron induced fissions with collision number. These two effects are shown that when combined, the probability of fission varies with collision number.

3. Chapter 4 then derives a new model which allows the probability of fission to vary with collision number, termed the Varying Probability of Fission Model. New equations of neutrons moments are derived. The accuracy of the VPF model is presented for a simulation of neutrons including all effects such as neutron energy variation and neutron capture, elastic, and inelastic reactions. This is done in comparison with the simplified physics of Chapter 3.

4. Chapter 5 then presents an application of using the VPF model to rapidly interpret images of neutron singles and doubles taken from a TNI system. Model parameters are determined from MCNP, then applied to the imaged data of several complicated geometries. The VPF model and determined parameters are incorporated into a least squares error minimizer to estimate the first collision probabilities and number of induced fissions from images of neutron singles and doubles. This is done over several geometries, and is able to provide accurate estimations of the number of fissions at each position without having to run a full Monte Carlo simulation for each geometry.

1.3 Fission Chains

1.3.1 Fission

At the center of non-destructive assay of fissile materials is the nuclear process of fission, in which a heavy atomic nucleus splits into two or more lighter daughter nuclei. Experimental evidence of fission was first observed by Enrico Fermi between 1934 and 1935 while exposing individual elements to neutron radiation [6]. The exposure of uranium was notable for creating radioactive material with multiple decay half lives. Ida Noddack proposed in 1935 that the uranium nuclei had burst into several lighter nuclei with individual half lives, but her explanation was ignored partly due to a lack of supporting evidence [6]. During 1937 in Paris, Irène Joliot-Curie and Pavel Savić came close to identifying one of the products as the lighter element lanthanum but instead incorrectly attributed it as the heavier but chemically similar element actinium. Concurrent experiments in Berlin starting in 1934 by Lise Meitner, Otto Hahn, and Friedrich Strassman also examined the exposure of uranium to neutron radiation. After systematically ruling out the production of elements neighboring uranium, Meitner urged Hahn and Strassman in 1938 to investigate the possibility of the light element barium being produced. At this time Hahn and Strassman remained in Berlin while Meitner, being an Austrian citizen and raised in a jewish household, had fled to Sweden after Hitler's invasion of Austria and imposition of work restrictions on people with jewish ancestry. Hahn and Strassman were able to verify that barium was produced from uranium exposed to neutron radiation, not the heavier element radium as was previously believed [6]. Hahn and Strassman published a paper of these results at the start of 1939 [7], and in 1944 Otto Hahn would receive the Nobel prize in chemistry for the discovery of fission. A month after the experimental confirmation Lise Meitner and Otto Frisch provided a theoretical interpretation [8] in which they introduced the word 'fission' and described the uranium nuclei bombarded by neutron radiation as an excited drop of liquid which then split into smaller droplets.

Niels Bohr and John Wheeler further developed Meitner's droplet model into the Bohr-Wheeler Liquid-Drop model (LDM) of fission which provides a quantitative analysis of the mechanism of nuclear fission [6], [9]. As described by the liquid model, the nucleus is pulled apart by the coulomb repulsion of the protons but held together by a surface tension via the nuclear force. This interplay creates a energy threshold, called the fission barrier. For a compound nucleus which has absorbed a neutron and may fission, a nuclei may begin to cross the fission barrier. The nucleus elongates into an elliptical shape, begins to break apart through the process of scission, and finally split into two lighter daughter nuclei which repel each other and separate as shown in Figure 1.1. This model largely remains intact today through its modern equivalent, the macroscopic-microscopic model of fission [6].

1.3.2 Fission Neutrons

For safeguards the relevant portion of fission is the generation of neutron and gamma particles, which occurs throughout the entire fission process. As this work is focused on neutrons, we list the steps of fission in terms of the emission of neutrons as described in [10].

1. A nucleus absorbs either a neutron or gamma, creating an excited compound state which can overcome the fission barrier. In this pre-fission state neutrons may be emitted, known as multi-chance fission. First-chance fission is the emission of zero neutrons before fission, second-chance is the emission of one neutron before fission, et cetera. This occurs on the scale of 10^{-21} seconds [10].

2. As the neutron splits or scissions, some neutrons in the shrinking neck may be orphaned as the daughter nuclei rapidly separate. These scission neutrons are predicted by some models; however, they have not been confirmed experimentally [10].

3. The now separated daughter nuclei are in excited states. Both neutrons and gammas are emitted through an evaporation process to dissipate the additional energy. The specific number of neutrons emitted is dependent on the isotope of the daughters and the geometry of the nucleons during scission, but generally the fragments are neutron rich. Neutrons are emitted on the time scales of the strong nuclear force within 10^{-17} seconds [10].

4. After the process of fission and primary neutron emission, the fragments are in their ground states but may remain neutron rich and undergo beta decay. This process is governed by the weak nuclear force and occurs between milliseconds to minutes [10].

Neutrons emitted from steps 1-3 are referred to as *prompt* neutrons, and neutrons emitted afterwards in step 4 are *delayed* neutrons.

In the center-of-mass frame of reference, the energies of prompt neutrons are described by a Maxwellian distribution which describes an evaporative process. In the lab frame of reference this results in the Watt neutron energy spectrum. In MCNP, one of the popular computer codes for modelling neutron transport, the Watt spectrum is expressed as a parameterized equation

$$f(E) = Ce^{-E/a} \sinh \sqrt{bE} \tag{1.1}$$

where C is a normalizing constant and a and b are fit for specific isotopes [11]. For neutron induced fission these constants also depend on the energy of the incident neutron.

The number of prompt neutrons emitted, called the neutron multiplicity, is a function of the excitation energy present in each fragment. Thus it is a function of both the mass of the fragment, and the excitation energy present in the pre-fission compound nucleus provided by the initiating neutron or gamma [6]. For safeguards applications typically only the second dependence is considered, and neutron multiplicity is averaged over the fragment mass and is a function of the incident neutron or gamma energy which imparts its energy to the pre-fission nuclei. Previous experiments have measured the multiplicity distributions over a range of isotopes for incident neutron and photon energies [12], as shown in Figure 1.2 for uranium-235 with several incident neutron energies.

1.3.3 Chain Reactions

In 1934, before the discovery of fission, Leo Szilard was granted a patent for "nuclear transmutation leading to the liberation of neutrons . . . by maintaining a chain reaction in which particles which carry no positive charge ... or a multiple thereof form the lines of the chain" [13]. Despite Szilard's petitioning of many scientists including Rutherford, only after the experimental confirmation of fission in 1939 was serious investigation made on determining if a fission driven chain reaction connected by neutrons was possible.

Following the discovery of fission, there remained three properties of fissioning nuclei which affect the ability to sustain a chain reaciton: the number of neutrons produced in a fission reaction, the probability of a neutron to induce fission, and the relative rate of non-fission neutron absorption reactions. During 1939, work in France by Halban, Joliot, and Kowarski estimated 3.5 neutrons liberated per fission. Although this was above the correct value of 2.6, their conclusion that "the fission chain will perpetuate itself" intensified efforts to investigate the possibility of a nuclear chain driven weapon, both in United States and Nazi Germany [14]. Fission chains in natural uranium proved difficult; however, George Placzek identified the importance of the second contribution. If too much natural uranium or absorbing material was present, enough neutrons would be captured to prevent the chain from continuing. As the properties of both uranium-235 and uranium-238 became better understood, it was suspected by many scientists that a self sustaining nuclear reaction was, in fact, possible. This culminated in the 1939 letter written by Albert Einstein and Szilard to President Roosevelt, establishing the Manhattan Project as the US government investigation of using neutron driven fission chains as a weapon of war. During the Manhattan project and after several initial experiments the first self-sustaining nuclear chain reaction was achieved on December 2, 1942 on the rackets court at the University of Chicago led by Enrico Fermi and Leo Szilard [14]. This first reactor used pure carbon to scatter neutrons, removing much of their energy and increasing the probability of fission. However, by this time it was understood that a nuclear chain sustained by only the unmoderated fast neutrons emitted directly by fission could also maintain a fission chain given in a configured mass of material enriched in uranium-235 [15].

1.3.4 Simulation

The statistical properties of fission chains are best illustrated with a program simulating a population of neutrons in fissile material. Energy, time, and position are neglected. The material is fully specified by two quantities: the multiplicity distribution $P(\nu)$ of a fission releasing ν neutrons with probability $P(\nu)$, and the probability p_f that any neutron will induce a fission. The program is outlined in Algorithm 1 and begins with a neutron population of one. Each neutron in the population is given a chance p_f of initiating a fission. If a fission is created, ν neutrons are sampled from the fission multiplicity distribution $P(\nu)$ and added to the neutron population. Each fission removes one neutron from the population to initiate the fission, and neutrons which do not fission are removed and added to the leaked neutron population representing the number of neutrons which have escaped or leaked from the material.

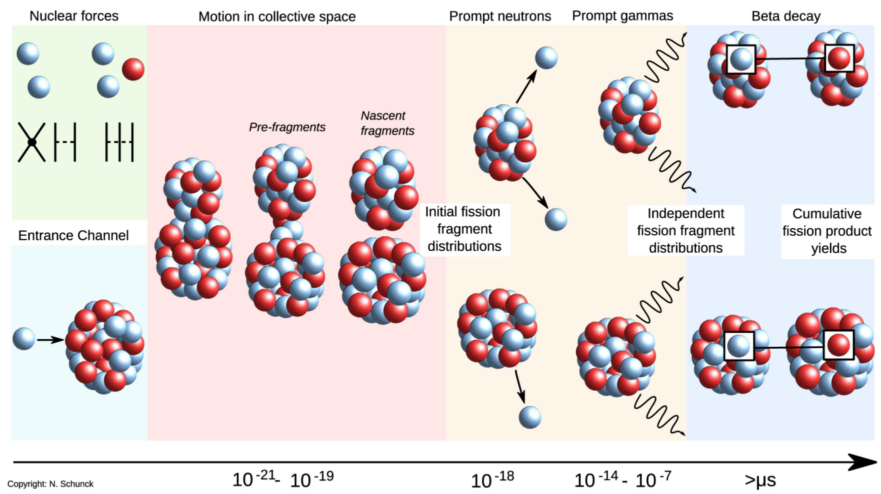

FIGURE 1.1: Illustration of the fission process as a parent compound nucleus deforms into separate excited fragment nuclei. The excited fragments emit prompt gammas and neutrons in addition to beta decay over a longer time period. Reprinted from Progress in Particle and Nuclear Physics, 125, Nicolas Schunck, David Regnier, Theory of nuclear fission, pg. 3, Copyright 2022, with permission from Elsevier.

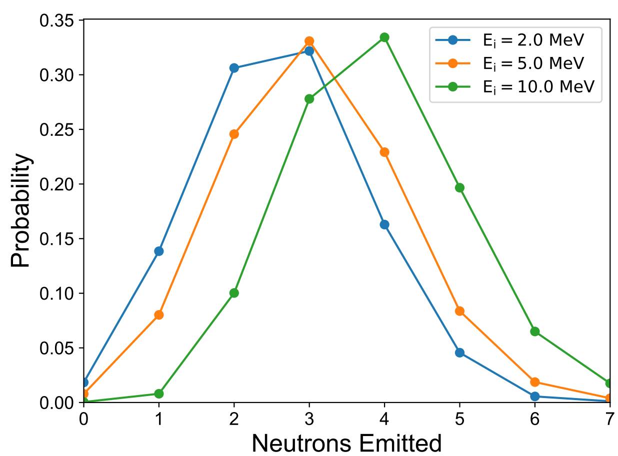

FIGURE 1.2: Multiplicity distribution of neutrons emitted from neutron induced fission on uranium-235 for neutrons of 2 MeV, 5 MeV and 10 MeV. Data shown is taken from [12].

Algorithm 1 Calculate number of neutrons emitted by a fission chain

---

Require: p_f, $P(\nu)$
  $n_{pop} \leftarrow 1$ {neutron population}
  $n_T \leftarrow 0$ {# neutrons (total)}
  $n_L \leftarrow 0$ {# neutrons (leak)}
  $n_F \leftarrow 0$ {# fissions}
  while $n_{pop} \geq 1$ **do**
    for $i = 1$ to n_{pop} **do**
      if $p_f >$ randf **then**
        $n_F = n_F + 1$
        $n_\nu \sim P(\nu)$ {Create ν fission neutrons with $P(\nu)$ probability}
        $n_{pop} = n_{pop} + n_\nu - 1$
        $n_T = n_T + n_\nu$
      else
        $n_{pop} = n_{pop} - 1$
        $n_L = n_L + 1$
      end if
    end for
  end while

1.3.5 Neutron Multiplication

Fissile materials multiply the number of neutrons introduced to a system, commonly referred to as multiplication. Robert Serber in 1945 clarified the definition of neutron multiplication to distinguish between total multiplication and net or leakage multiplication [3]. Total multiplication $\mathbf{M_T}$ is defined as the total number of neutrons created in a fissile material after introducing one source neutron. This can be expressed mathematically as

$$\mathbf{M_T} = 1 + \sum_{i=0}^{n_F} \nu_i \tag{1.2}$$

$$\overline{\mathbf{M_T}} = 1 + \overline{n_F}\bar{\nu} \tag{1.3}$$

where n_F is the number of fissions occurring. Taking the average of both sides yields (1.3) where $\overline{n_F}$ is the average number of fissions in each chain and $\bar{\nu}$ is the average number of neutrons emitted per fission [3]. Common usage of total multiplication refers to the averaged quantity $\overline{\mathbf{M_T}}$ over many chains, so it is customary to refer to (1.3) as the total multiplication $\mathbf{M_T}$.

Alternatively total multiplication can be expressed with the probability p_f that any single neutron induces fission. Starting with a single neutron, there is a p_f chance a fission occurs and creates on average $\bar{\nu}$ neutrons, $1 + p_f\bar{\nu}$. Each of these neutrons also have a p_f chance to initiate fission, creating on average $1 + p_f\bar{\nu}(1 + p_f\bar{\nu})$ neutrons. This process continues indefinitely for many fissions, with a net multiplication

$$\mathbf{M_T} = 1 + p_f\bar{\nu}(1 + p_f\bar{\nu}(1 + p_f\bar{\nu}(1 + p_f\bar{\nu} \cdots))). \tag{1.4}$$

Expanding the terms yields a geometric series

$$\mathbf{M_T} = 1 + p_f\bar{\nu} + (p_f\bar{\nu})^2 + (p_f\bar{\nu})^3 + \cdots \tag{1.5}$$

which where $p_f\bar{\nu} < 1$ corresponding to a subcritical assembly converges to the solution

$$\mathbf{M_T} = \frac{1}{1 - p_f\bar{\nu}}. \tag{1.6}$$

Net or leakage multiplication $\mathbf{M_L}$ quantifies the number of neutrons which leave a system given one source neutron. In this simplified model, the only neutrons which do not leave are those used to induce fission. This can be expressed as,

$$\mathbf{M_L} = 1 + n_F\bar{\nu} - n_F = 1 + n_F(\bar{\nu} - 1) \tag{1.7}$$

and is related to the total multiplication by

$$\mathbf{M_L} = (1 - p_f)\mathbf{M_T} = \frac{1 - p_f}{1 - p_f\bar{\nu}}. \tag{1.8}$$

Using the parameters shown in the simulation of Figure 1.3b where $p_f = 0.2$ and $\bar{\nu} = 2.637$

with (1.6) and (1.8) yields $\mathbf{M_T} = 2.116$ and $\mathbf{M_L} = 1.693$. This matches the expected values of $\mathbb{E}[n_T] = 2.116$ and $\mathbb{E}[n_L] = 1.693$ of the leaked neutron distribution n_L shown for the simulation of Figure 1.3b created using Algorithm 1.

1.3.6 Moments of Emitted Fission Neutrons

In addition to multiplication another important quantity of fission chains are the relative rates of one, two, or more neutrons being emitted from each fission chain. A detection system which records the timing information of detected neutrons can measure these rates, and provides additional information about the properties of the fission chain.

Instead of using the count probabilities, it is more common to measure the combinatorial moments of the leaked neutron distribution $n_L(i)$. The jth combinatorial moment $\mathcal{M}_j$ measures the number of unique ways of counting j items from i objects sampled from a discrete distribution $P(i)$ [16],

$$\mathcal{M}_j = \sum_i \binom{i}{j} P(i) = \mathbb{E}_{P(i)}\left[\binom{i}{j}\right]. \tag{1.9}$$

The first three combinatorial moments of the leaked neutron distribution $n_L(i)$ are

$$\mathcal{M}_1 = \sum_i \binom{i}{1} n_L(i) = \sum_i i n_L(i) = \mathbb{E}_{n_L(i)}[i] \tag{1.10}$$

$$\mathcal{M}_2 = \sum_i \binom{i}{2} n_L(i) = \frac{1}{2!}\sum_i i(i-1) n_L(i) = \frac{1}{2}\mathbb{E}_{n_L}[i(i-1)] \tag{1.11}$$

$$\mathcal{M}_3 = \sum_i \binom{i}{3} n_L(i) = \frac{1}{3!}\sum_i i(i-1)(i-2) n_L(i) = \frac{1}{6}\mathbb{E}_{n_L}[i(i-1)(i-2)]. \tag{1.12}$$

If 6 neutrons escape the first three combinatorial moments are 6, 16, and 20. As (1.10) is equal to the average number of neutrons leaked from a system, for one starting neutron, $\mathcal{M}_1 = \mathbf{M_L}$.

The values of the first three moments are simulated using Algorithm 1 for various values of p_f and shown in Figure 1.4.

1.4 Neutron Non Destructive Analysis

1.4.1 Nuclear Security and Safeguards

The textbook by Doyle et. al list three main objectives in nuclear security for the post-Cold War and post-9/11 era [17]

- "The states that possess nuclear weapons, materials, and knowledge must effectively control and protect them from theft or misuse".
- "The proliferation of nuclear weapons, both within states that possess them and to additional states, should be prevented".

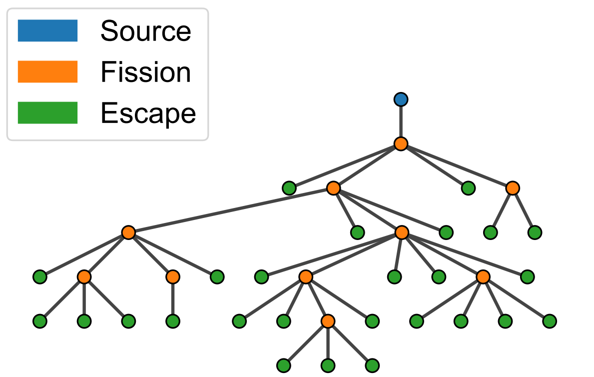

(A) One simulated fission chain. Nodes are events, connecting lines are neutrons. The total number of neutrons n_T are the number of connecting lines. The number of leaked neutrons n_L are the number of escape events. For the chain shown, $n_T = 36$ and $n_L = 26$.

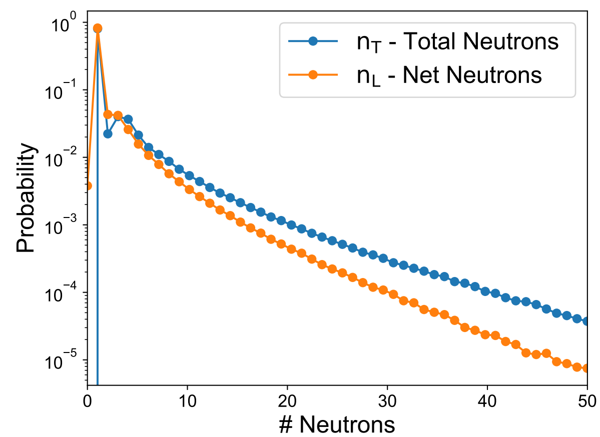

(B) Aggregate statistics of total and leaked neutrons over 10^7 simulated chains using $p_f = 0.2$. $P(\nu)$ is the 2.0 MeV neutron induced multiplicity distribution of Figure 1.2.

FIGURE 1.3: The output of Algorithm 1 for a single chain (left) and aggregated over 10^6 chains (right) displaying the probability of any chain producing n_T total neutrons and n_L leaked neutrons.

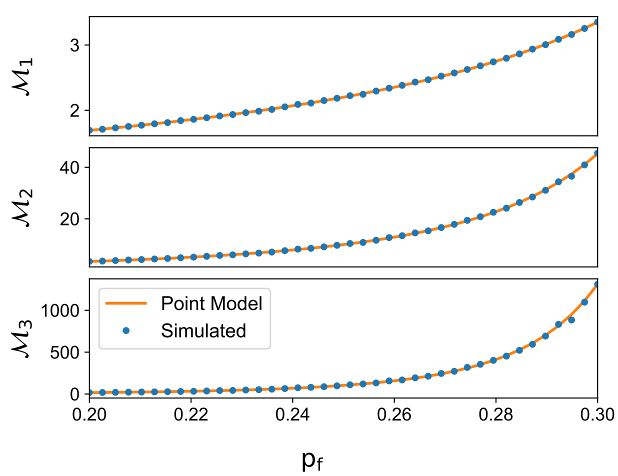

FIGURE 1.4: The first three combinatorial moments for trials of 10^6 simulated fission chains with $p_f = 0.2 - 0.3$. The moments using the simulation of Algorithm 1 is shown (blue) in comparison with the point model equations (2.36)-(2.38) (orange).

- "All states must make efforts to prevent nuclear terrorism".

Approaches to meet these objectives fall into two categories, nuclear security and nuclear safeguards. Security aims to prevent the theft of nuclear materials, while safeguards aim to detect the diversion of materials of peaceful nuclear programs for undeclared weapons programs. Security is mainly controlled by individual states guided by the IAEA document "Physical Protection of Nuclear Material and Nuclear Facilities" (INFCIR/225/Rev.4) [17]. Safeguards are performed both by individual states seeking to prevent against external and insider threats and through international agreements enforced by the International Atomic Energy Agency (IAEA) via the Comprehensive Safeguards Agreement (INFCIRC/153) and the Additional Protocol (INFCIRC/540) [17].

The use of technology for the measurement and accounting of nuclear materials is essential for security and the compliance of international agreements. This can be through destructive assay or analysis (DA) where a small sample of an interrogated item is collected and analyzed to determine isotopic composition. Common DA methods include analytical chemistry and mass spectrometry. However DA requires the ability to remove a small portion of the material which is not possible for assembled items which inspectors are not able to alter due to classification or security concerns.

The alternative is to perform non destructive analysis or assay (NDA) which measures properties of nuclear materials without destruction or direct contact. Most NDA methods rely on measuring either photons (x-ray or gamma) or neutrons, both of which are electrically neutral and pass through many materials. When detected, the spectrum of energetic photons provide direct measurement of uranium and plutonium isotopic composition. However for high Z materials such as uranium and plutonium metal most photons are re-absorbed limiting information to the first few millimeters below the surface if the material is not already shielded. Neutrons readily pass through high Z materials but their energies do not give significant isotopic or mass estimates. However as fission chains occur within several to hundreds of nanoseconds the timing correlations of detected neutrons are distinguishable from background sources [18]. The intensity of these correlations are proportional to the amount of fissile material present. The ability to rapidly assay large and dense samples is the reason neutron based NDA methods are popular for nuclear material accounting scenarios in nuclear security and safeguards.

1.4.2 Neutron Counting, Coincidence Counting, and Multiplicity Analysis

Most measurements using the emission of neutrons emitted by an interrogated material can be divided using two categories, first being whether an external source of neutron radiation is used. Passive measurements use neutrons generated within the material, either through spontaneous fission or (α, n) emission. Active measurements rely on an external source of neutrons to begin fission chains. As the neutron emission rate of plutonium-240 is 920 neutrons$/(sec \cdot g)$, 3.0×10^{-4} neutrons$/(sec \cdot g)$ for uranium-235 and 0.0136 neutrons$/(sec \cdot g)$ for uranium-238, plutonium measurements can be done using passive assays while measurements of uranium typically require an active assay [19].

The second category is the number of variables recorded by the detector electronics and used in the analysis. Neutron counting records the rate neutron of neutrons emitted by a system, proportional to the first combinatorial moment $\mathcal{M}_1$ (1.10). Neutron coincidence counting includes occurrences of two neutrons in a time gate, which is proportional to the second combinatorial moment $\mathcal{M}_2$ (1.11). Neutron multiplicity analysis also includes the third moment $\mathcal{M}_3$ (1.12) of neutron triple coincidences. Higher moments may be included, however the lower detection efficiency generally prevents the signal from being useful. In theory for each additional moment measured it is possible to infer another property of the material being assayed.

In addition to the combinatorial moments all of the neutron rates are proportional to the source term, that is the strength of either the spontaneous fission, (α, n) reaction, or fissions induced by external neutron source of a known strength. The source strength increases with mass, allowing an estimate of the mass for an unknown object given a previous measurement of an object with known source strength and mass. For low multiplication where $\mathcal{M}_1 \approx 1$, neutron counting is a possible choice for estimating plutonium mass in a passive assay. However other neutron sources such as ambient backgrounds and neutrons scattered from the environment must be accounted for. Coincidence counting avoids these discriminates against these backgrounds by selecting only neutrons which are correlated in time.

There exist several comprehensive descriptions of how neutron counting, coincidence, and multiplicity counters are designed and operate [20]. However for the purpose of this thesis only the main points are outlined. Assayed fissile materials are surrounded by a moderating material such as high density polyethylene to lower the emitted neutron energy via elastic scatter on hydrogen which are then detected by embedded gas tubes of helium-3. The recoil proton of the neutron and helium-3 capture reaction produces a charge, which is then amplified and recorded as a digital pulse. A multiplicity shift register then sorts the pulse stream into correlated and uncorrelated events. This is performed by delaying the input pulse stream by a predelay amount and then counting the number of pulses within a set gate width. When another pulse comes in, the number of pulses stored is counted in scalar electronics counting whether zero, one, two, three, or more pulses were within the gate, which is a combination of real and accidental coincidences. This process is repeated but replacing the short predelay by a much longer delay, where the scalars measure the accidental uncorrelated multiplet coincidences. Subtracting the second set of scalars from the first then yields the detected multiplicity distribution, the 'reals', from which the neutron singles, doubles, and triples rates are determined.

Alternative systems which instead detect the fast neutrons emitted from the fission chain without moderation have been developed. These systems have the advantage that in addition to no moderator, the detection uses proton recoil present in organic scintillators which has a much faster response time on the order of nanoseconds compared to the milliseconds of traditional helium-3 counters. This avoids the need for long time gates, allowing the acquisition of multiplicity counts more frequently yielding improved counting statistics [21]. The disadvantage of scatter based systems are the lower absolute detection efficiency, the need to discriminate against gamma rays, and the ability of a neutron to scatter multiple times across several detectors.

In both systems the measurements are compared with either a simulation of neutron transport to estimate fissile mass, or make use of an analytical model describing the rates for the moments of neutron coincidences. The most popular of these is the 'point model' formalized by Böhnel, Hage, and Cifarelli and is covered in Chapter 2 [1] [22].

1.4.3 Associated Particle Imaging

An alternative method to passive and active neutron multiplicity assays utilizes the associated particle technique. In this approach fast neutrons are generated in a two body collision reaction which also produces a charged particle. If the energy and direction of the incident particle is known, recording the solid angle of the charged particle determines the emitted solid angle of the fast neutron. Additionally, counting the charged particle in coincidence with products of fast neutron induced reactions allow a selection against background events [23].

One reaction is the fusion deuterium-tritium (DT) reaction, in which a deuteron is emitted from an ion source and accelerated onto a target enriched in tritium. The reaction creates a 3.5 MeV alpha particle and a 14.1 MeV neutron, emitted in nearly opposite directions, as shown in Figure 1.5 [24]. By recording the position of the alpha particle, the direction of the outgoing fast neutron is known within a small solid angle. This setup is often referred to as tagged neutron interrogation (TNI) system as each neutron has been tagged in time, energy, and direction of travel.

TNI systems provides two significant capabilities over traditional neutron multiplicity systems. By including a neutron detector adjacent to an inspected object, the fraction of fast neutrons passing through the object can be selected in coincidence with alpha particles at different solid angles. By repeating this process over several rotation angles a fast neutron transmission object can be formed using medical imaging reconstruction methods, analogous to a computed tomography image. The second capability is using the kinematics of fast neutron induced reactions to associate detected neutrons with induced reactions. Fission neutrons travel at a slower energy of 2 MeV and arrive later in time relative to the 14.1 MeV fast neutron. By selecting neutrons relative to the time of recorded alpha particle which arrive after any possible transmitted 14.1 MeV neutrons, neutrons created through induced fission can be selected as seen in Figure 1.6. Multiple fission neutrons may be detected akin to multiplicity assays. With the directional information of the tagged inducing fast neutron, the detected neutron singles and doubles can be organized as imaged data where the pixel or voxel intensity represents the number of detected neutron singles or doubles per path length of the tagged neutron. However an analytic model for interpreting these models does not exist. Instead Monte Carlo simulations are used to estimate material properties based on these images, which require both computation time and the time and effort of an operator to perform the simulation. This is described in greater detail in Section 2.5.4. This dissertation presents a model which can create quantitative interpretations of imaged neutron singles and doubles from TNI systems in real time.

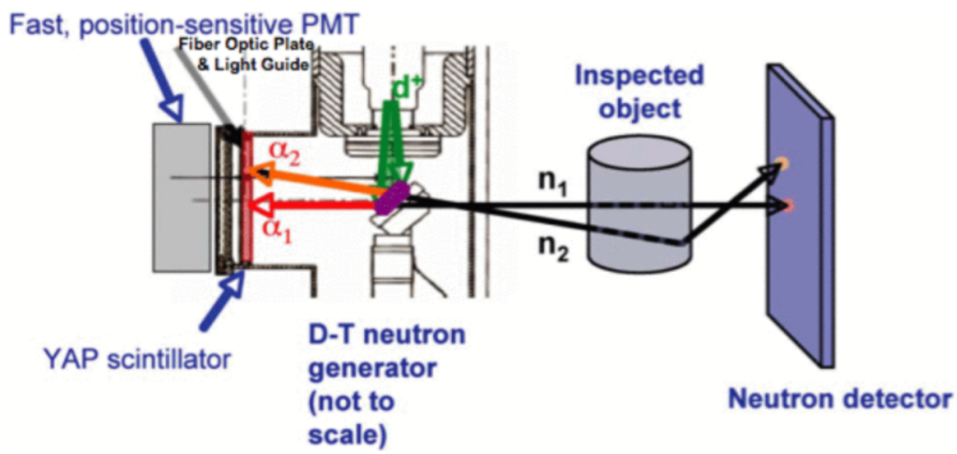

FIGURE 1.5: Figure 1 from [24] showing deuterons colliding with a tritium enriched source inside a D-T neutron generator. A position sensitive scintillator records the time and position of the alpha particle in coincidence with the emitted fast neutron and any fast neutron induced reaction products within an inspected object. Reprinted from [24] © 2012 IEEE.

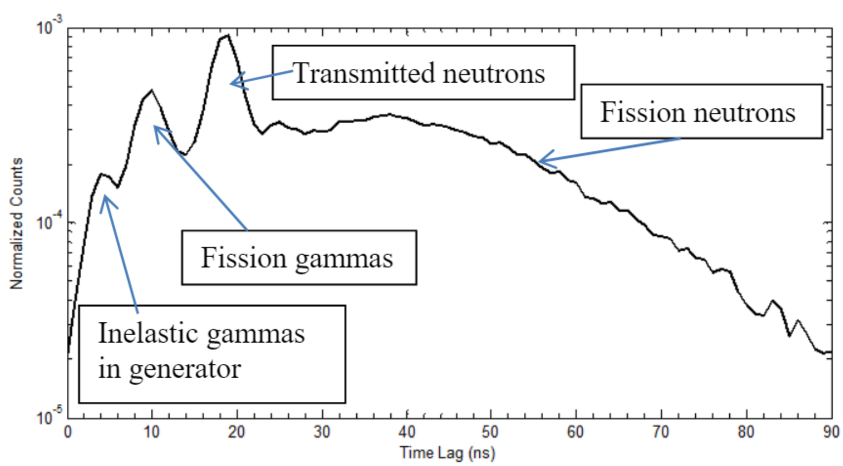

FIGURE 1.6: Figure 2 from [25] showing the time response of a neutron detected in a tagged neutron interrogation system with fissile material present. The transmitted neutrons and induced fission neutrons can be selected by the time lag between the neutron detection and the associated alpha particle.

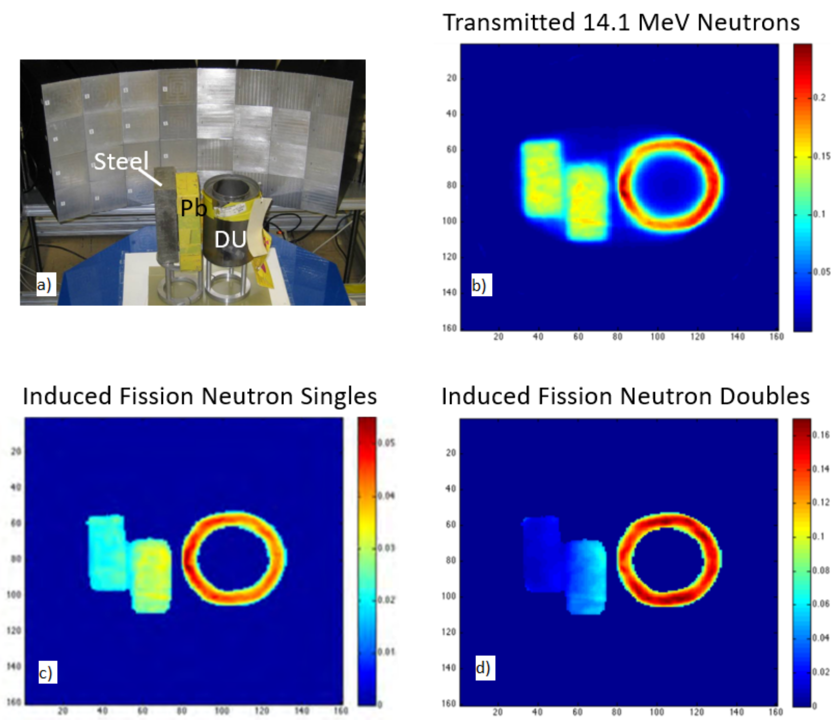

FIGURE 1.7: A combination of Figures 6, 7, 9, and 100 from [26] showing the imaged data of tagged neutron transmission and induced neutron singles and doubles from the Advanced Portable Neutron Imaging System (APNIS) developed at Oak Ridge National Laboratory.

Chapter 2

The Point Model of Neutron Fission Chains for Nuclear Safeguards

2.1 Probability Generating Functions

2.1.1 History

Similar problems to the fission chain process of Section 1.3.4 have been analyzed mathematically beginning in 1874 with Sir Francis Galton and Reverend H. W. Watson [27]. Together they provided a solution to the analogous problem of determining the size of a family name after several generations given probabilities p_n that each man of the family name produces n sons.

This problem was revisited in the 1920s and 1930s to study the survival of gene mutations, chemical chain reactions, and the multiplication of electrons in an amplifying device [27]. The discovery of neutron induced fission [7], [8] then necessitated the need to describe nuclear chain reactions. One approach by Stanislaw Ulam and David Hawkins at Los Alamos described neutron chains using the probability generating function technique [28]. After the war, multiplicative and branching processes were further developed by Ted Harris at the RAND corporation [27], [29] and have found many applications in the fields of ecology, genetics, and biology.

Probability generating functions (PGF) remain one of the main tools for describing neutron chain reactions to the present day, with Böhnel's paper on the point model of neutron transport [1] being the main reference in nuclear safeguards applications. The probability generating function technique is now described according to the text by Grimmet and Stirzaker [30].

2.1.2 Definition

For a sequence $a = \{a_i : i = 0, 1, 2 \cdots\}$, the *generating function* $G_a(s)$ is defined as

$$G_a(s) = \sum_{i=0}^{\infty} a_i s^i. \tag{2.1}$$

where s is a latent or dummy variable. Considering a discrete random variable X which can take non-negative integer values $\{0, 1, 2, \dots\}$, the sequence $f_i = \Pr(X = i)$ specifies the distribution.

The generating function $G_X(s)$ of the discrete probability mass function f_i is called a *probability generating function* (PGF) with property

$$G_X(s) = \sum_{i=0}^{\infty} f_i s^i = \sum_{i=0}^{\infty} s^i \Pr(X = i) = \mathbb{E}(s^X). \tag{2.2}$$

For example, the side of one rolled fair die has distribution $f_i = \Pr(X = i) = 1/6$ for $1 \leq i \leq 6$ with a probability generating function

$$G_{\text{dice}}(s) = \frac{1}{6}s + \frac{1}{6}s^2 + \frac{1}{6}s^3 + \frac{1}{6}s^4 + \frac{1}{6}s^5 + \frac{1}{6}s^6. \tag{2.3}$$

The PGF of a coin flip with probability $(1 - p)$ of landing tails $\Pr(X = 0)$ and probability p of heads $\Pr(X = 1)$ is written as

$$G_{\text{coin}}(s) = (1 - p) + ps. \tag{2.4}$$

In general, the PGF for the distribution of a discrete positive integer X is always an integer polynomial $\sum_i f_i s^i$ where the coefficient of each term f_i is the probability and the realization of $X = i$ is indicated by the power of s^i.

2.1.3 Properties

The power of generating functions lies with the following useful properties.

Sum of Two Random Variables

If X, Y are independent variables with the sum $S = X + Y$, the relation of the respective generating functions is

$$G_S(s) = G_X(s) G_Y(s). \tag{2.5}$$

Thus the PGF for the sum of two rolled fair dice is

$$G_{\text{two dice}}(s) = G_{\text{dice}}(s) G_{\text{dice}}(s) = \frac{1}{36}s^2 + \frac{1}{18}s^3 \cdots + \frac{1}{18}s^{11} + \frac{1}{36}s^{12}. \tag{2.6}$$

Random Sum of Random Variables

A random discrete positive integer variable N has associated generating function $G_N(s)$, and X is a different random discrete positive integer variable with generating function $G_X(s)$. The sum S of X added N times, $S = X_1 + X_2 + \ldots X_N$ then has generating function

$$G_S(s) = G_N(G_X(s)). \tag{2.7}$$

For the coin and die example, consider rolling the die and flipping a number of coins equal to the die face. The generating function for the sum of coins which landed heads is then

$$G_{\text{dice then coin}}(s) = G_{\text{dice}}(G_{\text{coin}}(s)) = \frac{1}{6}((1-p)+ps) + \cdots + \frac{1}{6}((1-p)+ps)^6 \tag{2.8}$$

Derivatives of Generating Functions

The original probability distribution $f_k = \Pr(X = k)$ can be calculated from the associated PGF $G_X(s)$ by

$$f_k = \Pr(X = k) = \frac{1}{k!}\left.\frac{d^k}{ds^k}G_X(s)\right|_{s=0}. \tag{2.9}$$

The kth factorial moment of X is calculated from the associated PGF as

$$\mathbb{E}[X(X-1)\cdots(X-k+1)] = \left.\frac{d^k}{ds^k}G_X(s)\right|_{s=1}. \tag{2.10}$$

Given a generating function, computing the factorial moment is often easier than the probabilities.

Iterations of Generating Functions

Consider again the process of (2.3) of rolling a die, abbreviated as $G_1(s) = G_{\text{dice}}(s)$. Now the process is repeated where one die is rolled and the die face specifies the number of additional dice that are rolled afterwards. The new PGF $G_2(s)$ for this twice iterated process can be written as

$$G_2(s) = G_1(G_1(s)). \tag{2.11}$$

This process can then be repeated again, yielding $G_3(s) = G_1(G_2(s))$ and for N iterations $G_N(s) = G_1(G_{N-1}(s))$. In general the n-fold iterate of a PGF $G(s)$ is

$$G_N(s) = G(G(\ldots(G(s))\ldots)) \tag{2.12}$$

where $G(G(\ldots(G(s))\ldots))$ is $G(s)$ nested inside itself N times.

Generating Functions for Mixture Models

A mixture or hierarchical model allows formulating a probability distribution as a series of steps where one or more latent variables are sampled which determine the distribution of an observable variable. They can be written in a hierarchical manner as,

$$Y \sim f(Y) \tag{2.13}$$
$$X|Y \sim g(X|Y) \tag{2.14}$$

where Y is drawn first, determining the distribution $g(X|Y)$ that X is drawn from.

Alternatively, the single distribution $g(X)$ can be written as a mixture by summing over possible Y values,

$$g(X) = \sum_Y f(Y)g(X|Y) = \sum_j \Pr(Y=j)g(X|Y=j) \tag{2.15}$$

The generating function for $g(X)$ is then

$$G_X(s) = \sum_i s^i \Pr(X=i) = \sum_i s^i \sum_j \Pr(Y=j)\Pr(X=i|Y=j) \tag{2.16}$$

$$G_X(s) = \sum_j \Pr(Y=j) \sum_i s^i \Pr(X=i|Y=j) = \sum_j \Pr(Y=j) G_{X|Y=j}(s). \tag{2.17}$$

Thus the generating function for a hierarchical or mixture model is a weighted sum of the individual generating functions.

Continuing the coin and dice examples, consider two dice A and B with associated PGFs $G_A(s)$ and $G_B(s)$. A coin flip of heads probability p and tails probability $(1-p)$ determines which die is rolled, with tails rolling die A and heads rolling die B. The generating function of the number on the die face for this two step process is

$$G_{\text{coin,dice}}(s) = \Pr(\text{Coin} = \text{Tails})G_A(s) + \Pr(\text{Coin} = \text{Heads})G_B(s) \tag{2.18}$$

$$G_{\text{coin,dice}}(s) = (1-p)G_A(s) + pG_B(s) \tag{2.19}$$

2.2 Böhnel's Equation

The example of (2.19) can model a single neutron initiating fission, where $p = p_f$ is the probability of one neutron initiating fission and $(1-p_f)$ is the neutron leaving the material. A fission process $f(s)$ is the associated PGF for neutrons emitted by a neutron induced fission. The PGF describing one neutron possibly initiating one fission is

$$h_1(s) = (1-p_f)s + p_f f(s) \tag{2.20}$$

$$f(s) = \sum_{i=0}^{N_f} f_i s^i \tag{2.21}$$

and the coefficients $f_0, f_1, \cdots, f_{N_f}$ correspond to the probabilities of a neutron induced fission emitting $0, 1, \cdots, N_f$ neutrons.

Now instead of starting with one neutron, we begin with a fission process $f^*(s)$. Each of the neutrons emitted from the $f^*(s)$ process then proceed according to $h_1(s)$. The sum for the number of total emitted neutrons is given by (2.7)

$$g_1(s) = f^*(h_1(s)) \tag{2.22}$$

Now again alter the starting event to be a neutron with probability p_f^* of initiating the fission process $g_1(s)$ and $(1-p_f^*)$ of escaping. This process is written

$$h_2^*(s) = (1-p_f^*)s + p_f^* g_1(s) = (1-p_f^*)s + p_f^* f^*(h_1(s)). \tag{2.23}$$

For $p_{f^*} = p_f$ and $f^*(s) = f(s)$,

$$h_2(s) = (1-p_f)s + p_f f(h_1(s)) \tag{2.24}$$

showing two generations of neutron induced fissions, beginning with one neutron. The previous derivation can be repeated for N generations of fissions

$$h_N(s) = (1-p_f)s + p_f(h_{N-1}(s)) \tag{2.25}$$

It is not known how many generations a fission chain may continue, however the limit of (2.17) can be taken as $N \to \infty$,

$$\lim_{N\to\infty} h_N(s) = \lim_{N\to\infty} h_{N-1}(s) = h(s) \tag{2.26}$$
$$h(s) = (1-p_f) + p_f f(h(s)) \tag{2.27}$$

Equation (2.27) is referred to as the Böhnel equation, and together with the following analysis forms the point model theory. Note that this equation describes the number of neutrons which *leave* a fission chain.

2.2.1 Point Model Moments

The kth factorial moment ϕ_k of (2.27) is calculated according to (2.10)

$$\phi_k = \left.\frac{d^k h(s)}{ds^k}\right|_{s=1} \tag{2.28}$$

The first three moments ϕ_1, ϕ_2, ϕ_3 yield

$$\phi_1 = 1 - p_f + p_f \nu_1 \phi_1 \tag{2.29}$$
$$\phi_2 = p_f(\nu_2 \phi_1^2 + \nu_1 \phi_2) \tag{2.30}$$
$$\phi_3 = p_f(\nu_3 \phi_1^3 + 3\nu_2 \phi_1 \phi_2 + \nu_1 \phi_3) \tag{2.31}$$

where ν_k are the kth factorial moments of the material specific neutron induced fission multiplicity distribution $f(s)$

$$\nu_k = \left.\frac{d^k f(h(s))}{dh(s)^k}\right|_{s=1} = \sum_{i=k}^{N_f} k! \binom{i}{k} f_i \tag{2.32}$$

and are usually assumed known either through compiled nuclear data libraries or previous calibration. The equations of (2.29)-(2.31) can then be solved algebraically for the first three neutron moments

$$\phi_1 = \frac{1-p_f}{1-p_f\nu_1} \tag{2.33}$$

$$\phi_2 = \left(\nu_2\phi_1^2\right)\left(\frac{p_f}{1-\nu_1 p_f}\right) = \frac{\nu_2 p_f(1-p_f)^2}{(1-\nu_1 p_f)^3} \tag{2.34}$$

$$\begin{aligned}\phi_3 &= \left(\nu_3\phi_1^3 + 3\nu_2\phi_1\phi_2\right)\left(\frac{p_f}{1-\nu_1 p_f}\right) \\ &= \frac{p_f(1-p_f)^3(3p_f\nu_2^2+\nu_3-p_f\nu_1\nu_3)}{(1-\nu_1 p_f)^5}\end{aligned} \tag{2.35}$$

The equations (2.33)-(2.35) can alternatively be written in terms of the leakage multiplication $\mathbf{M_L}$

$$\mathbf{M_L} = \frac{1-p_f}{1-p_f\nu_1} \tag{2.36}$$

$$\phi_1 = \mathbf{M_L} \tag{2.37}$$

$$\phi_2 = \mathbf{M_L}^2\left[\nu_2\left(\frac{\mathbf{M_L}-1}{\nu_1-1}\right)\right] \tag{2.38}$$

$$\phi_3 = \mathbf{M_L}^3\left[3\nu_2^2\left(\frac{\mathbf{M_L}-1}{\nu_1-1}\right)^2 + \nu_3\left(\frac{\mathbf{M_L}-1}{\nu_1-1}\right)\right]. \tag{2.39}$$

These equations match the previous simulated moments of Figure 1.4 exactly.

2.2.2 Modified Source Event

If the first event is either spontaneous fission or induced fission by an external neutron of higher energy, the multiplicity distribution of neutrons produced in this first reaction will differ from that in (2.21). Denoting this altered source distribution as

$$g(s) = \sum_{i=0}^{N_g} g_i s^i, \tag{2.40}$$

with associated moments $\nu_{g,k}$ defined by (2.32). The PGF of (2.27) can be modified to use th the source event $g(s)$

$$h_g(s) = g\left(h(s)\right). \tag{2.41}$$

The kth factorial moments $\phi_{g,k}$ for emitted neutrons due to source event $g(s)$ are calculated using (2.28),

$$\phi_{g,1} = \nu_{g,1}\phi_1 \tag{2.42}$$
$$\phi_{g,2} = \nu_{g,2}\phi_1^2 + \nu_{g,1}\phi_2 \tag{2.43}$$
$$\phi_{g,3} = \nu_{g,3}\phi_1^3 + 3\nu_{g,2}\phi_1\phi_2 + \nu_{g,1}\phi_3. \tag{2.44}$$

As Böhnel notes, due to differences of the neutron energy for the source event and neutrons emitted from fission-neutron-induced fission the probability of fission will differ slightly for neutrons created from the source event [1]. Using p_x as the modified probability of fission for neutrons emitted from the source event, the modified PGF $h_x(u)$ is written as

$$h_x(s) = (1 - p_x)s + p_x g(h(s)). \tag{2.45}$$

The modified moments are then calculated using (2.30)

$$\phi_{x,1} = 1 - p_x + p_x\nu_{g,1}\phi_1 \tag{2.46}$$
$$\phi_{x,2} = p_x\left(\nu_{g,2}\phi_1^2 + \nu_{g,1}\phi_2\right) \tag{2.47}$$
$$\phi_{x,3} = p_x\left(\nu_{g,3}\phi_1^3 + 3\nu_{g,2}\phi_1\phi_2 + \nu_{g,1}\phi_3\right). \tag{2.48}$$

2.3 Relation to Neutron Multiplicity Analysis

Pázsit et al have presented the canonical form of neutron multiplicity equations which relate the point model moments to the rates of detecting neutrons [31]. A derivation of these equations is now summarized. The notation of their manuscript that ν_k refers to the moments of nuclear data for neutrons emitted from a single fission reaction, and ϕ_k the moments of neutrons emitted by a fission chain initiated by a source event are maintained.

For a fission chain initiating source event a detector has a probability $P_d(n)$ of detecting n neutrons. The $P_d(n)$ distribution includes all detector effects and differs from the distribution of emitted neutrons from a fission chain. The expected values for the number of ways to detect 1, 2, and 3 neutrons per fission chain, which are by definition the first, second and third factorial moments, are

$$\phi_{d,1} = \sum_{n=0}^{\infty} nP_d(n) = \mathbb{E}_{P_d}[n] \tag{2.49}$$
$$\phi_{d,2} = \sum_{n=0}^{\infty} n(n-1)P_d(n) = \mathbb{E}_{P_d}[n(n-1)] \tag{2.50}$$
$$\phi_{d,3} = \sum_{n=0}^{\infty} n(n-1)(n-2)P_d(n) = \mathbb{E}_{P_d}[n(n-1)(n-2)] \tag{2.51}$$

where $\mathbb{E}_{P_d}$ is the expectation with respect to the distribution P_d. In general,

$$\phi_{d,k} = \mathbb{E}_{P_d}\left[\frac{n!}{(n-k)!}\right] = \mathbb{E}_{P_d}\left[k!\binom{n}{k}\right] = k!\,\mathbb{E}_{P_d}\left[\binom{n}{k}\right]. \tag{2.52}$$

As neutrons are identical and neutron detector systems record the number of unique combinations the factor of $k!$ is divided out by convention and known as the either the combinatorial or reduced factorial moment. Multiplying the combinatorial moments $\phi_{d,k}/k!$ by the number of fission chain starting events or the source intensity Q_s yields the detected neutron multiplets C_k recorded by a measurement system,

$$C_k = Q_s \frac{\phi_{d,k}}{k!}. \tag{2.53}$$

To relate the detected moments $\phi_{d,k}$ to the moments of emitted neutrons $\phi_{e,k}$ requires including the factors of detection efficiency. As derived in Section 2.4.2 a detector with a uniform efficiency ϵ for detecting any emitted neutron adds a factor of ϵ^k to each kth moment. Additionally, the second and third moments are triggered by the first neutron and wait for additional neutrons within a time gate. This adds an additional detector efficiency terms f_d, f_t to the second and third moments. Combining the factors of ϵ^k, f_d, f_t yields expressions relating the emitted neutron moments $\phi_{e,k}$ to the detected neutron moments $\phi_{d,k}$

$$\phi_{d,1} = \epsilon\phi_{e,1} \tag{2.54}$$
$$\phi_{d,2} = f_d\epsilon^2\phi_{e,2} \tag{2.55}$$
$$\phi_{d,3} = f_t\epsilon^3\phi_{e,3}. \tag{2.56}$$

Writing (2.53) with (2.54)-(2.56) yields expressions for the measurements of a neutron detection system,

$$\mathbf{S} = C_1 = Q_s\phi_{d,1} = Q_s\epsilon\phi_{e,1} \tag{2.57}$$
$$\mathbf{D} = C_2 = Q_s\frac{\phi_{d,2}}{2!} = Q_s f_d\epsilon^2\frac{\phi_{e,2}}{2} \tag{2.58}$$
$$\mathbf{T} = C_3 = Q_s\frac{\phi_{d,3}}{3!} = Q_s f_t\epsilon^3\frac{\phi_{e,3}}{6} \tag{2.59}$$

where **S** are commonly referred to as neutron singles, **D** doubles, and **T** triples.

The detector efficiency factors ϵ, f_d, f_t are determined using a spontaneous fission source such as Cf252 of known strength Q_s and emitted neutron moments $\phi_{e,k} = \nu_{e,k}$. Measurements of **S**, **D**, and **T** are used to solve for ϵ, f_d, and f_t using equations (2.57)-(2.59). Then for a calibrated system of known system parameters, measurements of **S**, **D**, and **T** and equations (2.57)-(2.59) enable solving for up to three desired properties of an assayed material. The forms of Q_s and $\phi_{e,k}$ differ depending on the type of assay and are now described.

2.3.1 Spontaneously Fissioning Pure Metal

In the case for fission chains initiated by spontaneous fission, the multiplicity distributions do not match those for neutron induced fission. The emitted neutron moments are described by (2.42)-(2.44). Writing (2.57)-(2.59) where $\phi_{e,k} = \phi_{sf,k} = \phi_{g,k}$ with the subscript $_{sf}$ for spontaneous fission and moments $\nu_{sf,k} = \nu_{g,k}$ with source strength $Q_s = Q_{sf}$,

$$\mathbf{S}_{sf} = Q_{sf}\ \epsilon\ \nu_{sf,1}\phi_1 \tag{2.60}$$

$$\mathbf{D}_{sf} = Q_{sf}\ f_d\epsilon^2\ \frac{1}{2}\left(\nu_{sf,2}\phi_1^2 + \nu_{sf,1}\phi_2\right) \tag{2.61}$$

$$\mathbf{T}_{sf} = Q_{sf}\ f_t\epsilon^3\ \frac{1}{6}\left(\nu_{sf,3}\phi_1^3 + 3\nu_{sf,2}\phi_1\phi_2 + \nu_{sf,1}\phi_3\right). \tag{2.62}$$

These equations are valid for spontaneously fissioning pure non-oxidized metals not in the presence of low-Z materials or moisture.

2.3.2 Oxide Materials and (α, n) Source Contributions

Many spontaneous fissioning sources also decay by emitting an energetic alpha particle. In the presence of low Z materials elements such as oxygen in a metal oxide or hydrogen and nitrogen for a material which has absorbed moisture, this leads to additional neutrons being created through (α, n) reactions and a greater number of fission chain starting events than the source strength Q_{sf} of equations (2.60)-(2.62).

If the contribution of fission chain events due to (α, n) reactions by a spontaneously fissioning source is Q_α, then the additional counts can be expressed using (2.60)-(2.62) with $Q_{sf} = Q_\alpha$ and $\nu_{sf,1} = 1$, $\nu_{sf,2} = 0$, $\nu_{sf,3} = 0$ as each (α, n) creates one neutron

$$\mathbf{S}_\alpha = Q_\alpha\ \epsilon\ \phi_1 \tag{2.63}$$

$$\mathbf{D}_\alpha = Q_\alpha\ f_d\epsilon^2\ \frac{1}{2}\phi_2 \tag{2.64}$$

$$\mathbf{T}_\alpha = Q_\alpha\ f_t\epsilon^3\ \frac{1}{6}\phi_3. \tag{2.65}$$

By convention, instead of Q_α the strength of the (α, n) contribution is written using the ratio $\boldsymbol{\alpha}$ of neutrons produced from (α, n) and spontaneous fission reactions

$$\boldsymbol{\alpha} = \frac{Q_\alpha}{Q_{sf}\nu_{sf,1}}. \tag{2.66}$$

Using $Q_\alpha = \boldsymbol{\alpha} Q_{sf} \nu_{sf,1}$ the total detector measurements are written

$$\mathbf{S} = \mathbf{S}_{sf} + \mathbf{S}_\alpha = Q_{sf} \epsilon \nu_{sf,1} \phi_1 (1 + \boldsymbol{\alpha}) \tag{2.67}$$

$$\mathbf{D} = \mathbf{D}_{sf} + \mathbf{D}_\alpha = Q_{sf} f_d \epsilon^2 \frac{1}{2} \left(\nu_{sf,2} \phi_1^2 + (1 + \boldsymbol{\alpha}) \nu_{sf,1} \phi_2 \right) \tag{2.68}$$

$$\mathbf{T} = \mathbf{T}_{sf} + \mathbf{T}_\alpha = Q_{sf} f_t \epsilon^3 \frac{1}{3} \left(\nu_{sf,3} \phi_1^3 + 3 \nu_{sf,2} \phi_1 \phi_2 + (1 + \boldsymbol{\alpha}) \nu_{sf,1} \phi_3 \right). \tag{2.69}$$

With the notation $\mathbf{F} = Q_{sf}$ and the forms of ϕ_k in equations (2.36)-(2.39) gives the equations present in [31] and [32]

$$\mathbf{S} = \mathbf{F} \epsilon \mathbf{M_L} \nu_{sf,1} (1 + \boldsymbol{\alpha}) \tag{2.70}$$

$$\mathbf{D} = \frac{\mathbf{F} \epsilon^2 f_d \mathbf{M_L}^2}{2} \left[\nu_{sf,2} + \left(\frac{\mathbf{M_L} - 1}{\nu_1 - 1} \right) \nu_{sf,1} (1 + \boldsymbol{\alpha}) \nu_2 \right] \tag{2.71}$$

$$\begin{aligned} \mathbf{T} = \frac{\mathbf{F} \epsilon^3 f_t \mathbf{M_L}^3}{6} & \left[\nu_{sf,3} + \left(\frac{\mathbf{M_L} - 1}{\nu_1 - 1} \right) [3 \nu_{sf,2} \nu_2 + \nu_{sf,1} (1 + \boldsymbol{\alpha}) \nu_3] \right. \\ & \left. + 3 \left(\frac{\mathbf{M_L} - 1}{\nu_1 - 1} \right)^2 \nu_{sf,1} (1 + \boldsymbol{\alpha}) \nu_2^2 \right]. \end{aligned} \tag{2.72}$$

The three measurements **S**, **D**, **T** are used to solve for **F**, $\mathbf{M_L}$, $\boldsymbol{\alpha}$.

For plutonium samples, a determined value of **F** allows to solve for the 240Pu effective mass

$$\mathbf{F} = Q_{sf} = \mathbf{m}_{\text{eff}}^{240} Y^{240} \tag{2.73}$$

where Y^{240} is the spontaneous fission rate per gram. For 240Pu, $Y = 473.5$ fissions s^{-1} g^{-1}. Additional details of the relation of effective mass and isotopic composition can be found in Appendix A.

2.3.3 Active Assay Using an External Neutron Source

For materials that do not have a useful spontaneous fission rate, such as uranium, the use of an external source of neutrons to begin fission chains is required. This modifies the source term Q_s. For U235

$$\mathbf{F} = Q_s = C_s \, Y_s \, \mathbf{m}_{\text{eff}}^{235} \tag{2.74}$$

where Y_s is the event rate of the external neutron sources and $\mathbf{m}_{\text{eff}}^{235}$ is the effective U235 mass. Not every neutron produced by the sources initiates a fission chain, this is accounted for by introducing the source coupling constant C_s which relates how many source events interact with the assayed material.

For pure uranium metal there are three required modifications of the measured neutron rates compared to (2.70)-(2.72). First, as there is no source of α particles in the sample the (α, n) contribution is ignored, $\boldsymbol{\alpha} = 0$. Second, as we are including additional neutrons into the system the singles rate will now also measure the source and must be accounted for. Lastly, the neutron moments for neutrons emitted by spontaneous fission are replaced with the moments for neutrons created in an induced fission by an external source, $\nu_{sf,n} \to \nu_{s,n}$.

This leads to the modified equations for **S**, **D**, **T**

$$\mathbf{S} = \mathbf{F}\epsilon\mathbf{M_L}\nu_{s,1} + S_0 + S_s \tag{2.75}$$

$$\mathbf{D} = \frac{\mathbf{F}\epsilon^2 f_d \mathbf{M_L}^2}{2}\left[\nu_{s,2} + \left(\frac{\mathbf{M_L}-1}{\nu_1 - 1}\right)\nu_{s,1}\nu_2\right] \tag{2.76}$$

$$\begin{aligned}\mathbf{T} = \frac{\mathbf{F}\epsilon^3 f_t \mathbf{M_L}^3}{6}\Bigg[\nu_{s,3} &+ \left(\frac{\mathbf{M_L}-1}{\nu_1 - 1}\right)\left[3\nu_{s,2}\nu_2 + \nu_{s,1}\nu_3\right] \\ &+ 3\left(\frac{\mathbf{M_L}-1}{\nu_1 - 1}\right)^2 \nu_{s,1}\nu_2^2\Bigg].\end{aligned} \tag{2.77}$$

The additional singles contributions are the detected neutrons from the source without a sample present S_0 and the change S_s of source neutrons scattering into the detector when the sample is present.

With two unknowns and three equations, typically only the **D** and **T** terms are used to solve for $\mathbf{M_L}$ and **F**, avoiding the need to determine S_0 and S_S. However, unlike for spontaneous fission the effective mass cannot be determined due to the additional C_s term present. This source coupling constant is a function of sample geometry, relative source position, sample mass, isotopic composition, moderation of the detection system, and other factors. Past approaches for active assay of uranium have relied on a heuristic functional form of C_s dependent on sample mass and multiplication for geometrically similar objects of the same composition. Parameters are determined using either calibrated standards of known mass or Monte Carlo simulation, allowing C_s to be estimated for a class of similar objects of varying mass and/or multiplication [2].

2.4 Extensions of the Point Model

An advantage of the PGF approach is that the Böhnel equation (2.27) is easily modified to include additional physics or detector effects. The resulting moments are then calculated as before using (2.28). A few common examples are described.

2.4.1 Neutron Capture and (n,xn) Reactions

Reactions other than fission alter the neutron population in a fissile material. These include neutron capture, in which an atomic nucleus absorbs a neutron and de-excites through gamma emission, and non-fission reactions which emit either 2 or 3 neutrons. These can be expressed with the respective probabilities p_c, p_{2n}, p_{3n}. Modifying the point model PGF to include these reactions explicitly yields

$$g^*(s) = p_c + (1 - p_f - p_c - p_{2n} - p_{3n})s + p_{2n}s^2 + p_{3n}s^3 + p_f f(g^*(s)). \tag{2.78}$$

While the moment equations can be written explicitly, it is more common to instead modify the definition of fission to include additional reactions, known as the super fission concept [1]. Then the point model PGF is written with the super fission probability p_f^* and modified nuclear data moments ν_j^*

$$p_f^* = p_f + p_c + p_{2n} + p_{3n} \tag{2.79}$$

$$g^*(s) = (1 - p_f^*)s + p_f^* f^*(g^*(s)) \tag{2.80}$$

$$f^*(s) = \frac{p_f \sum_{i=0}^{N_c} f_i s^i + p_c + p_{2n}s^2 + p_{3n}s^3}{p_f^*} \tag{2.81}$$

which results in the same moments as (2.33)-(2.35) where the neutron multiplicity data moments are altered $\nu_i \to \nu_i^*$

$$\nu_i^* = \frac{p_f}{p_f^*}\nu_i + 2\frac{p_{2n}}{p_f^*}\binom{2}{i} + 3\frac{p_{3n}}{p_f^*}\binom{3}{i} \tag{2.82}$$

For a specific enrichment, the ratios of interaction probabilities can be determined from the macroscopic cross sections Σ,

$$p_x = 1 - e^{-\Sigma_x l} \tag{2.83}$$

$$p_f^* = 1 - e^{-(\Sigma_f + \Sigma_c + \Sigma_{2n} + \Sigma_{3n})l} \tag{2.84}$$

where over a small distance l,

$$\frac{p_x}{p_f^*} \approx \frac{\Sigma_x}{\Sigma_f + \Sigma_c + \Sigma_{2n} + \Sigma_{3n}}. \tag{2.85}$$

ν_i^* can also be determined for a specific enrichment using a calibration source of known mass and adjusting the values of ν_i^* to match the measured neutron multiplicities, either through measurement or Monte Carlo simulation.

2.4.2 Detector Effects

If a detection system has uniform efficiency ϵ for detecting any neutron, the associated PGF is

$$\eta(s) = (1 - \epsilon) + \epsilon s \tag{2.86}$$

which expresses a $(1 - \epsilon)$ chance of detecting zero neutrons and ϵ chance of detecting one neutron [33].

For a fissile assembly where the number of neutrons emitted is described by PGF $g(s)$, the resulting PGF $g_\eta(s)$ of those neutrons then being detected is

$$g_\eta(s) = g(\eta(s)) \tag{2.87}$$

with moments

$$\phi_{\eta_1} = \epsilon\phi_1 \tag{2.88}$$

$$\phi_{\eta_2} = \epsilon^2\phi_2 \tag{2.89}$$

$$\phi_{\eta_3} = \epsilon^3\phi_3 \tag{2.90}$$

which is the origin of the ϵ^n factor in the equations (2.54)-(2.56) for the neutron singles, doubles, and triples.

Shin et al has extended this for scatter based detection systems, in which a neutron has a probability ϵ_0 of being detected once, ϵ_1 of being detected twice, and ϵ_2 of being detected three times [21]. The PGF of this process is written as

$$\eta(s) = (1-\epsilon_0) + \epsilon_0(1-\epsilon_1)s + \epsilon_0\epsilon_1(1-\epsilon_2)s^2 \tag{2.91}$$

and associated moment equations can be derived.

2.4.3 Photons and Multiple Particles

In addition to neutrons, photons are also emitted during the fission process according to a multiplicity distribution. The photon equivalent of the point model PGF [33], accounting for only fission interactions is

$$l(t) = (1-p_f) + p_f m(t) f(l(t)) \tag{2.92}$$

where each s^i term is a probability of i photons being emitted and $m(t)$ is the PGF for photons emitted from a neutron induced fission process

$$m(t) = \sum_{i=0}^{N_m} m_i t^i. \tag{2.93}$$

The photon PGF nests inside the neutron multiplicity PGF $f(t)$ to represent that some neutrons are created, which go on to induce fission which emits more gammas.

Instead of a separate equation, a combined PGF for emitted photons and neutrons can be written [33]

$$u(s,t) = (1-p_f)s + p_f m(t) f(u(s,t)) \tag{2.94}$$

and the PGFs of (2.27) and (2.92) are special cases of (2.94) when either $s = 1$ or $t = 1$. The joint moments $\phi_{i,j}$ for i neutrons and j photons can be calculated as

$$\phi_{i,j} = \frac{1}{i!j!}\left(\frac{\partial^i}{\partial s^i}\frac{\partial^j}{\partial t^j}u(s,t)\right)\Bigg|_{s=1,t=1} \tag{2.95}$$

where the order of the partial differentiation does not matter due to the continuity of $u(s,t)$ and all of the partial derivatives.

2.5 Limitations

While the point model and the approach provided by generating functions are a powerful analysis tool, the limitations of this approach arise from the assumptions used to write the PGF. For the neutron point model PGF (2.27), these assumptions are:

- Time: For each source event, all neutrons are emitted simultaneously at once.
- Energy: All neutrons have the same energy.
- Space: All neutrons are emitted from the same single point in space.
- Data: The moments of a single neutron induced fission, ν_j, are known.

These assumptions together allow the interaction and multiplicity probabilities, p_f and f_i, to be written as constant numbers independent of energy or position and with no time delay between interactions. The time, energy, and data assumptions are described briefly with recent approaches to relax them. Examining the single point approximation is the focus of this dissertation and is given an expanded discussion.

2.5.1 Instantaneous Time Assumption

Most neutron multiplicity systems are based on He3, which require thermalization of the emitted fission neutrons in order to be detected. The thermalization process occurs on the scale of tens of microseconds. Compared to the nanosecond timescale between fissions, previous neutron multiplicity systems have been insensitive to timing correlations of emitted fission neutrons.

Recent advances in fast neutron scatter scintillation based detectors and list-mode read out electronics provide the ability to measure down to the nanosecond scale. While not as efficient as He3 systems, this allows exploring the time correlations for characterizing fissile material signatures such as time between detected neutrons. In this mode the timing structure of neutron induced fission events can be distinguished from spallation or other background neutron producing reactions [34]. Recent work at LLNL has developed methods of describing the timing distributions of neutron counts using the probability generating function technique and method of characteristics [35]–[37].

However, even on the microsecond scale of slower He3 detectors there are two time related factors which affect the rate of neutron emissions. First is the contribution of delayed neutrons, in which neutrons are emitted up to tens of seconds after the prompt fission. Previous work has shown that in most safeguards application the impact of delayed neutrons is below current measurement sensitivities [38]. Second is the effect of thermalized neutrons returning back into the fissile material and restarting the fission chain [39]. For He3 detectors this is mitigated by surrounding the sample with a cadmium liner which absorbs thermalized neutrons traveling from the moderator into the sample cavity [2].

2.5.2 Monoenergetic Energy Assumption

Fission neutrons have energies over range of several MeV, which are then affected by scattering due to elastic and inelastic scattering both within the fissile assembly and surrounding materials. The interaction probabilities p_x are functions of nuclear cross sections and thus dependent on neutron energy. The induced neutron multiplicity distribution and the associated moments ν_i also vary with energy of inducing neutron. The point model ignores these variations by assuming all fission neutrons have an averaged value for energy. However due to Jensen's inequality these variations will consistently underestimate the correct value for neutron moments to some degree [40].

A significant source of bias in the equations (2.70)-(2.72) is the assumption that the average neutron energy from (α, n) reactions match those from spontaneous fission of 240Pu [41]. However neutrons (α, n) reactions are typically between 1-2 MeV higher than spontaneous fission. As the induced fission moments will differ by about 5% per MeV of the inducing neutron energy, this results in about a 0.5% change of $\nu_{i,1}$ between neutrons emitted from (α, n) sources and spontaneous fission [42]. Additionally the detection efficiency ϵ and gate fractions are dependent on the emitted neutron energy and can be affected by the higher (α, n) neutron energies. Two approaches for characterizing the average neutron energy difference is by measuring the fourth moment termed the quads, or through the ring ratio method of estimating emitted neutron energy through the ratios of neutron singles for detectors closer to the detector and those further away. These parameters have been introduced in modified point model equations and reduce the energy bias [41].

2.5.3 Enrichment Dependence of Data

The desired quantity in neutron multiplicity analysis is the estimate of effective mass $\mathbf{m}_{\text{eff}}$, which is determined from **F** and is dependent on the total amount and enrichment of a material. However in some assay scenarios it is difficult to correctly predict **S**, **D**, **T** without having enrichment or isotopic information a priori.

In cases of active assay of uranium using an AmLi neutron source with mean neutron energy of 0.3 MeV nearly all fissions are on U235 due to the drop off of the U238 neutron induced fission cross-section at 1.5 MeV. However, with a higher energy neutron source such as a 14.1 MeV DT neutron generator the induced fission, n2n, and n3n reactions on both U235 and U238 are significant. Thus the external source neutron induced fission moments $\nu_{s,1}, \nu_{s,2}, \nu_{s,3}$ are dependent on the isotopic composition. This has been shown to significantly bias the results of the point model equations if the isotopic composition is not known a priori [43].

2.5.4 Point Geometry Approximation

The point geometry assumption states that every neutron has the same probability p_f of initiating fission regardless of the position which neutrons are introduced in a fissile assembly. Specifically on the positions of that atoms which undergo spontaneous or induced fission by an external source, releasing additional neutrons and beginning the fission chain. This simplification was known to largely be incorrect as far back as 1945 by Serber who stated that "the multiplication of a subcritical assembly depends, of course, on the position in the active material at which the source of neutrons is introduced" [3].

This spatial dependence will bias assay results and is illustrated using an example [44] of two samples of equal fissile masses $m_1 = m_2 = m$ and equal number of initiating events $\mathbf{F}_1 = \mathbf{F}_2 = \mathbf{F}$ but with differing multiplications $\mathbf{M_{L}}_1 \neq \mathbf{M_{L}}_2$ due to either different shapes or different source distributions.

The point model equations for the singles and doubles,

$$\mathbf{S} = \mathbf{F}\,\mathbf{M_L} \tag{2.96}$$

$$\mathbf{D} = \frac{1}{2}\mathbf{F}\,\mathbf{M_L}\nu_2\left(\frac{\mathbf{M_L}-1}{\nu_1-1}\right) \tag{2.97}$$

can be inverted to solve for $\mathbf{F}$ and $\mathbf{M_L}$ given a measurement of $\mathbf{S}$ and $\mathbf{D}$

$$\mathbf{F} = \frac{\nu_2\mathbf{S}^2}{2\mathbf{D}(\nu_1-1)+\nu_2\mathbf{S}} \tag{2.98}$$

$$\mathbf{M_L} = 1 + \frac{2\mathbf{D}(\nu_1-1)}{\nu_2\mathbf{S}}. \tag{2.99}$$

If two separate assays are performed resulting in the measurements $(\mathbf{S}_1, \mathbf{D}_1), (\mathbf{S}_2, \mathbf{D}_2)$ the individual initiating events $\mathbf{F}_1$, $\mathbf{F}_2$ can be estimated using (). Combining the estimated initiating event rates yields $\mathbf{F}_1 + \mathbf{F}_2 = 2\mathbf{F}$.

If instead a single assay is performed of both masses m_1, m_2 together, the resulting singles and doubles measurements will be $(\mathbf{S}_1 + \mathbf{S}_2, \mathbf{D}_1 + \mathbf{D}_2)$. Solving for $\mathbf{F}$ and $\mathbf{M_L}$ yields

$$\mathbf{F}_{1+2} = \mathbf{F}\frac{(\mathbf{M_L}_1 + \mathbf{M_L}_2)^2}{\mathbf{M_L}_1^2 + \mathbf{M_L}_2^2} \tag{2.100}$$

$$\mathbf{M_L}_{1+2} = \frac{\mathbf{M_L}_1^2 + \mathbf{M_L}_2^2}{\mathbf{M_L}_1 + \mathbf{M_L}_2}. \tag{2.101}$$

For $\mathbf{M_L}_1 \neq \mathbf{M_L}_2$,

$$\mathbf{F}_{1+2} < \mathbf{F}_1 + \mathbf{F}_2 = 2\mathbf{F} \tag{2.102}$$

$$\min(\mathbf{M_L}_1, \mathbf{M_L}_2) < \mathbf{M_L}_{1+2} < \max(\mathbf{M_L}_1, \mathbf{M_L}_2). \tag{2.103}$$

This derivation illustrates that when measuring objects of differing multiplication, the combined $\mathbf{F}_{1,2,...}$ will be underestimated compared the true result $\mathbf{F}_1 + \mathbf{F}_2 + \dots$ from measuring each object individually. Thus the point model equations contain a bias of underestimating $\mathbf{F}$ and effective fissile mass when multiplication varies in an object.

Direct Bias Correction

One method is to simply alter the biased fissile mass by applying correction factors $f_m(\mathbf{M_L})$ and $f_m(\boldsymbol{\alpha})$ [44],

$$m_{\text{eff, corr}} = f_m(\mathbf{M_L}) \cdot f_m(\boldsymbol{\alpha}) \cdot m_{\text{eff}} \tag{2.104}$$

$$f_m(\mathbf{M_L}) = a_m + b_m(\mathbf{M_L} - 1) + c_m(\mathbf{M_L} - 1)^2 \tag{2.105}$$

$$f_m(\boldsymbol{\alpha}) = 1 + a_{\boldsymbol{\alpha}}\boldsymbol{\alpha} + b_{\boldsymbol{\alpha}}\boldsymbol{\alpha}^2. \tag{2.106}$$

The coefficients $a_m, b_m, c_m, a_{\boldsymbol{\alpha}}, b_{\boldsymbol{\alpha}}$ are determined from calibration against several objects with known effective masses. These coefficients only allow a correction to be applied for objects of similar isotopic composition and geometry [45]. Additionally, the mass correction does not correct the multiplication which is also a useful quantity.

Weighted Point Model

An alternative approach is to instead apply determined variable-multiplication weighting factors $w_D, w_T, w_D^{\boldsymbol{\alpha}}, w_T^{\boldsymbol{\alpha}}$ onto the second and third neutron moments. This forms an alternative set of point model equations termed the 'Weighted Point Model' equations

$$\mathbf{S} = \mathbf{F}\epsilon\nu_{s1}\mathbf{M_L}(1 + \alpha) \tag{2.107}$$

$$\mathbf{D} = \frac{1}{2}\mathbf{F}\epsilon^2 f_d \nu_{s2}\mathbf{M_L}^2(f_D + \boldsymbol{\alpha} f_D^{\boldsymbol{\alpha}}) \tag{2.108}$$

$$\mathbf{T} = \frac{1}{6}\mathbf{F}\epsilon^3 f_t \nu_{s3}\mathbf{M_L}^3(f_T + \boldsymbol{\alpha} f_T^{\boldsymbol{\alpha}}) \tag{2.109}$$

$$f_D = w_D(1 + c_1(\mathbf{M_L} - 1)) \tag{2.110}$$

$$f_D^{\boldsymbol{\alpha}} = w_D^{\boldsymbol{\alpha}} c_1(\mathbf{M_L} - 1) \tag{2.111}$$

$$f_T = w_T(1 + c_2(\mathbf{M_L} - 1) + c_3(\mathbf{M_L} - 1)^2) \tag{2.112}$$

$$f_T^{\boldsymbol{\alpha}} = w_T^{\boldsymbol{\alpha}}(c_4(\mathbf{M_L} - 1) + c_3(\mathbf{M_L} - 1)^2) \tag{2.113}$$

where the coefficients c_1, c_2, c_3, c_4 are expressions involving the known moments ν_{s1}, ν_{s2}, ν_{s3}, ν_{i1}, ν_{i2}, ν_{i3} [44]. The effective mass is then determined by solving for $\mathbf{F}$ using the usual point model inversion. The advantage of the weighted point model is that the weighting factors are more insensitive to sample geometry and mass [44]. Additionally the values of $\mathbf{M_L}$ and $\boldsymbol{\alpha}$ are corrected. The weighting factors are specific to the geometric shape, the values of w_D and w_T determined for cylindrical objects do not match those for spherical objects.

Follow up work has given a more physical interpretation of the weighting factors for higher moments [46] [4]. The traditional point model equations consider only one value of $\mathbf{M_L}$. For objects where the multiplication varies with position $\vec{r}$ within a volume V this translates into determining an average or expected value of neutron multiplication across the object,

$$\langle \mathbf{M_L} \rangle = \frac{\int_V \mathbf{M_L}(\vec{r}) d\vec{r}}{\int_V d\vec{r}} \tag{2.114}$$

The underestimation of the second and third neutron moments can be explained through Jensen's Inequality, which states that integrals or expected values of convex functions will be greater than the convex function applied onto the expectation or integral [40]

$$\phi(\langle X \rangle) \leq \langle \phi(X) \rangle \,. \tag{2.115}$$

Applying Jensen's inequality on the successive powers of multiplication present in the point model equations,

$$\langle \mathbf{M_L} \rangle^n \leq \langle \mathbf{M_L}^n \rangle \tag{2.116}$$

which can alternatively be expressed as a ratio measuring the discrepancy in the inequality

$$g_n = \frac{\langle \mathbf{M_L}^n \rangle}{\langle \mathbf{M_L} \rangle^n}. \tag{2.117}$$

The equations for the doubles, triples and higher moments are then written replacing all occurrences of $\mathbf{M_L}^n$ with $g_n \langle \mathbf{M_L} \rangle^n$. For triples this requires knowing the four coefficients g_2, g_3, g_4, g_5. For a specific geometry and composition the coefficients g_n can be determined through Monte Carlo simulation [46] [4].

Spatial Neutron PGF

The previous approaches have sought to account for the lack of spatial dependence by either altering the effective mass or the derived moment expressions. Alternatively, one can instead alter the original point model PGF to include spatial dependence at the start. Early approaches were made in 1D cases [47], [48], and recent work by Imre Pázsit and others have shown how to calculate neutron moments for several basic shapes and the procedure in the general case [49] [50] [51]. For a neutron introduced at position $\vec{r}$, the general space dependent PGF $g(z|\vec{r})$ with dummy variable z can be written as

$$g(z|\vec{r}) = zg_0(z|\vec{r}) + \frac{1}{4\pi} \int_{4\pi} d\vec{\Omega} \int_0^{l(\vec{r},\vec{\Omega})} dse^{-s} q_r[g(z|\vec{r} + s\vec{\Omega})] \tag{2.118}$$

$$g_0(z|\vec{r}) = \frac{1}{4\pi} \int_{4\pi} d\vec{\Omega} e^{-l(\vec{r},\vec{\Omega})} \tag{2.119}$$

where $\vec{\Omega}$ accounts for the directions the neutron can travel over a length s to the boundary of the object at $l(\vec{r}, \vec{\Omega})$ and q_r is the PGF of an induced fission reaction.

The moments can be calculated as before by taking the derivative with respect to z and then setting $z = 1$. This results in a recursive integral equation. For a source particle introduced at $\vec{r}$ the first moment $n(\vec{r})$ can be written as

$$n(\vec{r}) = n_0(\vec{r}) + \frac{\nu_{r,1}}{4\pi} \int_{4\pi} d\vec{\Omega} \int_0^{l(\vec{r},\vec{\Omega})} dse^{-s} n(\vec{r}'(s)) \tag{2.120}$$

$$n_0(\vec{r}) = \frac{1}{4\pi} \int_{4\pi} d\vec{\Omega} e^{-l(\vec{r},\vec{\Omega})}. \tag{2.121}$$

For a specific geometry specifying the form of $l(\vec{r}, \vec{\Omega})$, a recursive-free solution for the moment can be written as a series expansion

$$n(\vec{r}) = \sum_{k=0}^{\infty} n_k(\vec{r}) \tag{2.122}$$

$$n_k(\vec{r}) = \frac{\nu_{r,1}}{4\pi} \int_{4\pi} d\vec{\Omega} \int_0^{l(\vec{r},\vec{\Omega})} ds e^{-s} n_{k-1}(\vec{r}'(s)) \tag{2.123}$$

with similar expressions for the higher order moments. The integral expressions () and () can be evaluated numerically with specified shapes, which has been done for spherical and cylindrical cases [49], [50]. For a specified geometry and composition, this approach can provide the expected values of the neutron moments for large objects, or indicate the bias of the point geometry assumption.

Extensions for Associated Particle Imaging Data

Analysis of data taken by API systems has largely relied on the use of Monte Carlo simulations to infer material properties from the tagged neutron interrogation data. One approach by Swift is to create simulated data of known geometric and material information for an interrogated object [52]. By iterating over unknown properties such as enrichment or object radius and finding which simulation matches the data best, the unknown properties can be inferred. The accuracy of this approach has been demonstrated to determine uranium enrichment within 6% for simulated data.

Crye extended this approach on measurements of a shielded enriched uranium storage casting taken by the NMIS API system [53]. Different enrichment and shielding material configurations are simulated, and the measured and simulated neutron time correlation distributions are compared. This approach is able to determine that enrichment is greater than 80%, close to the actual enrichment of 93%. By comparing the total number of doubles the estimate is improved to at least 82% enrichment.

Despite their accuracy these Monte Carlo based approaches suffer from two drawbacks [53]. First is the computational time and resources needed to obtain Monte Carlo estimates. In Crye's work a total of 16 simulations are needed requiring between 2-5 hours of computation time each. These times are not reasonable for infield measurements where results should be immediately displayed. Second is that the modeling requires translating the imaged transmission data into the descriptive geometry used as input in Monte Carlo programs. This is done by hand by constructing the geometry out of simple shapes and makes it impractical to be done by a technician in a reasonable time.

The ideal situation for interpreting imaged data from API systems is akin to current practice in the medical imaging field where a measurement can be performed by a technician. Results are rapidly shown using automated software and enable real time decision making.

An alternative approach to pure Monte Carlo simulations is to derive a set of equations for estimating fissile mass and multiplication for API systems. Tweardy explored this approach by modifying the point model equations to account for a high energy interrogating neutron [54]. His modified point model equations were found to be very sensitive to the isotopic composition of the material, and unsuitable unless the isotopic composition was known a priori. A hybrid approach was developed which uses a suite of Monte Carlo simulations to estimate the dependence of leakage multiplication on uranium mass and sphericity [55]. While this approach was shown to accurately estimate leakage multiplication, estimates of enrichment showed a consistent bias. Tweardy mentions that one contributor of this bias may be the spatial dependence of leakage multiplication for objects which do not meet the point geometry assumption.

Chapter 3

Study of Point Geometry Assumption

In this chapter the accuracy of approximating the geometry of a fissile assembly as a single point is explored. This is done using a simplified version of the Monte Carlo N-Particle (MCNP) neutron transport program which has been modified as described in Section 3.1 to evaluate only the point geometry assumption. Additional analysis in Section 3.2 then explores the variation of the probability of fission with position of the fission reaction. The distribution of these fission reactions is shown to vary significantly with collision number for source distributions that differ from the fundamental mode of a fissile material, as detailed in Section 3.3. The net effect is a probability of fission which varies with collision number as described in Section 3.4. Section 3.5 compares the simulated and measured neutron moments using the collision dependent distributions of the probabilities of fission, and the mean of the distributions.

3.1 Monte Carlo Simulation and Analysis

The Monte Carlo neutron transport program MCNP version 6.2 is used in full analog mode to disable all weight splitting and variance reduction methods [11]. While the point model of neutron transport described in Chapter 2 approximates all neutrons to be monoenergetic and only induce fission reactions or escape, MCNP uses the nuclear cross section data files provided by ENDF in the ACE format to accurately model neutron transport. This includes emission of fission neutrons of different energies, the dependence of the number of fission neutrons on the energy of the neutron inducing fission, and the inclusion of additional reactions such as neutron capture and scattering and their modifications on the energy of the incident neutron. To resolve these additional differences between the point model and simulations using MCNP, two approaches may be taken. One approach is to modify the point model to include these additional reactions and energy dependence or to modify the MCNP source code such that all neutrons are monoenergetic and only fission reactions or escape are possible. This work takes the latter approach, allowing the use of MCNP to test only the point geometry assumption of the point model for various extended geometries. The modifications of MCNP are now described.

As this work examines the event-by-event correlations of neutrons within each fission chain, the full information provided by MCNP is recorded using the PTRAC option which yields a binary file containing the history of each particle. The ordering of the information is determined by the internal neutron bank, a first-in, last-out datatype which iterates on each neutron until it is terminated. To reconstruct the event by event information, the provided MCNPTools C++ and Python interfaces have been modified to create a graph representation [56]. This is accomplished using the Boost Graph Library and is shown in Figure 3.1 [57].

MCNP relies on the ENDF nuclear cross section files in ACE to determine which reaction a neutron undergoes in different materials and how often. This chapter has modified the cross section files using the NJOY21 code library which allows manipulating the cross section values for neutron induced reactions within ACE formatted files [58]. For each material the cross sections of all non fission reactions are set to zero. In the ENDF format, this corresponds to all MT numbers not equal to 18. The total cross section value is then set to equal the fission cross section.

To make all neutrons monoenergetic, the source code of MCNP is modified. This is done by enabling the FREYA model of induced neutron fission through the MCNP PHYS:N card option [11]. The FREYA submodule source code is modified so all neutrons returned to MCNP from FREYA are assigned energies of 2.0 MeV. The starting neutron of the simulation is also assigned a value of 2.0 MeV through the MCNP input card.

To ensure that the multiplicity distribution is known precisely, the FREYA module is modified to use the values measured by Zucker and Holden for U-235 for an incident neutron energy of 2.0 MeV [12]. The associated moments (2.34) are $\nu_1 = 2.637$, $\nu_2 = 5.623$, $\nu_3 = 9.476$.

Analysis of simulations using MCNP with these modifications verify that only fission reactions occur and all neutrons have energies of 2.0 MeV. The moments ν_1,ν_2,ν_3 are also verified to match the expected values. An example of a fission chain with these modifications is shown in Figure 3.2 where all neutrons are only 2.0 MeV and the only allowed interactions are induced fission or escape.

For every MCNP source neutron i up to a total of N_S, the number of neutrons produced for each source neutron is denoted $N(i)$. The jth neutron created from the ith source neutron is written $\mathbb{N}_{i,j}$. The PTRAC file is parsed to determine the fate of each neutron $\mathbb{N}_{i,j}$ and whether it induces a fission or escapes the boundary of the geometry. The notation $\mathbb{N}_{i,j}(f_{\text{escape}})$ is used to indicate that the neutron ended by escaping the geometry.

3.2 Variation of Probability of Fission with Position

The probability of a neutron to induce fission is dependent on the position of the neutron in an assembly of fissile material [3], $\vec{r}$, due to the variation of the amount of surrounding material. Using the PTRAC output of MCNP, a filter on $\vec{r}$ being contained in a voxel at position $\vec{s}$ with half length Δ, $\vec{r} \in \text{Voxel}(\vec{s}, \Delta)$ is created. By comparing the ratio of all neutrons passing this filter to neutrons which induce fission, a spatial dependent probability of fission is created and expressed mathematically as

$$p_f(\vec{r}) \approx \frac{\sum_i^{N_S} \sum_j^{N(i)} \mathbb{N}_{i,j}(f_{\text{fission}}, \vec{r} \in \text{Voxel}(\vec{s}, \Delta s))}{\sum_i^{N_S} \sum_j^{N_N(i)} \mathbb{N}_{i,j}(\vec{r} \in \text{Voxel}(\vec{s}, \Delta))} \tag{3.1}$$

and is shown in Figure 3.3 for a simulated 6 cm sphere of uranium-235 with $\Delta = (12/(2 \cdot 21))$ cm and $N_S = 5 \times 10^7$ source neutrons distributed uniformly.

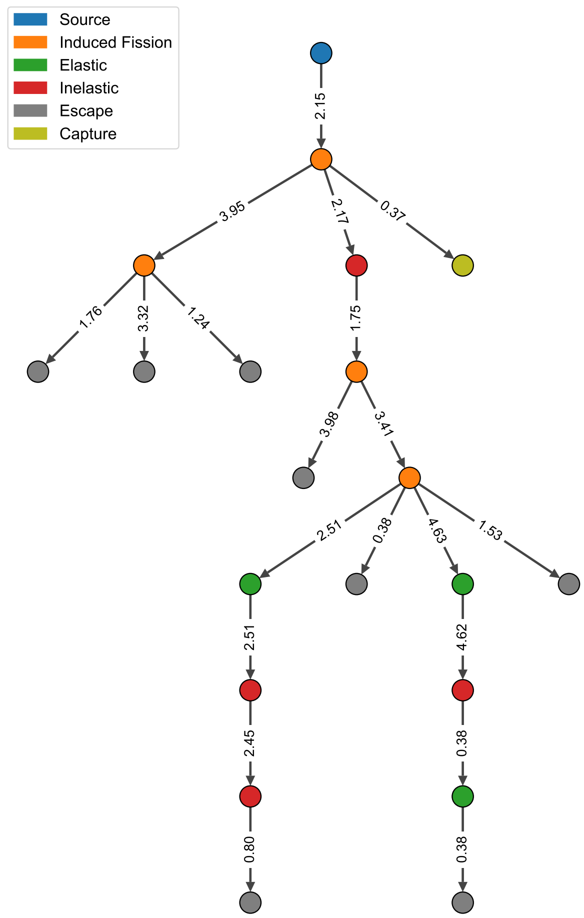

FIGURE 3.1: Graph representation of a single fission chain simulated using MCNP with all physics enabled. Each reaction is a node, connected by neutrons represented as the connecting lines. The label on the line indicates the neutron energy in MeV.

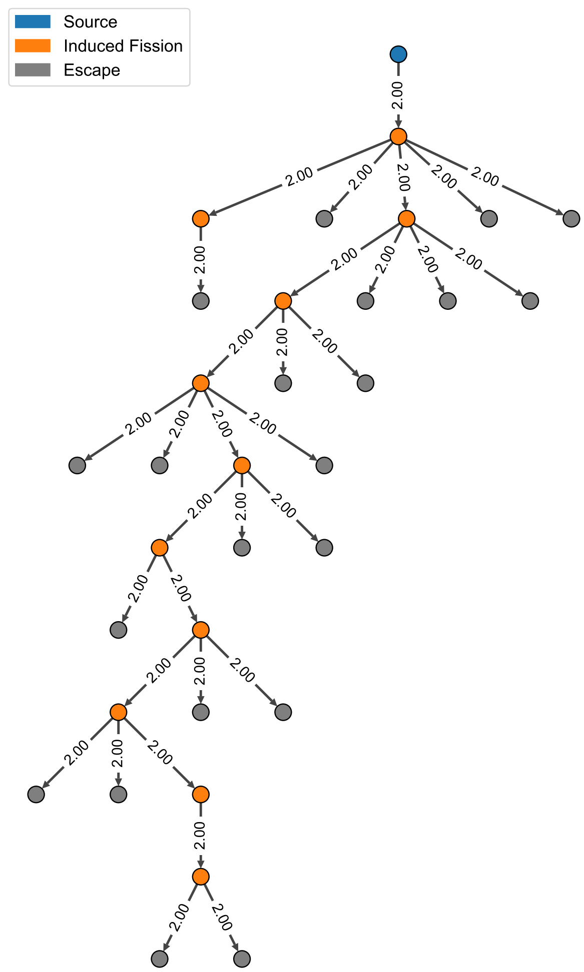

FIGURE 3.2: Graph representation of a single fission chain simulated using MCNP with only induced fission and escape reactions allowed. All neutrons are modified to have a single energy of 2.0 MeV.

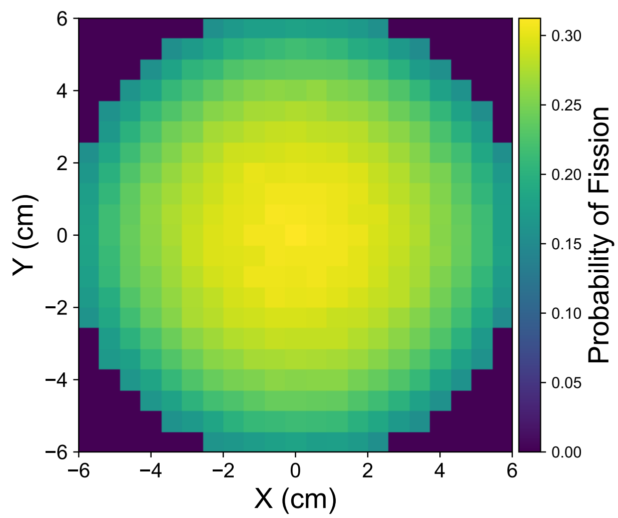

FIGURE 3.3: A simulated 6 cm radius sphere of pure uranium-235 showing the estimated probability of a 2.0 MeV isotropically emitted neutron to induce fission, dependent on the position at which the neutron is created.

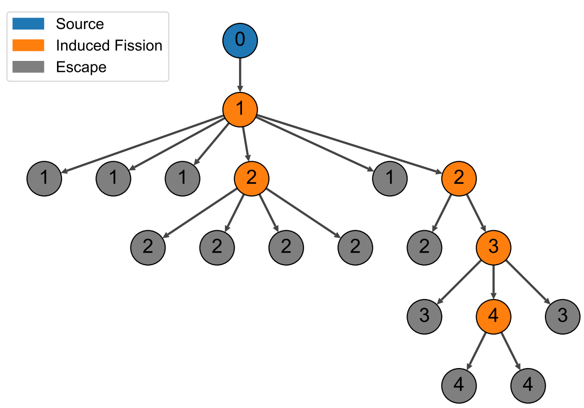

FIGURE 3.4: A processed event from MCNP which builds the history of the fission chain into a directed graph. Nodes are events, either a source, induced fission, or escape event. The directed lines are neutrons. The number of collisions in each node's history are displayed.

Neutrons which are emitted near the center have nearly twice the probability of initiating fission compared to neutrons emitted near the edge of the sphere. This is expected as the path length averaged over all directions is largest at the center. Thus, p_f is not constant and varies considerably with respect to the position at which each neutron is created. A previous approach to address this variation is the 'Weighted Point Model' described in Section 2.5.4.

3.3 Changing Source Distribution with Collision Number

Consider the behavior of a large burst of neutrons from a source neutrons at the center of the sphere of uranium-235 shown in Figure 3.3. Initially all neutrons are located at source position $\vec{r}_0 = 0$ cm. For those that do not escape, the remaining neutrons then induce fission at positions throughout the sphere. These first fission positions will form a distribution denoted as $\Psi(\vec{r}, 1|\vec{r}_0)$. Next, the neutrons emitted from these first induced fission positions will then again either escape or induce a second generation of fissions at positions which follow a distribution denoted $\Psi(\vec{r}, 2|\vec{r}_0)$. This process continues with additional generations of induced fission, called the collision number n.

To determine $\Psi(\vec{r}, n|\vec{r}_0)$ every neutron and fission reaction is assigned a collision number according to how many collisions occurred previously. To determine the collision number n, the time and positions of output neutrons are correlated to fission reactions and used to construct the fission chain event tree. With the node of the starting neutron at the top with a collision number of zero, the collision number for each reaction is the depth of the node in the graph data structure. The collision number of each neutron is the collision number of the parent reaction. Escape reactions are not collisions and do not increase the collision number. The representation of this process is shown for one fission chain in Figure 3.4. It can be shown that the graph and collision number representation of a fission chain is equivalent to the continuous time rate equation formulation of Feynman [28], [59].

This analysis is used to create a filter on collision number n. The described MCNP simulations and analysis can now be used to determine $\Psi(\vec{r}, n|\vec{r}_0)$

$$\Psi(\vec{r}, n|\vec{r}_0) \approx \frac{\sum_i^{N_S} \sum_j^{N_N(i)} \mathbb{N}_{i,j}(\vec{r} \in \mathrm{Voxel}(\vec{s}, \Delta), n|\vec{r}_0)}{\sum_i^{N_S} \sum_j^{N_N(i)} \mathbb{N}_{i,j}(n|\vec{r}_0)} \tag{3.2}$$

where $\mathbb{N}_{i,j}(\vec{r} \in \mathrm{voxel}(\vec{s}, \Delta), n|\vec{r}_0)$ is the jth neutron from the ith source particle that at collision number n has a position $\vec{r}$ contained within voxel$(\vec{s}, \Delta)$, using a simulation with a point source of neutrons emitted at $\vec{r}_0$. Fig. 3.5 shows $\Psi(\vec{r}, n|\vec{r}_0)$ of a 6 cm sphere of uranium-235 with two source positions at $\vec{r}_0 = 0$ cm and $\vec{r}_0 = 5$ cm for collision numbers $n = 2, 5$ and the sum of position with a collision number greater than or equal to 9. Near the beginning of the chain after two collisions most neutrons are created at positions near the source position $\vec{r}_0$. As the chain progresses with collision number the positions of induced fissions diffuse. After nine collisions the distribution of induced fissions appear identical regardless of initial source position $\vec{r}_0$.

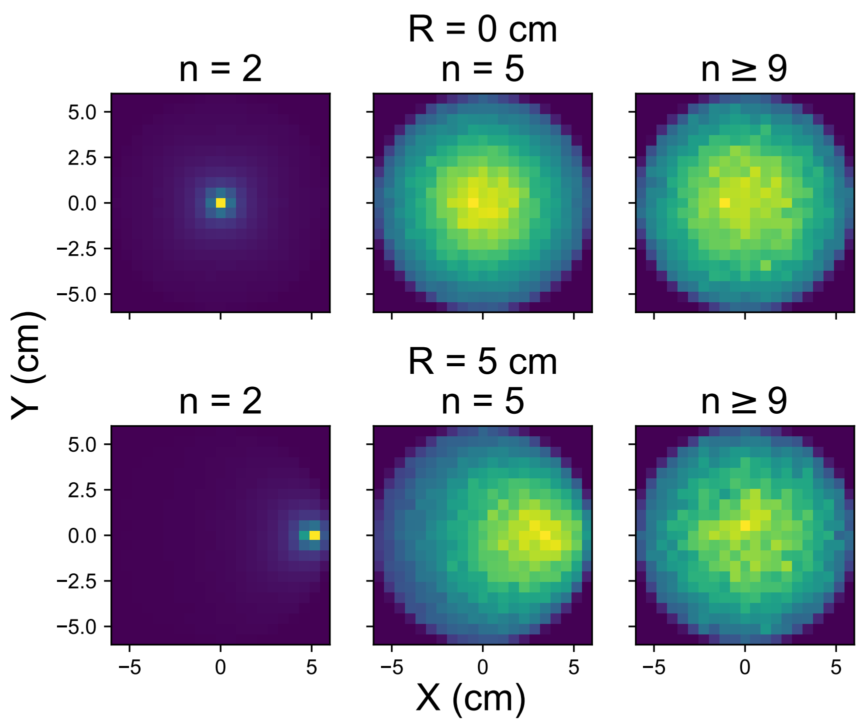

FIGURE 3.5: The intensity of the locations of induced fissions in a 6 cm sphere of uranium-235 for a point source of neutrons at the center (top row) and 5 cm offset from the center (bottom row). The left column shows the positions of fissions after two collisions, the center column after five collisions, and the right column for nine collisions. While the distribution of fission sites is dependent on the position $\vec{r}_0$ of the neutron source, after nine collisions the dependence has nearly disappeared and the distributions are nearly identical.

3.4 Behavior of Probability of Fission with Collision Number

The combined effect of the described spatial dependence of the probability of a neutron to induce fission shown in Section 3.2 and the changing spatial distribution of the neutrons and fissions with collision number described in Section 3.3 is a distribution of probabilities of fission which changes with collision number. This can be expressed mathematically as

$$p_f(\vec{r}|n,\vec{r_0}) = p_f(\vec{r})\Psi(\vec{r},n|\vec{r}_0). \tag{3.3}$$

The distributions of $p_f(\vec{r}|n,\vec{r_0})$ are shown in Figure 3.6 for the previous example of a simulated 6 cm sphere of uranium-235 with a source at the center, with the simplified modifications of MCNP. For several and fewer collisions, most neutrons have a very high probability to fission as they remain near the center. After several collisions they spread out into a distribution which does not change with additional collisions and is independent of the starting position of the source.

This behavior can be shown by looking at the averaged or expected values of $p_f(\vec{r}|n,\vec{r_0})$,

$$p_f(n,\vec{r_0}) = \mathbb{E}_{\vec{r}}\left[p_f(\vec{r}|n,\vec{r_0})\right] = \mathbb{E}_{\vec{r}}\left[p_f(\vec{r})\Psi(\vec{r},n|\vec{r}_0)\right]. \tag{3.4}$$

Figure 3.7 shows $p_f(n,\vec{r_0})$ for source positions $\vec{r}_0 = 0$ cm and $\vec{r}_0 = 5$ cm. For $n = 1$, $p_f(n = 1,\vec{r_0}) = p_f(\vec{r} = \vec{r}_0)$. After several collisions the values for both curves of $p_f(n,\vec{r_0})$ are near equal and $p_f(n,\vec{r_0}) \approx p_f(N)$ for some $N > 1$.

3.5 Analysis of Neutron Moments for Extended Geometries

The combinatorial moments (1.10)-(1.12) of the number of escaped neutrons can be estimated from the MCNP simulations as,

$$\phi_{1,\text{MCNP}} = \sum_i^{N_S} \sum_j^{N_N(i)} \mathbb{N}_{i,j}(f_{\text{escape}}) \tag{3.5}$$

$$\phi_{2,\text{MCNP}} = \frac{1}{2}\sum_i^{N_S} \sum_j^{N_N(i)} \mathbb{N}_{i,j}(f_{\text{escape}})\left(\mathbb{N}_{i,j}(f_{\text{escape}}) - 1\right) \tag{3.6}$$

$$\phi_{3,\text{MCNP}} = \frac{1}{6}\frac{1}{N_S}\sum_i^{N_S} \sum_j^{N_N(i)} \mathbb{N}_{i,j}(f_{\text{escape}})\left(\mathbb{N}_{i,j}(f_{\text{escape}}) - 1\right)\left(\mathbb{N}_{i,j}(f_{\text{escape}}) - 2\right). \tag{3.7}$$

The combinatorial moments are simulated for the simplified 6 cm sphere of uranium-235 with a source of neutrons at various radial positions and shown in Figure 3.8. The moments are shown to vary substantially based on where in the material the source is, for the triples the moment increases by three-fold for a source at the center compared to near the edge. This shows the sensitivity of a neutron multiplicity measurement with the spatial distribution of the source and the spatial variation of the probability of fission.

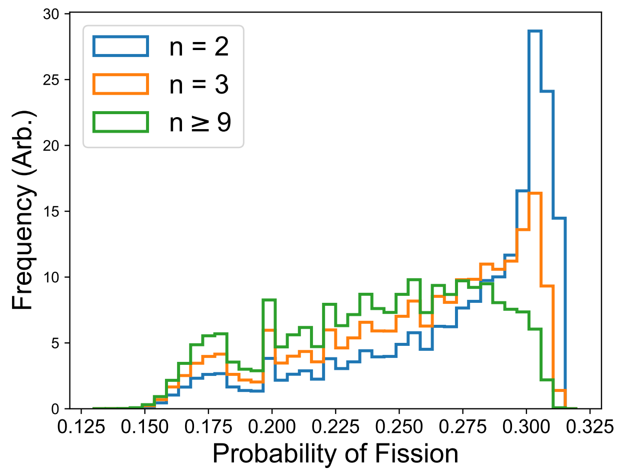

FIGURE 3.6: Distribution of the probabilities of fission for a sphere of uranium-235 with a source of neutrons at the center. The distributions are shown after 2, 3, and greater than or equal to 9 collisions.

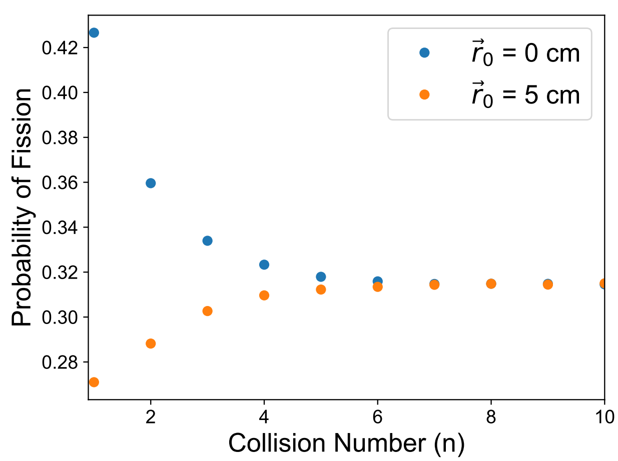

FIGURE 3.7: Mean values of the probability of fission with collision number for a source at the center (blue line) and near the edge (orange line) in a 6 cm sphere of uranium-235.

Now we examine how to reduce the knowledge required to estimate the moments of Figure 3.8 accurately. First we will estimate the moments using only the collision and source position dependent probability of fission distributions of Figure 3.6. Then we will approximate the distributions using only the mean or average with respect to the collision number. The simple Monte Carlo Algorithm 1 of Section 1.3.4 is modified and used to calculate the moments and compare with the values from the simulation.

3.5.1 Calculation of Moments Using Collision and Position Dependent Distributions of the Probability of Fission

As a first step the collision and position dependent distributions for the probabilities of fission as shown in Figure 3.6 are calculated for each source position using (3.3). Algorithm 1 of Section 1.3.4 is modified to keep track of the collision number, and use a probability of fission which changes with generation number. Then for a specified source position, each neutron chain uses the probabilities of fission are sampled from the N distributions shown in Figure 3.6. This process is repeated, building the escaped neutron distribution and the moments are calculated using (3.5)-(3.7). These moments, $\phi_{i,p_f(\vec{r}|n)}(\vec{r}_0)$ are then compared to those calculated directly from MCNP $\phi_{i,\mathrm{MCNP}}(\vec{r}_0)$ at different radial positions $\vec{r}_0$.

The outcome of this analysis, combined with the monoenergetic and fission only simulation, is determining how accurately the moments can be estimated by considering the variation of the probability of fission with *only position*. What is not included is the variation of the probability of fission with *position and direction*. Figure 3.9 shows the percent error of $\phi_{i,p_f(\vec{r}|n)}(\vec{r}_0)$ compared to $\phi_{i,\mathrm{MCNP}}(\vec{r}_0)$. The last two positions near the radius suffer from a lack of statistics as most neutrons exit the assembly immediately, leading to relatively few neutrons available to estimate the probability of fission distributions for additional collision numbers. Excluding these last two points, the average error is summarized in Table B.1. While the singles are estimated accurately, the doubles and triples have a consistent overestimation.

The reason for the bias and the relation with neutron direction can be understood through a simple one dimensional example shown in Figure 3.10. A fission occurs at position $\vec{r} = x$, in a one dimensional fissile material of length L. The probability of fission is

$$p_f(x, \mu) = \left(1 - e^{-l(x,\mu)\ \Sigma_f}\right) \tag{3.8}$$

where Σ_f is the macroscopic fission cross section and l is the path length for a given position x and direction μ. As we are assuming isotropic fission, the probability of fission averaged over direction μ is,

$$\langle p_f(x, \mu)\rangle_\mu = \frac{1}{2}\left(1 - e^{-x\ \Sigma_f}\right) + \frac{1}{2}\left(1 - e^{-(L-x)\ \Sigma_f}\right) \tag{3.9}$$

$$p_f(x, \langle\mu\rangle) = \left(1 - e^{-\frac{x+(L-x)}{2}\ \Sigma_f}\right) = \left(1 - e^{-(L/2)\ \Sigma_f}\right) \tag{3.10}$$

$$\langle p_f(x, \mu)\rangle_\mu \leq p_f(x, \langle\mu\rangle) \tag{3.11}$$

$$\phi_i(\langle p_f(x, \mu)\rangle_\mu) \leq \phi_i(p_f(x, \langle\mu\rangle)). \tag{3.12}$$

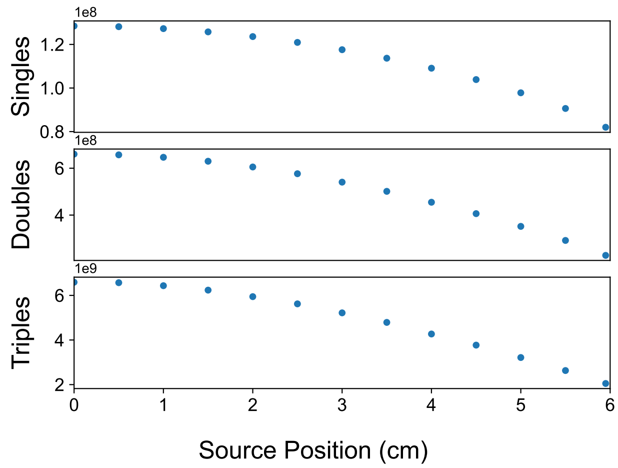

FIGURE 3.8: Simulated combinatorial moments (Singles, Doubles, Triples) for the 6 cm sphere of uranium-235 in a monoenergetic fission only MCNP simulation. The moments are shown at different positions of a point source of 5e7 neutrons.

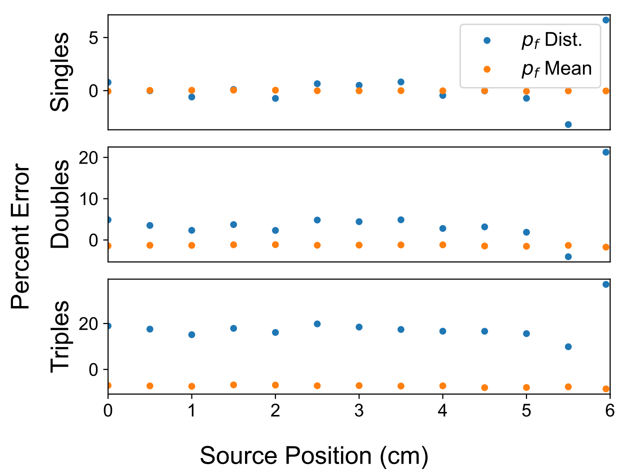

FIGURE 3.9: Simulated error of combinatorial moments (Singles, Doubles, Triples) compared to the simulated moments of Figure 3.8 using a modified version of Algorithm 1 where the values of p_f vary with generation. The values of p_f are sampled from the collision dependent distributions of Figure 3.6 (in blue) and the mean of the distributions (in orange) shown in Figure 3.7.

This example illustrates that the moments for fission at a specific position, averaged over direction, is greater than the direction average of the position and direction specific moments. Thus sampling the position distribution of Figure 3.6, instead of a distribution dependent on both position and direction, will overestimate the moments determined from a full Monte Carlo simulation as seen in Figure 3.9.

3.5.2 Calculation of Moments Using Collision Dependent Values of Probability of Fission Averaged over Position

Ignoring direction, now we consider the effect of using the expectation of the position dependent probability of fission per collision (3.4). As the moments are a concave function, we can apply Jensen's inequality [40]

$$\phi_i(\mathbb{E}_{\vec{r}}\left[p_f(\vec{r}|n,\vec{r_0})\right]) \leq \mathbb{E}_{\vec{r}}\left[\phi_i(p_f(\vec{r}|n,\vec{r_0}))\right] . \tag{3.13}$$

Thus the outcome of then averaging over position $\vec{r}$ will be an underestimation compared to the simulated Monte Carlo moments as seen in Figure 3.9 and Table B.1.

The conclusion is that the combinations of the two simplifications, each of which introduce a significant bias, act against each other. The net bias is not quantified in this work, but will be assumed to be a smaller number than either effect alone.

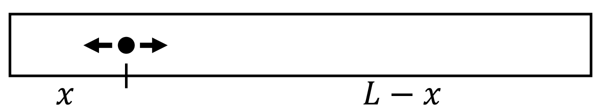

FIGURE 3.10: A simple illustration of neutrons emitted from a fission at position x in a 1D rod of fissile material of length L, which can either travel x or $L - x$ length through the rod depending on emitted direction.

Chapter 4

Varying Probability of Fission Model

The varying probability of fission (VPF) model begins with the recursive derivation of the fission chain probability distribution presented by Prasad and Snyderman [59], which extends the earlier work of Hawkins and Ulam [28]. Prasad and Snyderman begin with a generating function $F(x,y)$ with latent variables x to track neutrons within the system and y for neutrons those that escape and do not perpetuate the fission chain. The first-generation generating function of a fission creating ν fission neutrons with probability C_ν which can either escape or remain in the system to perpetuate the chain is

$$F(x,y) = F_1(x,y) = \sum_{\nu=0}^{\nu_{\max}} C_\nu [px + (1-p)y]^\nu \tag{4.1}$$

where each of the ν fission neutrons has probability p to induce a new fission and probability $(1-p)$ to escape. The generating function for n generations of fissions is the nth iterate of $F(x,y)$

$$F_n(x,y) = F[F_{n-1}(x,y),y] = F[\cdots F[F[F(x,y),y],y],\cdots,y] \tag{4.2}$$

where for each generation, x is replaced by $F(x,y)$ allowing each of the internal neutrons possibly to generate ν fission neutrons with probability C_ν and continue the chain. For a fission chain beginning with a single fission energy neutron the probability generating function after n generations $f_n(x,y)$ is,

$$f_n(x,y) = (1-p)y + pF_n(x,y). \tag{4.3}$$

The limit of $f_n(x,y)$ for infinite collisions where the fission chain has ended and the internal neutron population is zero yields the Böhnel equation [1] of the point model

$$h(y) = \lim_{x\to 0}\left[\lim_{n\to\infty} f_n(x,y)\right] \tag{4.4}$$

$$h(y) = (1-p)y + p\sum_{\nu=0}^{\nu_{\max}} C_\nu [h(y)]^\nu \tag{4.5}$$

where the nth factorial moment ϕ_n is obtained as

$$\phi_n = \left.\frac{d^n h(y)}{dh(y)^n}\right|_{y=1} \tag{4.6}$$

and the resulting equations have been previously derived (2.33)-(2.35).

4.1 Derivation of VPF Moments

The above analysis assumes that the probability of fission p is independent of generation number i. We now derive the case where this is not assumed and all neutrons for generation i have a fission probability p_i and escape probability $(1 - p_i)$. Instead of beginning with an induced fission we write the generating function $g_1(x, y)$ for a single first generation fission energy neutron which may escape with probability $(1 - p_1)$ or fission with probability p_1 and create ν internal neutrons with count probability C_ν,

$$g_1(x, y) = (1 - p_1)y + p_1 C(x). \tag{4.7}$$

In general an ith generation fission energy neutron has the probability generating function

$$g_i(x, y) = (1 - p_i)y + p_i C(x). \tag{4.8}$$

The PGF for multiple fissions is written by replacing x with the PGF for the next generation $g_i(x \to g_{i+1}(x, y), y)$. For a neutron of generation i, the PGF of internal and escaped neutrons for later generation j is then

$$g_{i,\ldots,j}(x, y) = g_i(g_{i+1}(g_{i+2}(\cdots g_{j-1}(g_j(x, y), y) \cdots, y), y), y) \tag{4.9}$$

$$g_{i,\ldots,j}(x, y) = (1 - p_i)y + p_i C(g_{i+1,\ldots,j}(x, y)). \tag{4.10}$$

The factorial moments are now derived for one neutron of generation i continuing to generation j. The notation will be $\phi'_{i,\ldots,j}, \phi''_{i,\ldots,j}, \phi'''_{i,\ldots,j}$ for the first, second, and third factorial moments.

The first y partial derivative of (4.10) followed by setting $x = y = 1$ yields

$$\left(\frac{\partial}{\partial y} g_{i,\ldots,j}(x, y)\right)_{x=y=1} = (1 - p_i) + p_i \left(\frac{dC}{dz}(z = g_{i+1,\ldots,j}(x, y))\right)_{x=y=1} \left(\frac{\partial}{\partial y} g_{i+1,\ldots,j}(x, y)\right)_{x=y=1}. \tag{4.11}$$

As $g_j(x = 1, y = 1) = 1$ then $g_{j-1,j} = g_{j-1}(g_j(x = 1, y = 1) = 1, y = 1) = 1$ which implies $g_{i,\ldots,j}(x = 1, y = 1) = 1$. Thus the kth derivative of $C(g_{i+1,\ldots,j}(x, y))$ is the kth factorial moment ν_k

$$\left(\frac{d^k C}{dz^k}(z = g_{i+1,\ldots,j}(x, y))\right)_{x=y=1} = \sum_{\nu=0}^{\nu_{\max}} C_\nu \frac{\nu!}{(\nu - k)!} = \nu_k. \tag{4.12}$$

The relation of (4.11) yields a recursive equation,

$$\phi'_{i,\ldots,j} = 1 - p_i + p_i \nu_1 \phi'_{i+1,\ldots,j} \tag{4.13}$$

where

$$\phi'_{i,\ldots,j} = \left(\frac{\partial}{\partial y} g_{i,\ldots,j}(x,y) \right)_{x=y=1}. \tag{4.14}$$

Writing out the first several terms of (4.14) yields,

$$\phi'_{i,\ldots,j} = (1-p_i) + p_i\nu_1(1-p_{i+1}) + p_i\nu_1 p_{i+1}\nu_1(1-p_{i+2}) + p_i\nu_1 p_{i+1}\nu_1 p_{i+2}\nu_1\phi'_{i+3,\ldots,j}. \tag{4.15}$$

The terms of (4.15) imply the closed form of the first factorial moment $\phi'_{i,\ldots,j}$

$$\phi'_{i,\ldots,j} = \sum_{a=i}^{j}(1-p_a)\prod_{b=i}^{a-1} p_b\nu_1. \tag{4.16}$$

The same procedure can be repeated for the second, third, and higher moments. For brevity, only the recursive relations and the closed forms of the second and third moments are shown:

$$\phi''_{i,\ldots,j} = p_i\nu_2(\phi'_{i+1,\ldots,j})^2 + p_i\nu_2 p_{i+1}\nu_1(\phi''_{i+2,\ldots,j}) \tag{4.17}$$

$$\phi'''_{i,\ldots,j} = p_i\nu_3(\phi'_{i+1,\ldots,j})^3 + 3p_i\nu_2 p_{i+1}(\phi'_{i+1,\ldots,j})(\phi''_{i+1,\ldots,j}) + p_i\nu_1\phi'''_{i+1,\ldots,j} \tag{4.18}$$

$$\phi''_{i,\ldots,j} = \nu_2\sum_{a=i}^{j-1} p_a(\phi'_{a+1,\ldots,j})^2\prod_{b=i}^{a-1} p_b\nu_1 \tag{4.19}$$

$$\phi'''_{i,\ldots,j} = \nu_3\sum_{a=i}^{j-1} p_a(\phi'_{a+1,\ldots,j})^3\prod_{b=i}^{a-1} p_b\nu_1 + 3\nu_2\sum_{a=i}^{j-1} p_a(\phi'_{a+1,\ldots,j})(\phi''_{a+1,\ldots,j})\prod_{b=i}^{a-1} p_b\nu_1. \tag{4.20}$$

The first three moments $\Phi'_n, \Phi''_n, \Phi'''_n$ beginning with the first collision $i = 1$ to the nth collision are

$$\Phi'_n = \phi'_{1,\ldots,n} = \sum_{a=1}^{n}(1-p_a)\prod_{b=1}^{a-1} p_b\nu_1 \tag{4.21}$$

$$\Phi''_n = \phi''_{1,\ldots,n} = \nu_2\sum_{a=1}^{n-1} p_a(\phi'_{a+1,\ldots,n})^2\prod_{b=1}^{a-1} p_b\nu_1 \tag{4.22}$$

$$\Phi'''_n = \phi'''_{1,\ldots,n} = \nu_3\sum_{a=1}^{n-1} p_a(\phi'_{a+1,\ldots,n})^3\prod_{b=1}^{a-1} p_b\nu_1 + 3\nu_2\sum_{a=1}^{n-1} p_a(\phi'_{a+1,\ldots,n})(\phi''_{a+1,\ldots,n})\prod_{b=1}^{a-1} p_b\nu_1. \tag{4.23}$$

In the case of neutrons having a uniform probability of fission per collision, $p_i = p$, the infinite collision limit $n \to \infty$ yields the point model moments listed as equations (21)-(23) in the work by

Böhnel [1] and in the previous chapter as (2.33)-(2.35).

$$\lim_{n\to\infty} \Phi_n^{'}(p_i = p) = \lim_{n\to\infty} (1-p) \sum_{a=1}^{n} (p\nu_1)^{a-1} = \frac{1-p}{1-p\nu_1} \tag{4.24}$$

$$\lim_{n\to\infty} \Phi_n^{''}(p_i = p) = \lim_{n\to\infty} \nu_2 p \sum_{a=1}^{n-1} (\phi_{a+1,\ldots,n}^{'})^2 (p\nu_1)^{a-1} = \frac{\nu_2 p(1-p)^2}{(1-\nu_1 p)^3} \tag{4.25}$$

$$\begin{aligned} \lim_{n\to\infty} \Phi_n^{'''}(p_i = p) &= \lim_{n\to\infty} \left(\nu_3 p \sum_{a=1}^{n-1} (\phi_{a+1,\ldots,n}^{'})^3 (p\nu_1)^{a-1} + 3\nu_2 p \sum_{a=1}^{n-1} \phi_{a+1,\ldots,n}^{'} \phi_{a+1,\ldots,n}^{''} (p\nu_1)^{a-1} \right) \\ &= \frac{p_f(1-p_f)^3(3p_f\nu_2^2 + \nu_3 - p_f\nu_1\nu_3)}{(1-\nu_1 p_f)^5} \end{aligned} . \tag{4.26}$$

Lastly, approximating the VPF equations such that after N collisions the probability of fission is constant leads to the following equations

$$\Phi_i^{'} = \sum_{a=i}^{N} (1-p_a) \prod_{b=i}^{a-1} p_b\nu_1 + \left(\prod_{b=i}^{N} p_b\nu_1 \right) \phi_1 \tag{4.27}$$

$$\Phi_i^{''} = \nu_2 \sum_{a=i}^{N} p_a (\Phi_{a+1}^{'})^2 \prod_{b=i}^{a-1} p_b\nu_1 + \left(\prod_{b=i}^{N} p_b\nu_1 \right) \phi_2 \tag{4.28}$$

$$\Phi_i^{'''} = \sum_{a=i}^{N} p_a \left(\nu_3 (\Phi_{a+1}^{'})^3 + 3\nu_2 (\Phi_{a+1}^{'})(\Phi_{a+1}^{''}) \right) \prod_{b=i}^{a-1} p_b\nu_1 + \left(\prod_{b=i}^{N} p_b\nu_1 \right) \phi_3 \tag{4.29}$$

where ϕ_1, ϕ_2, ϕ_3 are the original point model moments (2.33)-(2.35). The final VPF moment equations, over all collisions for $i = 1$ where $p_i = p$ for $i > N$, are thus $\Phi^{'} = \Phi_{i=1}^{'}$, $\Phi^{''} = \Phi_{i=1}^{''}$, and $\Phi^{'''} = \Phi_{i=1}^{'''}$. This formulation is computationally faster than using a large number of p_i values.

4.2 Validation of VPF Moments

The VPF equations (4.21)-(4.23) are now shown to accurately model the moments of a system with a varying probability of fission per generation. A simple Monte Carlo program was written in Python, which begins with an internal neutron population of one and either induces a fission with probability p_1 and generates ν additional internal neutrons sampled from a fission multiplicity distribution $P(\nu)$, or is transferred to the escape neutron population with probability $(1 - p_1)$. This process is repeated for successive generations on every neutron in the current generation internal neutron population until no internal neutrons remain and the chain has ended. Each neutron generation uses a different value for the probability of fission.

In this simulation the collision dependent probability of fission p_i is given the functional form

$$p_i = (1-\alpha)^{i-1} p_1 + p_\infty \alpha^{i-1} \tag{4.30}$$

where $p_1 = 0.3$, $p_\infty = 0.2$, and $\alpha = 0.6$.

The simulation is then run for $F = 10^7$ source events using the multiplicity distribution of uranium-235 induced by a 2.0 MeV neutron measured by Zucker and Holden where $\nu_1 = 2.637$, $\nu_2 = 5.623$, $\nu_3 = 9.476$ [12]. The number distribution of escaped neutrons per generation is recorded and shown in Figure 4.1.

The generation dependent leaked neutron distributions are used to calculate the Monte Carlo estimated generation dependent neutron singles S_i^{MC}, doubles D_i^{MC}, and triples T_i^{MC} where

$$S_i^{\mathrm{MC}} = F\,\mathbb{E}[n_L(i)] \tag{4.31}$$

$$D_i^{\mathrm{MC}} = F\,\frac{1}{2}\mathbb{E}[n_L(i)(n_L(i)-1)] \tag{4.32}$$

$$T_i^{\mathrm{MC}} = F\,\frac{1}{6}\mathbb{E}[n_L(i)(n_L(i)-1)(n_L(i)-2)]. \tag{4.33}$$

These are plotted and compared with the VPF singles S_i^{VPF}, doubles D_i^{VPF} and triples T_i^{VPF}

$$S_i^{\mathrm{VPF}} = F\,\Phi_i' \tag{4.34}$$

$$D_i^{\mathrm{VPF}} = F\,\frac{1}{2}\Phi_i'' \tag{4.35}$$

$$T_i^{\mathrm{VPF}} = F\,\frac{1}{6}\Phi_i''' \tag{4.36}$$

in Figure 4.2 and are in agreement with the results obtained using the VPF equations.

4.3 Including All Physics in the VPF Model

The MCNP program of Section 3.1 is now reverted back to the original version of MCNP which includes all neutron physics such as energy variation and capture and scattering.

4.3.1 Additional Neutron Reactions

The inclusion of neutron capture and (n,xn) reactions into the point model has been discussed previously in Section 2.4.1 as the 'superfission' approach. The VPF model takes the same approach, replacing p_i with the superfission probability $p_i^* = p_{i,f} + p_{i,c} + p_{i,2n} + p_{i,3n}$ where $p_{i,f}$ is the probability of a neutron in the ith generation to induce fission, $p_{i,c}$ to be captured, and $p_{i,2n}$, $p_{i,3n}$ to undergo a (n,2n) or (n,3n) reaction, respectively.

It is assumed that the ratio of each reaction probability to the total probability does not change with position or generation number. This approximation is reasonable if the material is bare and homogeneous. Additional materials, nonuniform enrichment, or surrounding shielding will violate this assumption.

With the other modifications described, the superfission neutron multiplicity distribution is determined by tallying the number of daughter neutrons using the graph representation of the MCNP PTRAC data, and shown in Figure 4.3. The associated moments are $\nu_1 = 2.352$, $\nu_2 = 4.957$

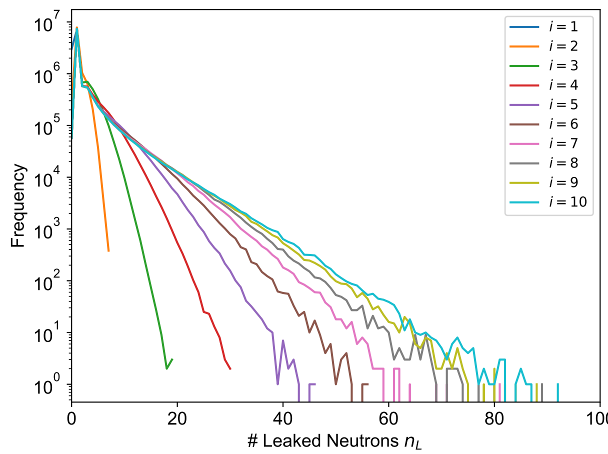

FIGURE 4.1: The escaped neutron population distributions for successive generations of fission.

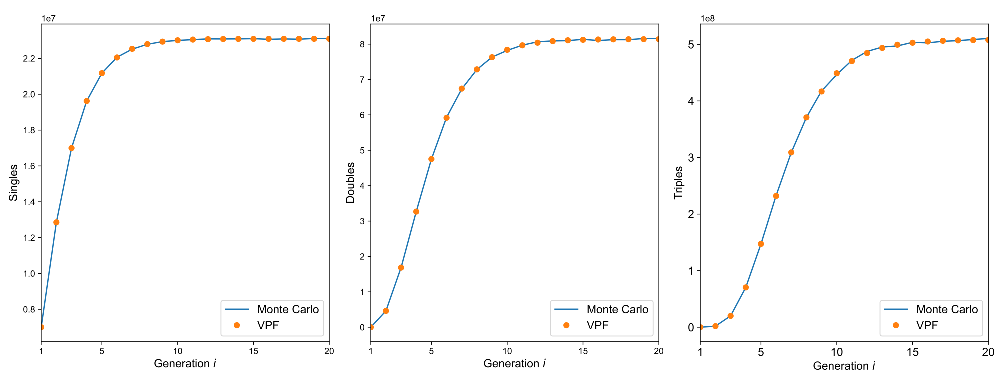

FIGURE 4.2: The escaped neutron population distributions for successive generations of fission. The simulated values using a collision dependent probability of fission in Algorithm 1 match those of the VPF moment equations (4.21)-(4.23).

and $\nu_3 = 8.232$. The simulation is a uniformly distributed source of neutrons in a 6 cm radius sphere of pure uranium-235.

4.3.2 Matching Source and Fission Neutron Energies

Previously in the simplified MCNP program the source neutron energy matched the energy of neutrons emitted from fission. This again must be maintained otherwise the first collision probabilities will be biased. The energies of the neutrons emitted per each 'superfission' event are recorded. Then the source neutron energy spectrum is modified to match the superfission neutron energy spectrum as closely as possible. The results are shown in Figure 4.4, where the superfission spectrum was found to match a Maxwellian spectrum with parameter $a = 1.333$. This spectrum takes into account energy variations due to neutrons inelastically scattering.

However, the variations of the probability of fission with energy are not taken into account. As neutrons which inelastically scatter will have lower energies than those that induce fission immediately, the probability of fission will vary significantly. This is expected to give a similar bias as averaging over neutron direction described in Section 3.5.1. The values of the probability of fission are shown in Figure 4.5 for both the simple model and the full physics for a 6 cm sphere of uranium-235 at source positions at the center and near the sphere edge.

4.4 Results of VPF Model Moment Equations

The accuracy of the VPF moment equations (4.34)-(4.36) to describe the simulated moments, in the simplified and the full physics simulations, is now presented in Figure 4.6. In both cases the input parameters are the calculated moments of neutrons emitted from fission, and the input true values of the probability of fission dependent on source position and collision number. The results show excellent agreement, with the bias introduced by using the full physics simulation shown in Table B.2. As with the averaging over direction described in Section 3.5.1, averaging over neutron energy introduces a positive bias.

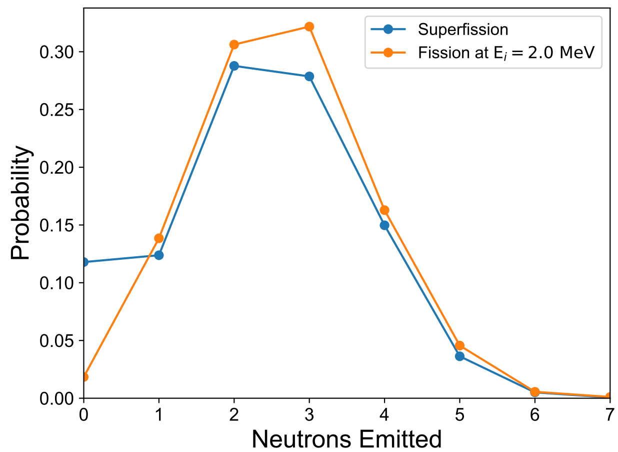

FIGURE 4.3: Multiplicity distribution of neutrons emitted from neutron induced fission on uranium-235. The original fission only distribution is shown (orange), along with the distribution for all neutron energies (blue) and including neutron capture and (n,xn) as fission.

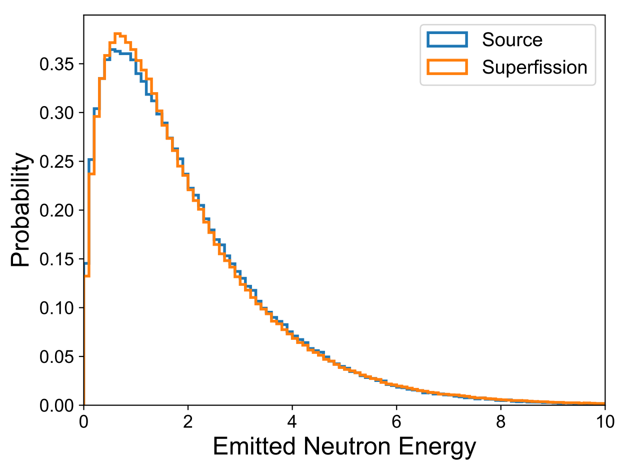

FIGURE 4.4: Energy distribution of neutrons emitted from all fission and (n,xn) reactions. The source neutron spectrum is modified until it matches the emitted fission neutron distribution.

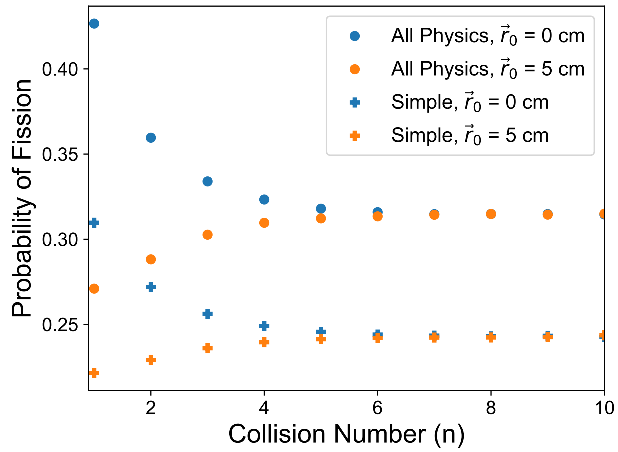

FIGURE 4.5: Mean values of the probability of fission with collision number for a source at the center (blue line) and near the edge (orange line) in a 6 cm sphere of uranium-235. These are shown for the simplified physics of Section 3.1, previously shown in Figure 3.7, and without any simplification of the physics or neutron transport. In the latter case the probability of fission includes capture and (n,xn) reactions.

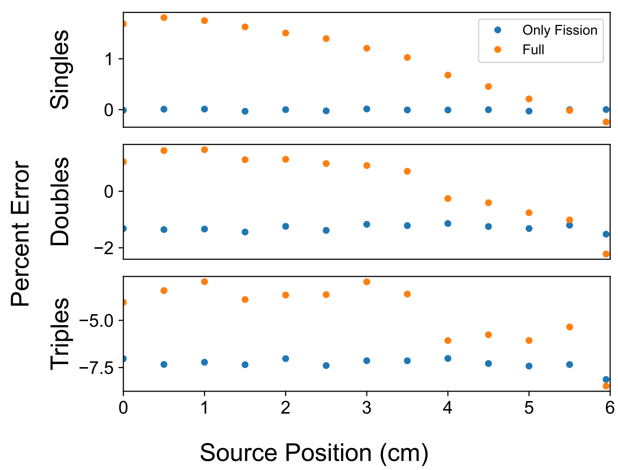

FIGURE 4.6: Simulated error of combinatorial moments (Singles, Doubles, Triples) of those predicted by the VPF moment equations and directly estimated from the distribution of escaped neutrons of the MCNP simulations. The error is shown for two cases, with the simplified version of MCNP described in Section 3.1, and for all physics including energy and neutron scattering as described in Section 4.3.

Chapter 5

Interpreting Simulated Imaged Data of API Measurements using the VPF Model

In this chapter we proceed to develop a way to interpret simulated API data using the VPF model. The goal is to use images of singles and doubles, $S(\vec{r}), D(\vec{r})$ to estimate the number of chain starting events $F(\vec{r})$ and the spatial dependent probability of fission $p(\vec{r})$. For the simulated sphere of Section 4.3 the transmission image and singles and doubles $S(\vec{r})$, $D(\vec{r})$ are shown in Figure 5.1. The goal is to use these images to reconstruct $F(\vec{r})$ and $p_f(\vec{r})$ as shown in Figure 5.2.

The procedure for doing so will be as follows. First, we must create a forward model which inputs the true images $F(\vec{r})$ and $p_f(\vec{r})$ and creates the imaged singles and doubles data $S(\vec{r})$, $D(\vec{r})$. The VPF model requires the probabilities of fission for each collision. The first problem to address will be to estimate the values of $p_f(n,\vec{r}_0)$ given only $p_f(\vec{r})$. Second, this forward model is incorporated into an optimization routine to minimize least squares error and estimate $F(\vec{r})$ and $p_f(\vec{r})$ from the transmitted, singles and doubles images.

5.1 Constructing the Forward Model

5.1.1 Estimating Intermediate Values of the Probability of Fission

We begin by revisiting the curve of $p_f(n,\vec{r}_0)$ shown in Figure 3.7. Given the values $p_f(n=1,\vec{r}_0)$ and $p_f(n\to\infty,\vec{r}_0) = p_f(\infty)$ we seek to find a functional form to find the intermediate values of $p_f(n,\vec{r}_0)$. The form used previously in (4.30)

$$p_f(n,\vec{r}_0) = (1-\alpha)^{i-1} p_f(1,\vec{r}_0) + p_f(\infty)\alpha^{i-1}. \tag{5.1}$$

The curves of (5.1) are fit for the sphere simulation at various radial positions, with α and $p_f(\infty)$ as variables to determine. The result is shown in Figure 5.3, where the best fit value is $\alpha = 0.39$ determined by minimizing over all radial positions $\vec{r}_0$. The additional error in the VPF moments (4.34)-(4.36) of using the functional form (5.1) is shown in Figure 5.4. It's seen that the functional form well approximates the curves of $p_f(\vec{r}_0, n)$ near the center of the sphere, but towards the edge introduces a few percent of additional error.

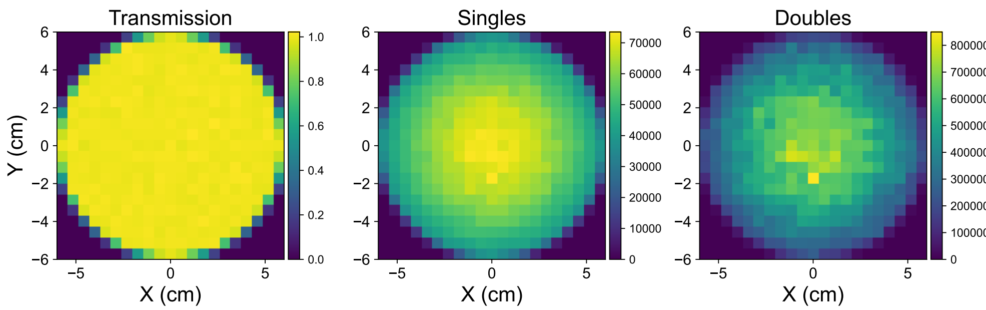

FIGURE 5.1: Simulated API data for a 6 cm radius sphere of U235 using MCNP for 10^7 uniformly distributed neutrons. All of the physics is enabled as described in Section 4.3.

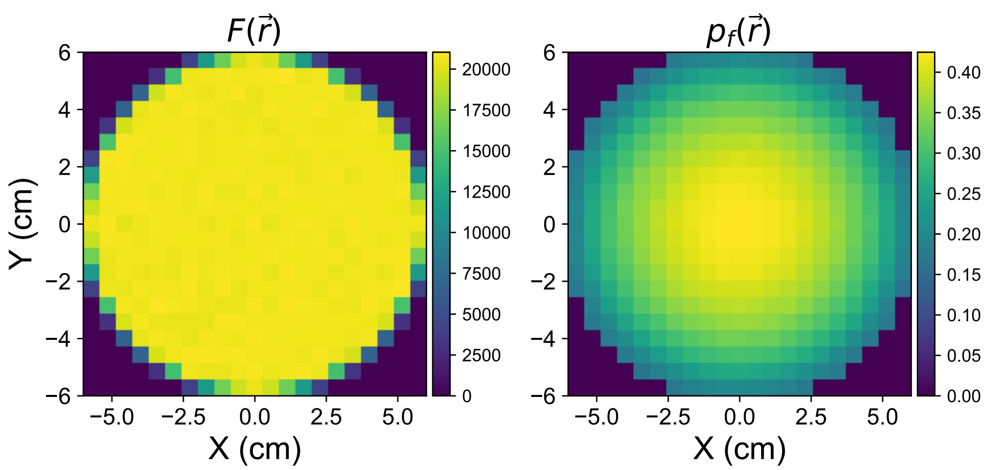

FIGURE 5.2: The true values of the number of source neutrons emitted at each voxel position $F(\vec{r})$ and the probability of a neutron emitted from a voxel to induce fission $p_f(\vec{r})$. All physics are enabled as described in Section 4.3.

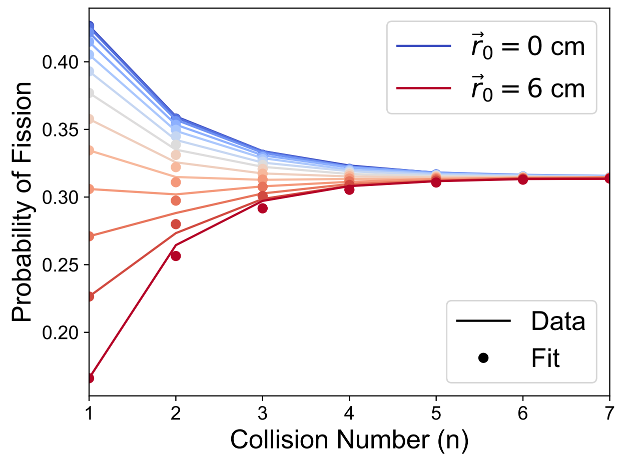

FIGURE 5.3: The values of $p_f(\vec{r}_0, n)$ fit with the functional form of (5.1) of values $\alpha = 0.40$ and $p_f(\infty) = 0.314$. The fit values are those which minimizes the least squares error over all radial positions.

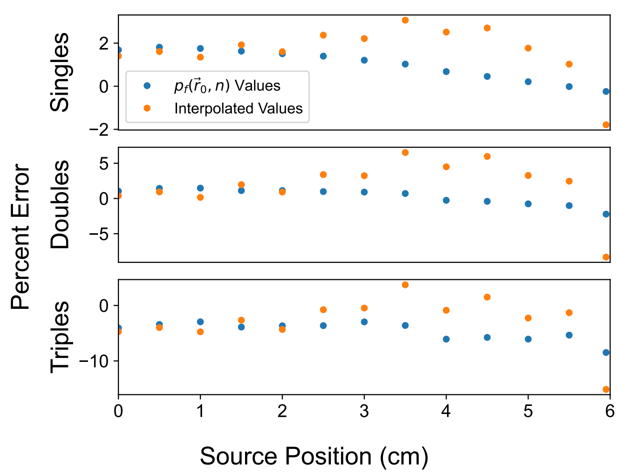

FIGURE 5.4: The additional error introduced by approximating $p_f(\vec{r}_0, n)$ (blue) with the functional form of (5.1) (orange). The additional error is minimal near the center of the sphere but increases towards the edge.

5.1.2 Estimating the Asymptotic Value of the Probability of Fission

The functional form of (5.1) still requires knowing the asymptotic value $p_f(\infty)$. Here it is shown one approach in which this can be approximated using the transmission image and the values of $p_f(\vec{r}_0, n=1)$. We return back to the form (3.4) which for $n \to \infty$ is,

$$p_f(\infty) = p_f(n \to \infty, \vec{r}_0) = \mathbb{E}_{\vec{r}}\left[p_f(\vec{r}|n \to \infty, \vec{r}_0)\right] = \mathbb{E}_{\vec{r}}\left[p_f(\vec{r})\Psi(\vec{r}, n \to \infty|\vec{r}_0)\right] \tag{5.2}$$

$$p_f(\infty) = \mathbb{E}_{\vec{r}}\left[p_f(\vec{r})\Psi(\vec{r}, \infty)\right] \tag{5.3}$$

where $\Psi(\vec{r}, \infty)$ is the fundamental node shown previously for $n \geq 9$ in Figure 3.5. Since we are already assuming that we know $p_f(\vec{r}) = p_f(n=1, \vec{r})$, what is left is to approximate $\Psi(\vec{r}, \infty)$.

To do so we turn to the transmission image shown in Figure 5.1. As the fundamental node reflects the distributions of fissions after many previous collisions the general behavior is that $\Psi(\vec{r}, \infty)$ is highest at positions where there is the most surrounding material, and lowest towards the edges of the object. Using the transmission image, which is proportional to the density of material, we look for a kernel $k(\vec{r} - \vec{r'})$ which when convolved with the transmission image $I(\vec{r})$ will approximate the fundamental node

$$\Psi(\vec{r}, \infty) \approx \int_V I(\vec{s})k(\vec{s} - \vec{r})d\vec{s}. \tag{5.4}$$

A simple choice would be a spherical kernel where

$$k_{\text{sphere}}(\vec{r} - \vec{r'}, r_\beta) = \begin{cases} 1, & |\vec{r} - \vec{r}'| \leq r_\beta \\ 0, & |\vec{r} - \vec{r}'| > r_\beta \end{cases}. \tag{5.5}$$

Knowing previously that $p_f(\infty) = 0.314$, spherical kernels of varying r_β are tested radii to find that which yields the correct value. The best radius is found to be $r_\beta = 4.1$ cm which yields $p_f(\infty) = 0.309$. The kernel and resulting approximation of $\psi(\vec{r}, \infty)$ are shown in Figure 5.5.

5.1.3 Forward VPF Model for API

With the parameters $\alpha = 0.40$ and $r_\beta = 4.1$ cm of Sections 5.1.1 and 5.1.2, and the determined superfission moments $\nu_1 = 2.352$ and $\nu_2 = 4.957$ of Section 4.3.1, a forward model for transforming the images of $F(\vec{r})$ and $p_f(\vec{r})$ of Figure 5.2 is constructed. The VPF equations 4.34-4.36 are used where the intermediate values of the fission probability are given by (5.1) with $p_f(\vec{r}, n=1) = p_f(\vec{r})$ and $p_f(\infty)$ determined by (5.3) and (5.4). The result is shown in Figure 5.6. The distribution of the percent error for each bin of the forward model and the simulated values from MCNP is shown in Figure 5.7. It is seen that the singles are much better estimated than the doubles. Comparing the sums of the singles and doubles yields error estimates of $S^{err}_{total} = -0.42\%$ and $D^{err}_{total} = -7.11\%$. The conclusion is that the VPF forward model is slightly biased to underestimate the number of singles and doubles, and that the doubles are more sensitive to the simplifications of the VPF model compared to the singles.

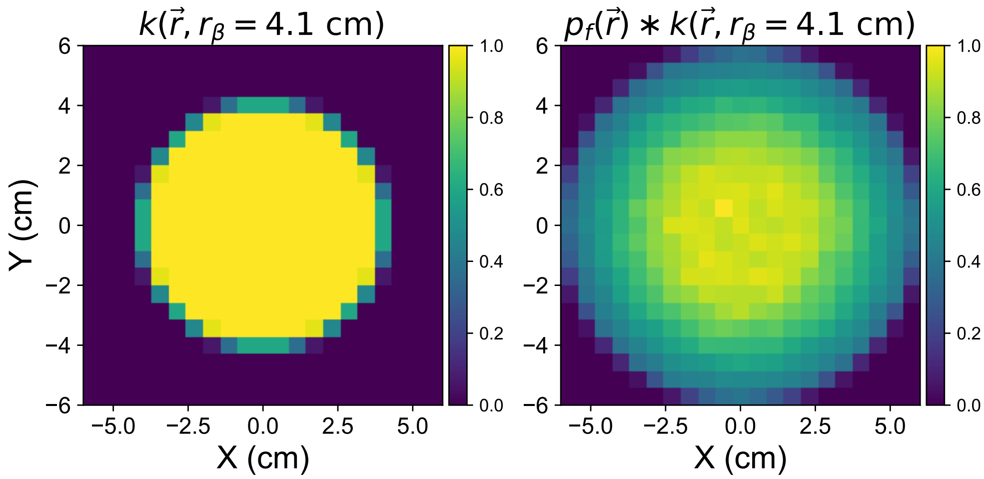

FIGURE 5.5: Applying the spherical kernel (left) on the transmission image (Figure 5.1) yields an approximation of $\Psi(\vec{r}, \infty)$. The spherical radius $r_\beta = 4.1$ cm yields a best value of $p(\infty) = 0.309$.

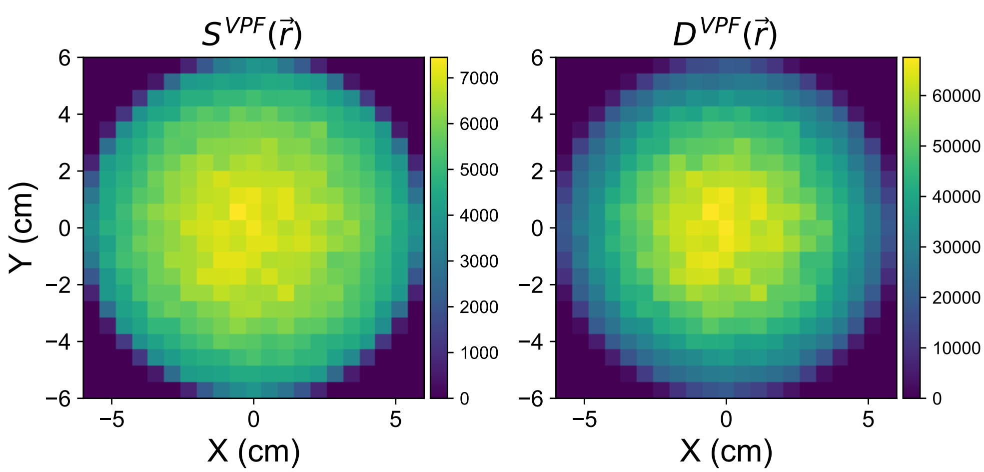

FIGURE 5.6: Estimate of the singles and doubles using the forward model with the VPF equations.

5.2 Estimate of $F(\vec{r})$ and $p_f(\vec{r})$ from $S(\vec{r})$ and $D(\vec{r})$ Using VPF Model

With a forward model now in place, it is possible to go in the reverse direction and find the images $F(\vec{r})$, $p_f(\vec{r})$ which minimizes the weighted sum of squares error between the forward projected images $S^{VPF}(\vec{r})$, $D^{VPF}(\vec{r})$ and the simulated imaged data $S(\vec{r})$, $D(\vec{r})$. This procedure is outlined now.

1. The VPF model parameters (α, r_β, ν_1, ν_2) are determined from an MCNP simulation of a 6.0 cm radius sphere of uranium-235. These are ($\alpha = 0.40$, $r_\beta = 4.1$ cm, $\nu_1 = 2.3517$, $\nu_2 = 4.9568$).

2. Images of the 14.1 MeV neutron transmission, emitted singles $S(\vec{r})$ and doubles $D(\vec{r})$ are prepared for a geometry and source distribution which are not known a priori in the reconstruction.

3. An initial estimate of $F(\vec{r})$ and $p_f(\vec{r})$ is determined using the point model equations for each voxel of $S(\vec{r})$ and $D(\vec{r})$.

4. An objective function to minimize is computed, being the weighted sum of squared errors (WSSE) of the input data $S(\vec{r})$ and $D(\vec{r})$ and the forward projections $S^{VPF}(\vec{r})$ and $D^{VPF}(\vec{r})$ summed over all voxels $\vec{r}_i$,

$$\mathrm{WSSE} = \sum_{\vec{r}_i} I(\vec{r}_i) \left| \frac{S(\vec{r}_i) - S^{VPF}(\vec{r}_i)}{\sqrt{S(\vec{r}_i)}} \right|^2 + I(\vec{r}_i) \left| \frac{D(\vec{r}_i) - D^{VPF}(\vec{r}_i)}{\sqrt{D(\vec{r}_i)}} \right|^2 \tag{5.6}$$

   where the weights are the reciprocal of the variance of the singles or doubles simulated values, $\sqrt{S(\vec{r}_i)}$ and $\sqrt{D(\vec{r}_i)}$, times the relative density $I(\vec{r}_i)$.

5. An optimization routine is used to find new estimates of $F(\vec{r})$ and $p_f(\vec{r})$ which yields a lower WSSE. In this work the Python library Scipy-optimization implementation of the Broyden–Fletcher–Goldfarb–Shanno limited-memory unconstrained nonlinear optimization algorithm (L-BFGS-B) [60].

6. The optimization routine is run for a fixed number of 250 iterations, returning estimates of $F(\vec{r})$ and $p_f(\vec{r})$. Additional iterations were not found to yield any improved results.

The above procedure is now applied on several different geometries of uranium-235 metal with density of 18.74 g/cm^3. In each case, the source neutrons are distributed uniformly throughout the volume with isotropic directions and an energy spectrum matching Figure 4.4. The geometries simulated are shown in Figure 5.8 and listed now.

1. A sphere of uranium-235 with radius of 6.0 cm.

2. A square triangular prism of uranium-235 with side length of 6.0 cm.

3. A 161-type storage casting of uranium-235 consisting of an annular cylinder with inner diameter of 8.890 cm, outer diameter 12.700 cm, and 14.856 cm height.

4. The University of Tennessee 'Power T' logo composed of uranium-235 with side length of 20.0 cm and depth of 10.0 cm.

5.3 Results

The previously described procedure for reconstruction of $F(\vec{r})$ and $p_f(\vec{r})$ for the geometries of Figure 5.8 are now computed. For each geometry 10^8 source particles are distributed uniformly and 3D voxellized images of both the emitted singles and doubles $S(\vec{r})$, $D(\vec{r})$ are computed along with the underlying true values of $F(\vec{r})$ and $p_f(\vec{r})$. The output of the reconstruction estimates of $F^{VPF}(\vec{r})$ and $p_f^{VPF}(\vec{r})$ are shown for the four geometries in Figures 5.9, 5.10, 5.11, 5.12.

The results are overall excellent, correctly reconstructing the values of $F(\vec{r})$ and $p_f(\vec{r})$. For the largest geometry of the 'Power T' logo, there is a slight overestimation of p_f towards the center with an underestimation of F. Due to the large directional variation of p_f at the center it is likely that the previously described bias in Section 3.5.2 for assuming a single value of p_f limits the accuracy.

The results are summarized in Table B.3. As a simple comparison the total values of the reconstructed $F^{VPF}(\vec{r})$ is compared with the value yielded by the point model equations (2.57), (2.58) neglecting detection efficiency, $\epsilon = 1.0$. In all cases the VPF model improves the bias of the point model, yielding a better estimation of F as desired.

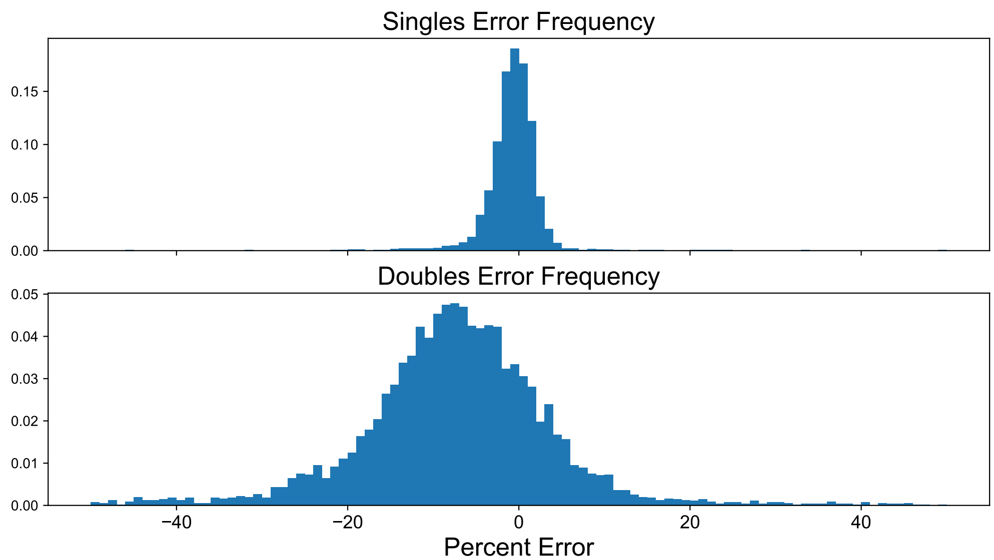

FIGURE 5.7: Histogram of the percent errors for each bin of the simulated singles and doubles (Figure 5.1) and the estimated singles and doubles for the forward model (Figure 5.6.)

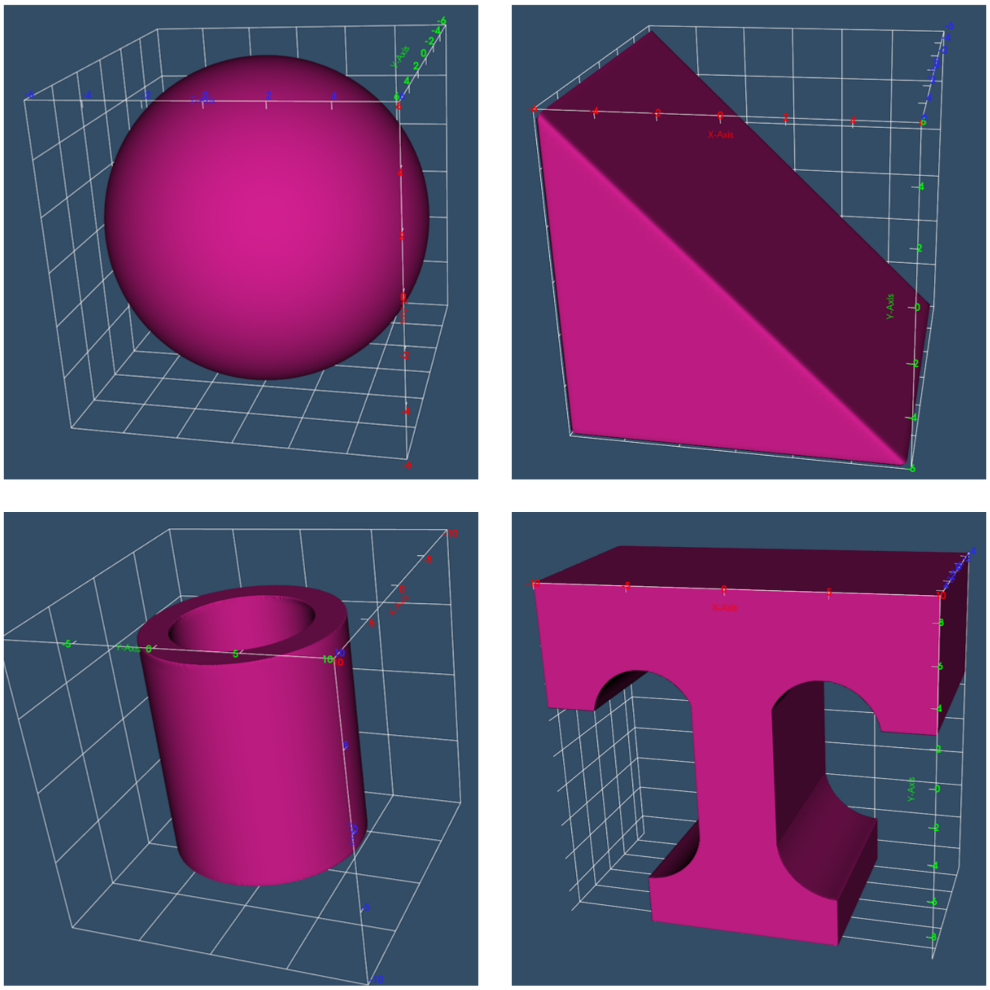

FIGURE 5.8: The simulated geometries from which simulated API data is created to evaluate the application of the VPF model. Descriptions of the geometries are listed in Section 5.2.

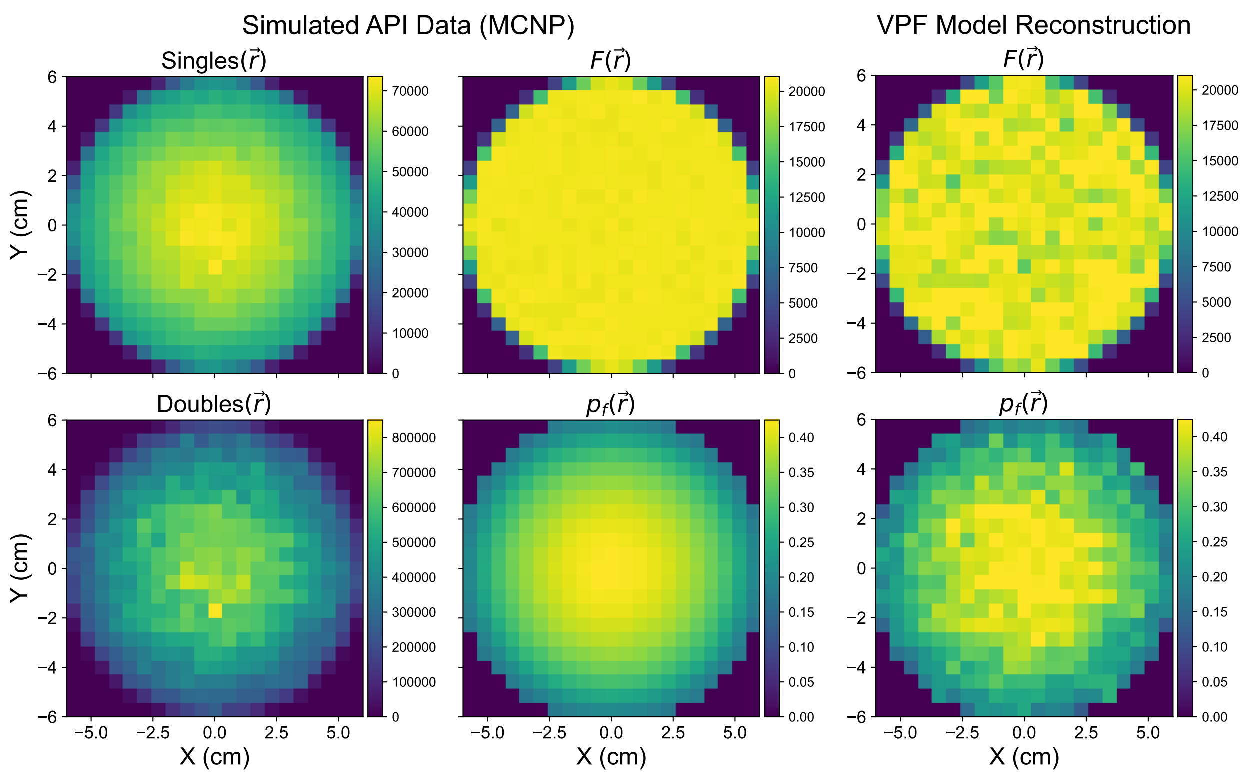

FIGURE 5.9: The simulated data (left) for a 6.0 cm radius sphere of uranium-235 and the VPF reconstruction results (right). Plots are shown for a two dimensional cross-section view through the origin on the X-Y plane.

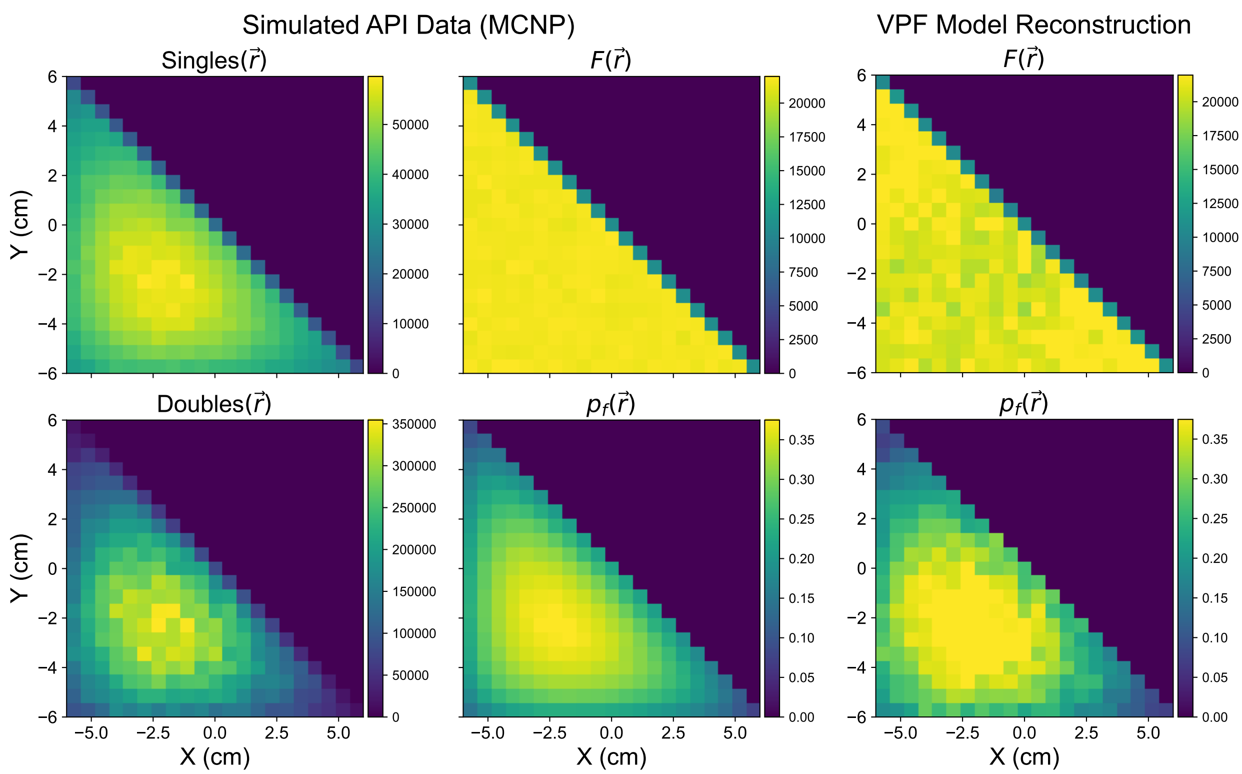

FIGURE 5.10: The simulated data (left) for a 6.0 cm radius sphere of uranium-235 and the VPF reconstruction results (right). Plots are shown for a two dimensional cross-section view through the origin on the X-Y plane

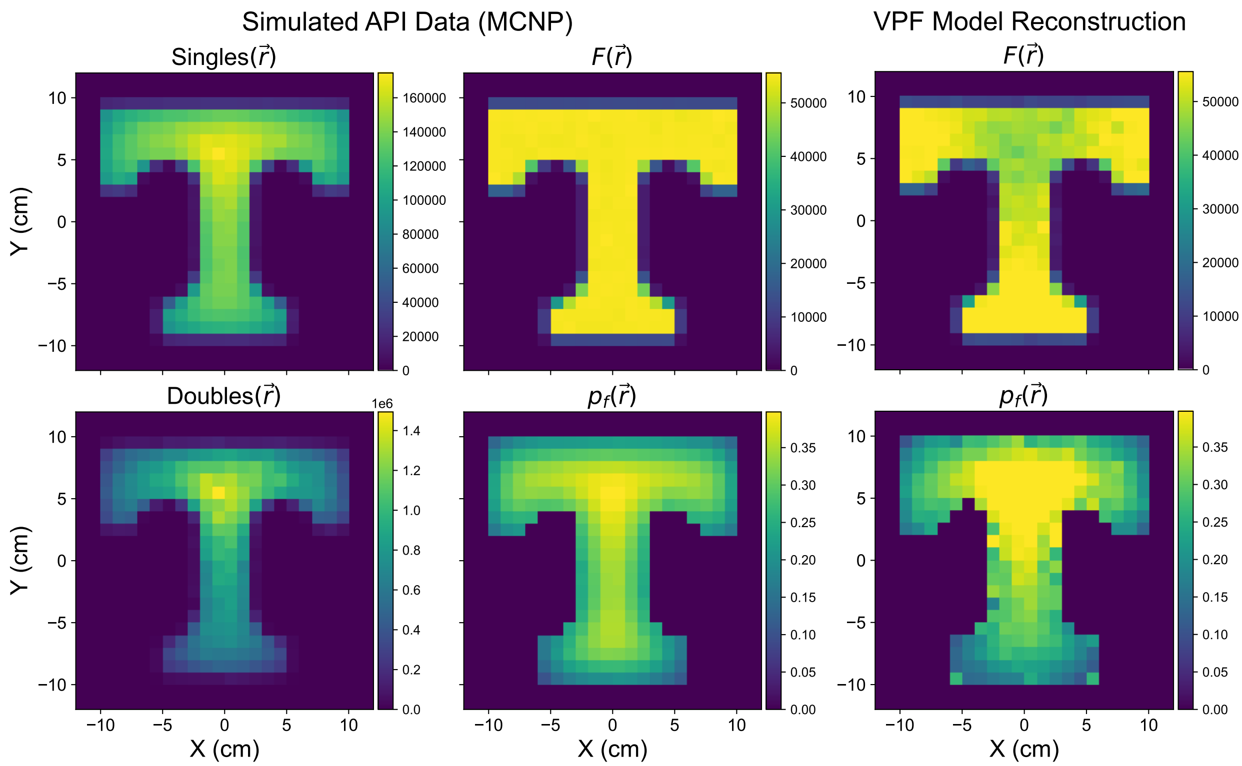

FIGURE 5.11: The simulated data (left) for a 20.0 side length and 10.0 cm depth 'Power T' of uranium-235 and the VPF reconstruction results (right). Plots are shown for a two dimensional cross-section view through the origin on the X-Y plane

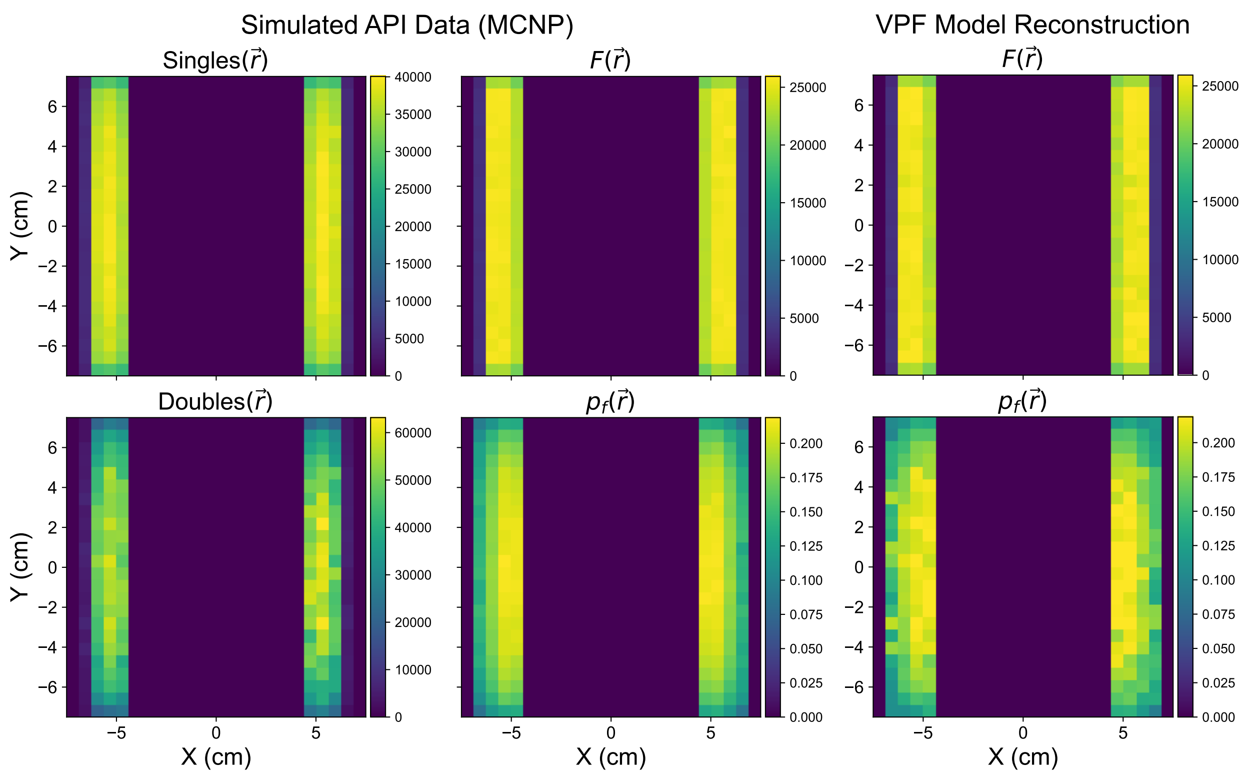

FIGURE 5.12: The simulated data (left) for a 161 casting geometry of uranium-235 and the VPF reconstruction results (right). Plots are shown for a two dimensional cross-section view through the origin on the X-Y plane

Chapter 6

Conclusions and Future Work

This dissertation presented an extension of the point model, the Varying Probability of Fission model, and a method for applying the VPF model to quantiatively interpret simulated imaged data from API systems. After altering the point model probability generating function with a probability of fission that varies with starting position of the neutron and the generation number, new moment equations for the neutron singles, doubles, and triples were derived (4.27), (4.28), (4.29). Section 4.4 showed these equations closely match the varying moments determined by MCNP simulation. A forward model was then created in Section 5.1 to create images of singles and doubles given the spatial dependent probability of fission and the number of source neutrons within a voxel. This was then applied in the reverse direction to estimate these quantities from simulated imaged data of singles and doubles directly. The results of Section 5.3 showed excellent agreement between the VPF reconstruction and the true images determined by MCNP.

Incorporating this work into existing API systems will enable real-time characterization of fissile materials, providing inspectors the information to make on-site evaluations and decisions. However, there are still several steps left to complete before this work can be applied for a larger variety of materials including plutonium, mixed oxide materials, and materials of unknown enrichment. These steps and other proposed future work include:

1. In the point model, an enrichment determination is made using the estimate of F and the specific activity and/or coupling parameter of an external neutron source. However, the model parameters ν_1, ν_2 have also shown to be highly dependent on enrichment [43] due to the variation of the capture to fission cross-section ratio. The possibility of modifying the presented reconstruction method with a global enrichment parameter should be explored.

2. The coupling parameter concept has not yet been explored in the VPF approach. The reconstructed values of $F(\vec{r})$ are proportional to the the external neutron source flux at $\vec{r}$ and the macroscopic cross-section of the 'superfission' at $\vec{r}$, which is dependent on enrichment. Previous work [54] should be extended to account for these factors using the VPF approach.

3. The use of imaged triples data may provide another set of variables that could be useful. For example, if shielded material is present there will be a large non-uniform scattering contribution which will not be proportional to $p_f(\vec{r})$. The use of triples may provide a method for creating a probability of scatter $p_s(\vec{r})$ image and allow the use of the VPF model for shielded fissile assemblies.

4. Other effects such as detector efficiency and cross-talk must be accounted for to incorporate the VPF model into existing API systems.

Lastly, we revisit a mentioned earlier approach in Section 2.5.4 developed in the past several years. This approach by Imre Pázsit and others includes the dependence neutron direction into to the probability of fission. Additionally the dependence on the macroscopic cross-section is made explicit. Investigating whether this approach is significantly faster than MCNP and whether it may provide a better way to explicitly account for enrichment estimation should be explored as well.

Bibliography

[1] K. Böhnel, "The Effect of Multiplication on the Quantitative Determination of Spontaneously Fissioning Isotopes by Neutron Correlation Analysis," *Nuclear Science and Engineering*, vol. 90, no. 1, pp. 75–82, 1985. DOI: 10.13182/nse85-2.

[2] P. Russo, "PASSIVE NONDESTRUCTIVE ASSAY OF NUCLEAR MATERIALS 2007 ADDENDUM," Tech. Rep., 2007.

[3] R. Serber, "The Definition of "Neutron Multiplication"," Los Alamos Scientific Laboratory, Tech. Rep., Jul. 1945.

[4] M. Göttsche and G. Kirchner, "Improving neutron multiplicity counting for the spatial dependence of multiplication: Results for spherical plutonium samples," *Nuclear Instruments and Methods in Physics Research Section A: Accelerators, Spectrometers, Detectors and Associated Equipment*, vol. 798, pp. 99–106, 2015, ISSN: 0168-9002. DOI: 10.1016/j.nima.2015.07.007.

[5] P. Hausladen, M. Blackston, D. Aykac, *et al.*, "3D Tomography and Image Processing Using Fast Neutrons Final Report," English, United States, Tech. Rep., Jan. 2020. [Online]. Available: https://www.osti.gov/biblio/1671428.

[6] W. Younes and W. D. Loveland, *An Introduction to Nuclear Fission* (Graduate Texts in Physics). 2021, ISBN: 9783030845919. DOI: 10.1007/978-3-030-84592-6.

[7] O. Hahn and F. Strassmann, "Über den Nachweis und das Verhalten der bei der Bestrahlung des Urans mittels Neutronen entstehenden Erdalkalimetalle," *Naturwissenschaften*, vol. 27, no. 1, pp. 11–15, 1939, ISSN: 0028-1042. DOI: 10.1007/bf01488241.

[8] L. MEITNER and O. R. FRISCH, "Products of the Fission of the Uranium Nucleus," *Nature*, vol. 143, no. 3620, pp. 471–472, 1939, ISSN: 0028-0836. DOI: 10.1038/143471a0.

[9] N. Bohr and J. A. Wheeler, "The Mechanism of Nuclear Fission," *Physical Review*, vol. 56, no. 5, pp. 426–450, 1939, ISSN: 0031-899X. DOI: 10.1103/physrev.56.426.

[10] P. Talou and R. Vogt, Eds., *Nuclear Fission*. Cham, Switzerland: Springer Nature Switzerland AG, 2023, ISBN: 9783031145445. DOI: 10.1007/978-3-031-14545-2.

[11] C. J. Werner, "MCNP Users Manual - Code Version 6.2," Los Alamos National Laboratory, Tech. Rep. LA-UR-17-29981, 2017.

[12] M. S. Zucker and N. E. Holden, "Energy Dependence of the Neutron Multiplicity P(nu) in Fast Neutron Induced Fission of U-235, U-238 and Pu-239," in *Proceedings of American Nuclear Society Annual Meeting*, Reno, Nevada, Jun. 1986. [Online]. Available: https://www.osti.gov/biblio/6974950.

[13] L. Szilard, "Improvements in or relating to the Transmutation of Chemical Elements," English, pat., Mar. 1936.

[14] L. Hoddeson, P. W. Henriksen, R. A. Meade, and C. L. Westfall, *Critical Assembly: A Technical History of Los Alamos during the Oppenheimer Years, 1943–1945*. Cambridge: Cambridge University Press, 1993, ISBN: 9780521441322. DOI: DOI:10.1017/CBO9780511665400.

[15] R. Rhodes, *The Making of the Atomic Bomb*. Simon & Schuster, 2012, ISBN: 9781439126226. [Online]. Available: https://books.google.com/books?id=aSgFMMNQ6G4C.

[16] S Walston, "Thoughts on Analyzing Neutron Multiplicity Data," English, United States, Tech. Rep., Jan. 2020. [Online]. Available: https://www.osti.gov/biblio/1777340.

[17] J. Doyle, *Nuclear Safeguards, Security and Nonproliferation: Achieving Security with Technology and Policy*, 1st ed. Butterworth-Heinemann, Jul. 2008, ISBN: 0750686731.

[18] K. S. Kim, L. F. Nakae, M. K. Prasad, N. J. Snyderman, and J. M. Verbeke, "Time Evolving Fission Chain Theory and Fast Neutron and Gamma-Ray Counting Distributions," *Nuclear Science and Engineering*, vol. 181, no. 3, pp. 225–271, Nov. 2015, doi: 10.13182/NSE14-120, ISSN: 0029-5639. DOI: 10.13182/nse14-120. [Online]. Available: https://doi.org/10.13182/NSE14-120.

[19] J. K. Shultis and R. E. Faw, *Fundamentals of Nuclear Science and Engineering*. CRC Press, 2019, ISBN: 9781498769297. DOI: 10.1201/9781315183183. [Online]. Available: https://books.google.com/books?id=Kw0DDQEACAAJ.

[20] N. Ensslin, M. S. Krick, D. G. Langner, and M. C. Miller, "Active Neutron Multiplicity Counting of Bulk Uranium," in *Proceedings Institute of Nuclear Materials Management Annual Meeting*, New Orleans, LA, Jul. 1991.

[21] T. H. Shin, M. Y. Hua, M. J. Marcath, *et al.*, "Neutron Multiplicity Counting Moments for Fissile Mass Estimation in Scatter-Based Neutron Detection Systems," *Nuclear Science and Engineering*, vol. 188, no. 3, pp. 246–269, 2017, ISSN: 0029-5639. DOI: 10.1080/00295639.2017.1354591.

[22] W. Hage and D. M. Cifarelli, "Correlation Analysis with Neutron Count Distributions in Randomly or Signal Triggered Time Intervals for Assay of Special Fissile Materials," *Nuclear Science and Engineering*, vol. 89, no. 2, pp. 159–176, 1985, ISSN: 0029-5639. DOI: 10.13182/nse85-8.

[23] H. H. Barschall, L. Rosen, R. F. Taschek, and J. H. Williams, "Measurement of Fast Neutron Flux," *Reviews of Modern Physics*, vol. 24, no. 1, pp. 1–14, Jan. 1952. DOI: 10.1103/revmodphys.24.1. [Online]. Available: https://link.aps.org/doi/10.1103/RevModPhys.24.1.

[24] J. W. Cates, J. P. Hayward, X. Zhang, P. A. Hausladen, and B. Dabbs, "Timing Resolution Study of an Associated Particle Detector for Fast Neutron Imaging," *IEEE Transactions on Nuclear Science*, vol. 59, no. 4, pp. 1750–1756, 2012, ISSN: 1558-1578. DOI: 10.1109/tns.2012.2201751.

[25] J. T. Mihalczo, P. R. Bingham, M. A. Blackston, *et al.*, "Fast-Neutron Imaging with API DT Neutron Generators," Moscow, Russia, Oct. 2012. [Online]. Available: `https://ntrl.ntis.gov/NTRL/dashboard/searchResults/titleDetail/DE20131079274.xhtml`.

[26] P. Hausladen, M. A. Blackston, J. A. Mullens, *et al.*, "Induced-Fission Imaging of Nuclear Material," 2010. [Online]. Available: `http://inis.iaea.org/search/search.aspx?orig\_q=RN:41096289`.

[27] T. E. Harris, *The Theory of Branching Processes*. 1964. [Online]. Available: `https://www.rand.org/content/dam/rand/pubs/reports/2009/R381.pdf`.

[28] D. Hawkins and S. Ulam, "Theory of Multiplicative Processes," Tech. Rep. LA-171, Nov. 1944. [Online]. Available: `https://permalink.lanl.gov/object/tr?what=info:lanl-repo/lareport/LA-00171` (visited on 01/31/2023).

[29] K. S. Alexander, "A conversation with Ted Harris," *Statistical Science*, vol. 11, no. 2, pp. 150–158, May 1996, ISSN: 0883-4237. DOI: `10.1214/ss/1038425658`.

[30] G. Grimmett and D. Stirzaker, *Probability and Random Processes*. OUP Oxford, 2020, ISBN: 9780192586865. [Online]. Available: `https://books.google.com/books?id=gfLuDwAAQBAJ`.

[31] I. Pázsit, A. Enqvist, and L. Pál, "A note on the multiplicity expressions in nuclear safeguards," *Nuclear Instruments and Methods in Physics Research Section A: Accelerators, Spectrometers, Detectors and Associated Equipment*, vol. 603, no. 3, pp. 541–544, 2009, ISSN: 0168-9002. DOI: `10.1016/j.nima.2009.03.018`.

[32] D. Langner, J. Stewart, M. Pickrell, M. Krick, N Ensslin, and W. Harker, "Application guide to neutron multiplicity counting," Los Alamos National Laboratory, Los Alamos, NM, Tech. Rep., 1998.

[33] I. Pázsit and L. Pál, *Neutron Fluctuations*. 2008, ISBN: 9780080450643. DOI: `10.1016/b978-0-08-045064-3.x5001-7`.

[34] L Nakae, G Chapline, A Glenn, *et al.*, "Safeguards Verification with Time-Correlated Fast Neutron Detection," English, in *Report Number: LLNL-CONF-461175*, Research Org.: Lawrence Livermore National Lab. (LLNL), Livermore, CA (United States), Oct. 2010. [Online]. Available: `https://www.osti.gov/biblio/1124928`.

[35] M. Prasad, N. Snyderman, J. Verbeke, and R. Wurtz, "Time Interval Distributions and the Rossi Correlation Function," *Nuclear Science and Engineering*, vol. 174, no. 1, pp. 1–29, 2013, ISSN: 0029-5639. DOI: `10.13182/nse11-87`.

[36] K. S. Kim, L. F. Nakae, M. K. Prasad, N. J. Snyderman, and J. M. Verbeke, "Time Evolving Fission Chain Theory and Fast Neutron and Gamma-Ray Counting Distributions," *Nuclear Science and Engineering*, vol. 181, no. 3, pp. 225–271, 2015, ISSN: 0029-5639. DOI: `10.13182/nse14-120`.

[37] M. Prasad, N. Snyderman, and S. Walston, "Neutron Time Interval Distributions with Background Neutrons," *Nuclear Science and Engineering*, vol. 186, no. 3, pp. 277–292, 2017, ISSN: 0029-5639. DOI: `10.1080/00295639.2016.1273620`.

[38] S. Croft and A. Favalli, "Incorporating delayed neutrons into the point-model equations routinely used for neutron coincidence counting in nuclear safeguards," *Annals of Nuclear Energy*, vol. 99, pp. 36–39, 2017, ISSN: 0306-4549. DOI: 10.1016/j.anucene.2016.08.012.

[39] K. S. Kim, L. F. Nakae, M. K. Prasad, N. J. Snyderman, and J. M. Verbeke, "Fission Chain Restart Theory," *Nuclear Science and Engineering*, vol. 188, no. 1, pp. 57–84, 2017, ISSN: 0029-5639. DOI: 10.1080/00295639.2017.1340691.

[40] J. L. W. V. Jensen, "Sur les fonctions convexes et les inégalités entre les valeurs moyennes," *Acta Mathematica*, vol. 30, no. 1, pp. 175–193, 1906, ISSN: 0001-5962. DOI: 10.1007/bf02418571.

[41] P. A. Santi and W. H. Geist, "Energy Dependent Bias in the Weighted Point Model.," English, in *Report Number: LA-UR-05-4287*, Research Org.: Los Alamos National Lab. (LANL), Los Alamos, NM (United States), Jan. 2005. [Online]. Available: https://www.osti.gov/biblio/977983.

[42] R. M. Jr, "Total Measurement Uncertainty in Neutron Coincidence Multiplicity Analysis," English, United States, Tech. Rep., Nov. 2020. [Online]. Available: https://www.osti.gov/biblio/1767868.

[43] M. C. Tweardy, S. M. McConchie, and J. P. Hayward, "An Evaluation of Systematic Biases of the Point Kinetics Model for Active Interrogation of Uranium," Jeju, South Korea, Apr. 2017. [Online]. Available: https://www.osti.gov/biblio/1479810.

[44] M. S. Krick, W. H. Geist, and D. R. Mayo, "A Weighted Point Model for the Thermal Neutron Multiplicity Assay of High-Mass Plutonium Samples," English, United States, Tech. Rep., Oct. 2005. [Online]. Available: https://www.osti.gov/biblio/876505.

[45] J. M. Burward-Hoy, W. H. Geist, M. S. Krick, and D. R. Mayo, "Achieving accurate nuetron-multiplicity analysis of metals and oxides with weighted point model equations.," English, in *Report Number: LA-UR-04-4357*, Research Org.: Los Alamos National Lab. (LANL), Los Alamos, NM (United States), Jan. 2004. DOI: 10.2172/876505. [Online]. Available: https://www.osti.gov/biblio/977717.

[46] S. Croft, E. Alvarez, P. M. Chard, R. McElroy, and S. Philips, "An alternative perspective on the weighted point model for passive neutron multiplicity counting," 2007.

[47] T. E. Harris, "On One-Dimensional Neutron Multiplication," RAND Corporation, Santa Monica, CA, Tech. Rep., 1960. [Online]. Available: https://www.rand.org/pubs/research_memoranda/RM2317.html.

[48] H. E. Conner, "A limit theorem for a position-dependent branching process," *Journal of Mathematical Analysis and Applications*, vol. 3, no. 3, pp. 560–591, 1961, ISSN: 0022-247X. DOI: 10.1016/0022-247x(61)90077-4.

[49] I. Pázsit and L. Pál, "Multiplicity theory beyond the point model," *Annals of Nuclear Energy*, vol. 154, p. 108 119, 2021, ISSN: 0306-4549. DOI: 10.1016/j.anucene.2020.108119.

[50] I. Pázsit and V. Dykin, "Transport Calculation of the Multiplicity Moments for Cylinders," *Nuclear Science and Engineering*, vol. 196, no. 3, pp. 235–249, 2021, ISSN: 0029-5639. DOI: 10.1080/00295639.2021.1973178.

[51] V. Dykin and I. Pazsit, "CALCULATION OF THE MULTIPLICITY MOMENTS FOR SHELLS IN A SPACE-DEPENDENT MODEL WITH INCLUSION OF SCATTERING," in *INMM Annual Meeting Proceedings*, 2020.

[52] A. Swift, "Materials and Configuration from NMIS Type Neutron Imaging and Gamma Spectroscopy," Ph.D. dissertation, 2012.

[53] J. Crye, "ENRICHMENT DETERMINATION OF URANIUM METAL IN SHIELDED CONFIGURATIONS WITHOUT CALIBRATION STANDARDS," Ph.D. dissertation, 2013.

[54] M. C. Tweardy, "Point Kinetics-based Methods for Uranium Assay in Tagged Neutron Interrogation," Ph.D. dissertation, University of Tennessee, Knoxville, 2018.

[55] M. C. Tweardy, S. McConchie, and J. P. Hayward, "Quantifying the determinants of leakage multiplication for large uranium objects using Monte Carlo simulations," *Nuclear Instruments and Methods in Physics Research Section A: Accelerators, Spectrometers, Detectors and Associated Equipment*, vol. 954, p. 161 684, 2020, ISSN: 0168-9002. DOI: `10.1016/j.nima.2018.11.143`.

[56] C. J. Solomon, C. Bates, and J. Kulesza, "The MCNPTools Package: Installation and Use," no. LA-UR-17-21779, Mar. 2017. [Online]. Available: `https://mcnp.lanl.gov/pdf\_files/TechReport\_2017\_LANL\_LA-UR-17-21779\_SolomonBates.pdf`.

[57] J. Siek, L. Lee, and A. Lumsdaine, *The Boost Graph Library: User Guide and Reference Manual, The* (C++ In-Depth Series). Pearson Education, 2001, ISBN: 9780321601612. [Online]. Available: `https://books.google.com/books?id=CPi7g1hjyIYC`.

[58] W. Haeck, *Processing files with NJOY - Reading and manipulating ACE files with ACEtk*, LA-UR-22-31190, Los Alamos, NM, Oct. 2022. [Online]. Available: `https://mcnpx.lanl.gov/pdf\_files/TechReport\_2022\_LANL\_LA-UR-22-31190\_Haeck.pdf`.

[59] M. K. Prasad and N. J. Snyderman, "Statistical Theory of Fission Chains and Generalized Poisson Neutron Counting Distributions," *Nuclear Science and Engineering*, vol. 172, no. 3, pp. 300–326, 2012, ISSN: 0029-5639. DOI: `10.13182/nse11-86`.

[60] P. Virtanen, R. Gommers, T. E. Oliphant, *et al.*, "SciPy 1.0: Fundamental Algorithms for Scientific Computing in Python," *Nature Methods*, vol. 17, pp. 261–272, 2020. DOI: `10.1038/s41592-019-0686-2`.

[61] H. A. Smith, "The Measurement of Uranium Enrichment," in *Passive Nondestructive Assay of Nuclear Materials*, D. Reilly, N. Ensslin, and H. Smith, Eds., Springfield, VA: National Technical Information Office, 1991, pp. 195–220, ISBN: 0160327245.

[62] IAEA, "The Text of the Agreement of 18 November 1977 Between the United States of America and the Agency for the Application of Safeguards in the United States of America," Tech. Rep., Nov. 1977. [Online]. Available: `https://www.iaea.org/publications/documents/infcircs/text-agreement-18-november-1977-between-united-states-america-and-agency-application-safeguards-united-states-america`.

[63] P. M. J. Chard and S Croft, "A Database of 240Pu_effective and 235U_effective Coefficients for Various Fertile and Fissile Isotopes," in *19th Annual Symposium on Safeguards and Nuclear Management*, 1997. [Online]. Available: `https://op.europa.eu/s/xSZG`.

[64] S Croft, L. C.-A. Bourva, D. R. Weaver, and H Ottmar, "Pu240 Effective Mass of Pu238 and Pu242 in Relation to Passive Neutron Coincidence and Multiplicity Counting," *Journal of Nuclear Materials Management*, 1st ser., vol. XXX, pp. 10–19, 2001.

[65] H Ottmar, P. v. Belle, S Croft, P. M. J. Chard, L. C.-A. Bourva, and U Blohm-Hieber, "An Empirical Measurement of the Specific 240Pu_Effective Mass of 238Pu and 242Pu," in *Proceedings of the 21st Annual Meeting: Symposium on Safeguards and Nuclear Material Management*, Sevilla, Spain, 2000, pp. 337–345. [Online]. Available: https://op.europa.eu/s/xSZN.

[66] S Croft, S Cleveland, and A Nicholson, "Calculation of the 240Pu_Effective Coefficients for Neutron Correlation Counting," Indian Wells, CA, USA, Jan. 2015. [Online]. Available: https://www.osti.gov/biblio/1214018.

Appendices

Appendix A

Enrichment and Effective Mass

A.1 Enrichment

Uranium enrichment is defined as the isotopic ratio of ^{235}U to all U isotopes, of which ^{238}U is the most dominant naturally [61]. The isotopic ratio can be defined as an atom fraction

$$E_a = \frac{\text{\# of atoms } ^{235}\text{U}}{\text{\# of atoms U}} \cdot 100\% \tag{A.1}$$

or as a weight fraction

$$E_w = \frac{\text{grams of } ^{235}\text{U}}{\text{grams of U}} \cdot 100\%. \tag{A.2}$$

The safeguards agreement between the United States and the IAEA (INFCIRC/288) alternatively defines enrichment as "the ratio of the combined weight of the isotopes uranium-233 and uranium-235 to that of the total uranium in question" [62]. In this work, uranium enrichment is defined using (A.2) and only the isotopes ^{235}U and ^{238}U are considered.

A.2 Neutron Counting Rates and Effective Mass

For an object composed of several isotopes i, the observed doubles rate $\dot{\mathbf{D}}$ is the sum of the doubles rate for each isotope,

$$\dot{\mathbf{D}} = \sum_i \dot{\mathbf{D}}_i = \sum_i \frac{1}{2} \mathbf{F}_i \epsilon_i^2 f_{D_i} (\nu_{2,i} \phi_2). \tag{A.3}$$

where $(\nu_{2,i}\phi_2)$ is the second neutron moment for a fission event from isotope i, ϵ_i is the detection efficiency for the neutrons emitted by isotope i and f_{D_i} is the associated doubles gate fraction [32]. Each isotope has an associated fission event rate $\mathbf{F}_i$. In general,

$$\mathbf{F}_i = m_i \alpha_i \tag{A.4}$$

where α_i is the event rate per unit mass and is dependent on the event process such as spontaneous or induced fission.

While isotopic composition is not known in general, typically an assay is interested in one fiducial isotope j. Most assay results report their results in terms of an *effective mass* which interprets the doubles rate as solely due to the j isotope, written as $\langle m_j \rangle_{\text{eff}}^{\mathbf{D}}$ [32]. This effective mass is derived by equating (A.3) to a single isotope j with an *effective* event rate $\langle \mathbf{F}_j \rangle_{\text{eff}}^{\mathbf{D}} = \langle m_j \rangle_{\text{eff}}^{\mathbf{D}} \alpha_j$ where the $\mathbf{D}$ superscript indicates this is for the doubles rate

$$\dot{\mathbf{D}} = \frac{1}{2} \langle \mathbf{F}_j \rangle_{\text{eff}}^{\mathbf{D}} \epsilon_j^2 f_{D_j} \nu_{2,j} \phi_2 \tag{A.5}$$

$$\sum_i \frac{1}{2} m_i \alpha_i \epsilon_i^2 f_{D_i} \nu_{2,i} \phi_2 = \frac{1}{2} \langle m_j \rangle_{\text{eff}}^{\mathbf{D}} \alpha_j \epsilon_j^2 f_{D_j} \nu_{2,j} \phi_2. \tag{A.6}$$

This yields an expression for the effective mass in terms of each isotope,

$$\langle m_j \rangle_{\text{eff}}^{\mathbf{D}} = \sum_i m_i \left(\frac{\alpha_i \nu_{2,i}}{\alpha_j \nu_{2,j}} \right) \left(\frac{\epsilon_i^2 f_{D_i}}{\epsilon_j^2 f_{D_j}} \right) = \sum_i m_i \gamma_{i,j}^{\mathbf{D}} \tag{A.7}$$

$$\gamma_{i,j}^{\mathbf{D}} = \left(\frac{\alpha_i \nu_{2,i}}{\alpha_j \nu_{2,j}} \right) \left(\frac{\epsilon_i^2 f_{D_i}}{\epsilon_j^2 f_{D_j}} \right). \tag{A.8}$$

The effective mass is thus a combination of the individual masses weighted by the coefficients $\gamma_{i,j}^{\mathbf{D}}$. The first portion of $\gamma_{i,j}^{\mathbf{D}}$ involving α_i and $\nu_{2,i}$ is a function of nuclear data and is detector independent. The second portion including ϵ_i and f_{D_i} is specific to a detection system and the energy spectra of neutrons emitted by isotope i. Generally this detector specific ratio is near unity [63].

If the isotopic composition of the material is available from a separate measurement providing the weight fractions $w_i = m_i / \sum_j m_j$, the total mass $m_{\text{tot}} = \sum_j m_j$ can be determined from $\langle m_j \rangle_{\text{eff}}^{\mathbf{D}}$,

$$m_{\text{tot}} = \frac{\langle m_j \rangle_{\text{eff}}^{\mathbf{D}}}{\langle w_j \rangle_{\text{eff}}^{\mathbf{D}}} \tag{A.9}$$

$$\langle w_j \rangle_{\text{eff}}^{\mathbf{D}} = \sum_i w_i \gamma_{i,j}^{\mathbf{D}} \tag{A.10}$$

where $\langle w_j \rangle_{\text{eff}}^{\mathbf{D}}$ is the effective weight fraction [64]. The calculation of (A.8) can be done in two ways listed below.

A.2.1 Detector Independent Calculation

Assuming the detection specific parameters ϵ_i and f_{D_i} do not vary with isotope i, $\gamma_{i,j}^{\mathbf{D}}$ can be approximated as

$$\gamma_{i,j}^{\mathbf{D}} \approx \left(\frac{\alpha_i \nu_{2,i}}{\alpha_j \nu_{2,j}} \right) \tag{A.11}$$

and for a specified assay mode can be calculated from known nuclear data.

For a passive neutron assay of spontaneously fissioning isotopes, $\alpha_i = g_i$ where g_i is the spontaneous fission event rate per unit mass

$$g_i = \frac{N_A}{A_i}\lambda_i \tag{A.12}$$

with N_A as Avogadro's constant, A_i the molar mass of isotope i and λ_i the associated decay constant.

A common task in passive neutron assay is the measurement of ^{240}Pu content with ^{238}Pu and ^{242}Pu present. Using the data listed in Table B.4 the effective mass equation is,

$$\langle m_{240}\rangle^{\mathbf{D}}_{\text{eff}} = m_{240} + 2.573\, m_{238} + 1.708\, m_{242}. \tag{A.13}$$

Similar equations for active assay and other modes of neutron counting for many isotopes can be derived. These have been compiled previously into a database which lists the doubles effective mass coefficients for many scenarios and isotopes [63].

A.2.2 Direct Measurement of Pure Isotopic Samples

Taking assay measurements to determine the ratio of the doubles rate for an isotope i and a fiducial isotope j is a another way to calculate $\gamma^{\mathbf{D}}_{i,j}$,

$$\frac{\dot{\mathbf{D}}_i}{\dot{\mathbf{D}}_j} = \frac{\frac{1}{2}m_i\alpha_i\epsilon_i^2 f_{D_i}\nu_{2,i}\phi_{2,i}}{\frac{1}{2}m_j\alpha_j\epsilon_j^2 f_{D_j}\nu_{2,j}\phi_{2,j}} = \gamma^{\mathbf{D}}_{i,j}\frac{m_i}{m_j}\frac{\phi_{2,i}}{\phi_{2.j}} \tag{A.14}$$

$$\gamma^{\mathbf{D}}_{i,j} = \frac{\dot{\mathbf{D}}_i}{\dot{\mathbf{D}}_j}\frac{m_j}{m_i}\frac{\phi_{2,j}}{\phi_{2,i}}. \tag{A.15}$$

In this case the sample dependent multiplication ratio $\phi_{2,j}/\phi_{2,i}$ must be either assumed unity or modelled through Monte Carlo simulation [65]. Thus if two known samples of isotopically pure isotopes are available, the mass coefficients which including the factors of detector response ϵ_i and f_{D_i} can be determined through experiment. This approach can also be done using only Monte Carlo simulation, provided an accurate detector model and post analysis.

The presented derivation for estimating effective mass has been done using only the doubles rates, however equivalent relations can be derived for both the singles and triples rates as well [64]. It is current practice to only consider the doubles rate derivation of effective mass, and nearly all literature refers to the doubles expression when discussing effective mass [66]. This is due in part to the popular use of coincidence counting, which relies only the the doubles rate for estimating effective mass. Additionally, a neutron multiplicity system will estimate a single value of **F** which is applied on the singles, doubles, and triples rate equations. To avoid the ambiguity of reporting three separate effective masses, only the doubles effective mass is reported and used in creating limits for safeguards.

Appendix B

Tables

TABLE B.1: Averaged Error of Figure 3.9 excluding the last two points due to poor statistics. The error is calculated for using the distributions of $p_f(\vec{r}|n, \vec{r}_0)$ shown in Figure 3.6 and the mean values $p_f(n, \vec{r}_0)$ shown in Figure 3.7, versus the moments determined from the number of escaped neutrons from MCNP.

	Singles Error	Doubles Error	Triples Error
Using $p_f(\vec{r}\|n, \vec{r}_0)$ Dist.	0.02%	3.657%	18.12%
Using $p_f(n, \vec{r}_0)$ Mean Val.	-0.02%	-1.32%	-7.21%

TABLE B.2: Averaged Error of Figure 4.6 excluding the last two points due to poor statistics. The error is for the VPF and simulated moments for the simplified physics and the full physics models.

	Singles Error	Doubles Error	Triples Error
Simple Physics	-0.01%	-1.29%	-7.21%
Full Physics	1.21%	0.67%	-4.19%

TABLE B.3: The summed values of the singles and doubles for the simulated API data of the geometries shown in Figures 5.9, 5.10, 5.11, 5.12. The percent error of the VPF reconstruction of the sum of $F(\vec{r})$ is made with the true value of 10^8. Additionally the total singles and doubles are used with the point model equations to estimate the total F. The VPF model shows a large improvement in estimating F compared to the point model.

	Total Singles	Total Doubles	Total $F^{VPF}(\vec{r})$ Error	Point Model Error
Sphere	2.43e8	1.82e9	-1.85%	-5.38 %
Prism	1.93e8	7.27e8	0.27%	-4.12 %
'Power T'	2.12e8	1.07e9	-1.34%	-5.09 %
161 Casting	1.46e8	1.81e8	-0.05 %	-0.55 %

TABLE B.4: Nuclear data of the spontaneous fission event rate g_i, the second moment of the number of neutrons emitted $\nu_{2,j}$ and the associated effective mass coefficient $\gamma^{\mathbf{D}}_{i,240}$ in reference to ^{240}Pu for isotopes ^{238}Pu and ^{242}Pu. Table and data are taken from [63].

^{i}Pu	g_i $(\mathrm{s}^{-1}\mathrm{g}^{-1})$	$\nu_{i,2}$	$\gamma^{\mathbf{D}}_{i,240}$
i = 238	1169.8	3.957	2.573
i = 240	475.01	2.154	1.0
i = 242	807.15	2.149	1.708

Vita

Aaron Nowack completed his B.S. in Physics from the University of California, Davis in 2011. While attending he conducted research on estimating the mass of large shear selected galaxy clusters with Dr. David Wittman, and later with Dr. Mani Tripathi to develop methods for tagging beam-halo background events for the monophoton search group for the Compact Muon Solenoid at the Large Hadron Collider. Afterwards he began a contract position at Sandia National Laboratories in Livermore, California for three years. While there he helped to develop novel approaches for imaging fission energy neutrons for detecting and characterizing fissile materials and nuclear materials. This work included developing data acquisition systems, modeling and simulation, and performing data analysis. After this period he joined the nuclear engineering department at the University of Tennessee, Knoxville as a PhD student under Dr. Jason Hayward. His doctoral research extended the traditional point model of neutron assay to account for large extended assemblies to better characterize fissile assemblies under active interrogation. This work is conducted in collaboration with the Advanced Radiation Detection, Imaging, Data Science, and Applications group at Oak Ridge National Laboratory under the supervision of Dr. Paul Hausladen.